Performance Investigation of Membranes Suitable for Osmotic Membrane Pressure Actuators

Gaute Tolås Trondsen

Abstract

Polybenzimidazole (PBI) membrane performance having hydrocarbons mixed with the feed water was investigated. Forward osmosis (FO) and pressure retarded osmosis (PRO) experiments were performed with different ratios of hydrocarbons. The membranes performed well under these conditions. The results did not conclusively indicate that there is a relationship between the hydrocarbon ratio and the water or salt permeability. It appeared that the contact between the water and the membrane surface is an important factor contributing to water permeation. The results indicated that exposure to hydrocarbons possibly increases the membrane's salt retention. It was also found that hydrocarbons possibly cause swelling of the membrane. This was done by measuring thickness before and after exposure under different circumstances. In experiments conducted in PRO mode pressure was generated on the draw side when hydrocarbons were mixed together with water in the feed. PRO experiments using pure water in the feed were performed at different pressure differences. The results showed no linear relationship between water flux and pressure difference. FO experiments using pure water in the feed were carried out to test the effect of temperature on the trans-membrane water and salt flux. It was found that both water and salt flux increase with temperature. The PBI membrane's thermal stability was investigated using thermogravimetric analysis. It was heated to temperatures just short of 600 °C with very little loss of mass. The membrane morphology was characterized by SEM, and its hydrophilic properties demonstrated by attempted contact angle measurements.

Sammendrag

Polybenzimidasol membraners ytelse ble undersøkt med hydrokarboner blandet med fødevannet. Eksperimenter ble utført ved vanlig osmose (FO) og trykk retardert osmose (PRO) med forskjellige forhold av hydrokarboner og vann. Membranene presterte godt under disse forholdene. Resultatene indikerte at det kanskje ikke var noen sammenheng mellom hydrokarbonforholdet og vann eller salt permeabiliteten. Det viste seg imidlertid at vannets kontakt med membranoverflaten kan være en viktig faktor som påvirker permeabiliteten i stor grad. Resultatene tydet også på at eksponering av membranene for hydrokarboner muligens fører til redusert salt permeabilitet. Målinger av membrantykkelsen før og etter eksponering for hydrokarboner ble utført. Resultatet av disse målingene tydet på at hydrokarboner kan forårsake membransvelling. Under eksperimenter utført i PRO modus ble det observert trykkøkning i trekkløsningen når hydrokarboner var blandet inn i fødevannet. PRO eksperimenter med rent fødevann ble utført ved forskjellige trykkforskjeller mellom trekk og fødesiden. Resultatene tydet ikke på at det var en lineær sammenheng mellom vannfluksen og trykkforskjellen. FO eksperimenter med rent fødevann ble utført for å undersøke effekten av temperatur på vann og salt fluksen gjennom membranen. Resultatet tydet på at både vann og salt fluks øker med temperaturen. PBI membranens termisk stabilitet ble undersøkt ved hjelp av termogravimetrisk analyse. Oppvarming til temperaturer i underkant av 600 ° C førte til lite tap av masse. Morfologi undersøkelser ble utført ved hjelp av SEM og membranens hydrofile egenskaper ble demonstrert med kontakt-vinkelmålinger.

Acknowledgements

Table of contents

Symbols and abbreviations

Symbol	Description	Units
A	Water permeability coefficient	[g m^{-2} bar^{-1} h^{-1}]
a_i	The activity of substance i	
B	Solute permeability coefficient	[g m^{-2} h^{-1}]
c	Solute concentration	[M]
		[mol L^{-1}]
d	Calibration constant	[mol cm μS^{-1} L^{-1}]
E	Membrane area	[m^2]
e	Calibration constant	[mol L^{-1}]
γ_i	The activity coefficient of substance i	
J_w	Water flux	[g m^{-2} h^{-1}]
J_s	Reverse salt flux	[mol m^{-2} h^{-1}]
k	Mass transfer coefficient	[g m^{-2} h^{-1}]
μ_i	Chemical potential of substance i in solution	[J mol^{-1}]
μ_i^0	Chemical potential of pure substance i	[J mol^{-1}]
M_w	Molar weight of water	[g mol^{-1}]
m	Weight	[g]
n_i	Number of substance i molecules	[mol]
P	Pressure	[bar]
		[Pa]
P_w	Permeability of water	[g m m^{-2} h^{-1}]
P_s	Permeability of salt	[g m m^{-2} h^{-1}]
π	Osmotic pressure	[bar]
		[Pa]
ρ	Density	[g L^{-1}]
σ	Reflection coefficient	
R	Ideal gas constant	[J K^{-1} mol^{-1}]
R_s	Salt rejection	[%]
s	Membrane thickness	[m]
T	Temperature	[°C]
t	Time	[s]
		[h]
V	Volume	[L]
		[m^3]
V_i	Volume of pure substance i	[m^3 mol^{-1}]
V_0	Start volume	[L]
x_i	Mole fraction of substance i	

Abbreviation	Description
CP	Concentration polarization
FO	Forward osmosis
PBI	Polybenzimidazole
HC	Hydrocarbons
PRO	Pressure retarded osmosis
RO	Reverse osmosis
SEM	Scanning electron microscope
TGA	Thermogravimetric analyzer
LPM	Liters per minute

1 Introduction

1.1 The background for the thesis

This master's thesis is a part of the Osmotic Membrane Pressure Actuator (OMPA) project. The OMPA project is a collaboration between the membrane research group at NTNU, Statoil, Inflow Control, Sintef Materials and Chemistry and ITM-CNR institute in Calabria, Italy. The project aims to develop an osmotic membrane pressure actuator that can be used to autonomously close off a valve in an oil or gas well drainage pipe when water is present. The actuator is initially intended for use in gas condensate wells in the Åsgard field, which will need this kind of water choking technology within a few years. A picture of the Åsgard B rig is shown in Figure 1-2.

Intrusion of water into the drainage pipes in wells decreases the recovery of gas and oil. In the last few years it has become increasingly common with horizontal and branched wells to improve reservoir utilization. When a well begins to produce water, expensive measures have to be taken to identify and close the water producing branch. If this identification and closing could be done autonomously, there is a large potential for reduced expenses [1]. The design of the actuator will be based on a patent held by Inflow Control and Statoil [2]. Figure 1-1 shows the proposed actuator design. The hydrocarbons and water from the well will enter into the feed chamber through an inlet hole. When water comes in contact with the semi permeable membrane the water will permeate through the membrane. The osmotic cell will feature a flexible impermeable membrane that enables the shutdown plate to move as osmotic pressure within the cell is generated. The shutdown plate will move to restrict the flow increasingly until it cuts off the flow from the reservoir completely [2].
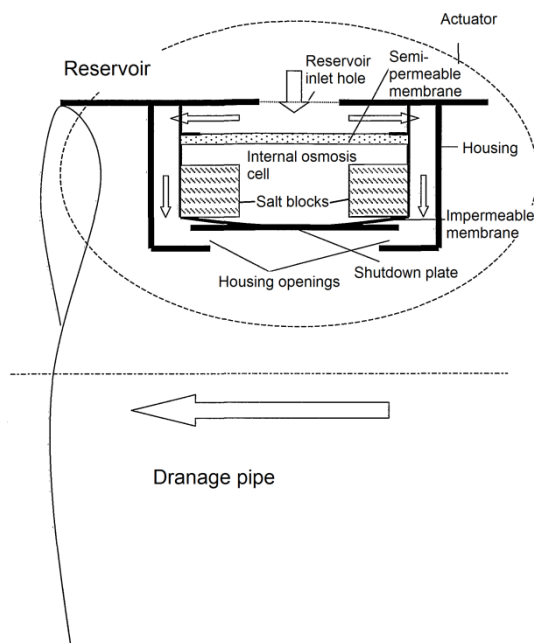

Figure 1-1: Figure of the OMPA actuator patent held by Statoil and Inflow control. Figure adapted from [2].

Figure 1-2: The Åsgard B rig in the North Sea. Picture: Statoil.

This master's thesis is a continuation of the student project "Investigation of Polybenzimidazole (PBI) Membrane Performance in Forward Osmosis". In that project, the PBI membrane performance using different salts at different concentrations for draw solution was investigated. The thesis work focuses on investigating the membrane performance when hydrocarbons are mixed with the feed water, as well as the temperature effect on water permeation through the membrane. Both forward osmosis and pressure retarded osmosis experiments are performed with this objective.

1.2   The problem of produced water in the offshore oil and gas industry

Water is naturally trapped in offshore oil and gas reservoirs. Even though efforts are made to recover the oil and gas selectively it is difficult to avoid bringing a fraction of the water to the surface along with the oil and gas. As wells mature, increased pressure is often needed. This can be achieved by injecting water to help force the oil to the surface. As a result, both the naturally occurring water from the reservoir and the injected water are produced together with the petroleum. In the worldwide offshore oil and gas production, roughly 17 million m^3 of water is produced daily, along with 14,3 million m^3 of oil. Forty percent of the produced water is discharged into the sea at the production site as a first treatment stage of the crude oil or gas. In the North Sea, roughly 1,1 million m^3 of produced water is discharged daily into the sea (2005). Gas fields tend to produce a lower volume of water relative to oil fields. However, the concentration of organic contaminants in the water from gas wells is higher than water from oil wells. Oil wells normally produce a larger volume of water, and this volume tends to increase as the amount of oil left in the reservoir decreases. In mature wells the volume of water may be as high as 10 times the volume of oil produced [3].

There are several problems related to produced water in oil and gas production. One of them is the environmental aspect. The environmental concern is related to the fact that the produced water contains contaminants. The contaminants are small quantities of hydrocarbons dissolved and dispersed in the water. This includes aromatic, aliphatic and cyclo-aliphatic substances. The water may also contain organic substances not related to oil, like phenols and fatty acids. Traces of naturally occurring radioactive material such as radium-226 and radium-228 with half-lives of 1601 years and 5 years respectively may be present in the produced water. Even though the concentrations of contaminants are low, there are some concerns that the contaminants may have a negative effect on marine life [3].

Another negative effect of the produced water is the impact it has on the capacity of the flow line, taking up valuable space that could otherwise be used for the oil and gas. It also impacts the topside process since the water has to be treated to meet the requirements before it can be discharged into the sea. The handling of produced water is a key challenge for most offshore oil and gas production sites. The possibility to reduce the production of water has a large potential for value creation [1].

1.3   The power of osmosis

Osmosis as a phenomenon was studied as early as 1740's by the French clergyman Jean-Antoine Nollet [4, 5]. The membranes used for experimentation in these early days consisted of material from plants and animals. Another hundred years went by before the first synthetic inorganic membrane was prepared by the German chemist Moritz Traube [4, 6]. Even though osmosis had been a known phenomenon for a long time, there weren't many studies published on the subject before the 1970's. Since osmosis is dependent on semi permeable membranes, it was not easy to investigate. However, in 1963, Loeb and Sourirajan prepared

an asymmetric cellulose acetate membrane with properties much superior to the synthetic membranes prepared up until this point [7]. This marked a significant breakthrough in membrane science and led to a large increase in published research on osmosis. Up until 1990, the number of published articles was still relatively modest, but from this point on it increased dramatically. Most of the published research was focused on reverse osmosis (RO). From the mid 2000's there has also been an increased number of published articles on forward osmosis (FO) and pressure retarded osmosis (PRO) [8].

Osmosis is a naturally occurring process where water flows through a selectively permeable membrane due to a concentration difference across the membrane. The water will flow from the side with low concentration to the side with high concentration of ions or molecules. A selectively permeable membrane allows the water to flow through, but rejects the solute [9].

PRO utilizes the free energy of mixing and converts it into potential mechanical energy. With today's climate situation, the need for green energy sources is growing. PRO technology has a large yet to be utilized potential for generating electric power. For Norway it is estimated that 25 TWh of osmotic electric power can be produced per year [10]. It should also be possible to utilize the potential mechanical energy generated by PRO to drive a hydraulic actuator cylinder. This actuator may then be used to close a valve in a water producing oil or gas well.

One of the challenges in developing an actuator based on PRO is to find a suitable membrane material that can withstand the tough conditions in an oil well with regard to pressure and temperature. A promising material candidate is polybenzimidazole, which has excellent thermal and chemical stability [11].

2 Theoretical background

2.1 Osmotic processes

Osmosis is the transport of water through a selectively permeable membrane. The driving force of the water transport is the difference in solute concentration on each side of the membrane. The flow of water is from the membrane side of low solute concentration, where the water chemical potential is high, to the side of high solute concentration, where the water chemical potential is low.

For a liquid mixture the activity of a component i is given as the product of the mole fraction x_i and the activity coefficient γ_i.

$$a_i = x_i\gamma_i \tag{2-1}$$

For a component i in a liquid mixture at constant temperature the chemical potential μ_i [J mol^{-1}] can be written as

$$\mu_i = \mu_i^0 + RTln(a_i) + V_iP \tag{2-2}$$

where μ_i^0 [J mol^{-1}] is the chemical potential of 1 mol of pure component at a pressure P [Pa] and a temperature T [K], V_i [m^3 mol^{-1}] is the volume of pure solvent, and R [J mol^{-1} K^{-1}] is the universal gas constant. When a concentrated and a and a dilute solution is separated by a semi permeable membrane the chemical potential for the concentrated solution, μ_w is given by

$$\mu_w = \mu_w^0 + RTln(a_w) + V_wP \tag{2-3}$$

Water is denoted by w. For the dilute solution the chemical potential $\mu_{w,d}$ can be written as

$$\mu_{w,d} = \mu_{w,d}^0 + RTln(a_{w,d}) + V_wP_d \tag{2-4}$$

At equilibrium the chemical potential is equal on both sides of the membrane.

$$\mu_w = \mu_{w,d} \tag{2-5}$$

A combination of Equation (2-1), (2-2) and (2-3) gives

$$RTln\left((a_{w,d}) - ln(a_w)\right) = (P - P_d)V_w = \Delta\pi V_w \tag{2-6}$$

where the pressure difference $(P - P_d)$ is the osmotic pressure $\Delta\pi$. When only pure solvent is situated on the dilute side of the membrane Equation (2-6) can be rewritten so that the osmotic pressure π is as a function of the water activity [12].

$$\pi = -\frac{ln(a_w)}{V_w}RT \tag{2-7}$$

For dilute solutions ($\gamma_i \to 1$) and Raoult's law can be used to simplify the expression.

$$\ln(a_w) = \ln(x_w \gamma_w) \approx \ln(x_w) \approx \ln(1 - x_s) = -x_s \tag{2-8}$$

x_s is the solute mole fraction which is given as

$$x_s = \frac{n_s}{n_s + n_w} \tag{2-9}$$

For dilute solutions $x_s = n_s/n_w$ since $n_s \ll n_w$ and $n_w V_w = V$ [m³] where n_s and n_w [mol] is the number of moles of solute and water respectively. Equation (2-7) can now be simplified to get an expression for the osmotic pressure for dilute solutions.

$$\pi = \frac{n_s}{V} RT \tag{2-10}$$

When equilibrium is reached the chemical potential of pure water (μ_w^0) is equal to the chemical potential of solvent in solution (μ_w). x_w is the mole fraction of solvent, π is the osmotic pressure and P is the pressure [12].

$$\mu_w^0 = \mu_w(x_w P + \pi) \tag{2-11}$$

The osmotic pressure ($\Delta\pi$) can also be defined as the pressure that needs to be applied to the side of high solute concentration to prevent water transport through the membrane. In FO the osmotic pressure is the driving force of the water transport. Reverse osmosis (RO) occurs when the applied hydraulic pressure to the membrane side with the higher solute concentration is greater than the osmotic pressure ($\Delta P > \Delta\pi$). This will cause water transport to be in the opposite direction relative to FO. PRO is an intermediate between FO and RO and occurs when ($\Delta P < \Delta\pi$) [9]. The different situations are illustrated in Figure 2-1 and Figure 2-2.

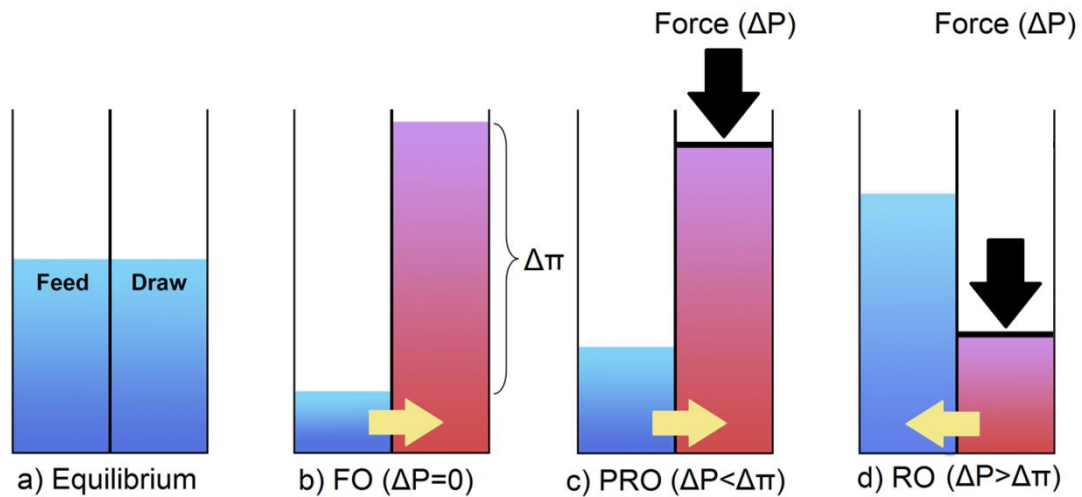**Figure 2-1: Illustration of the different scenarios in osmosis: a) Osmotic equilibrium, b) FO ($\Delta P = 0$), PRO ($\Delta P < \Delta\pi$) and RO ($\Delta P > \Delta\pi$). Illustration adapted from [9].**
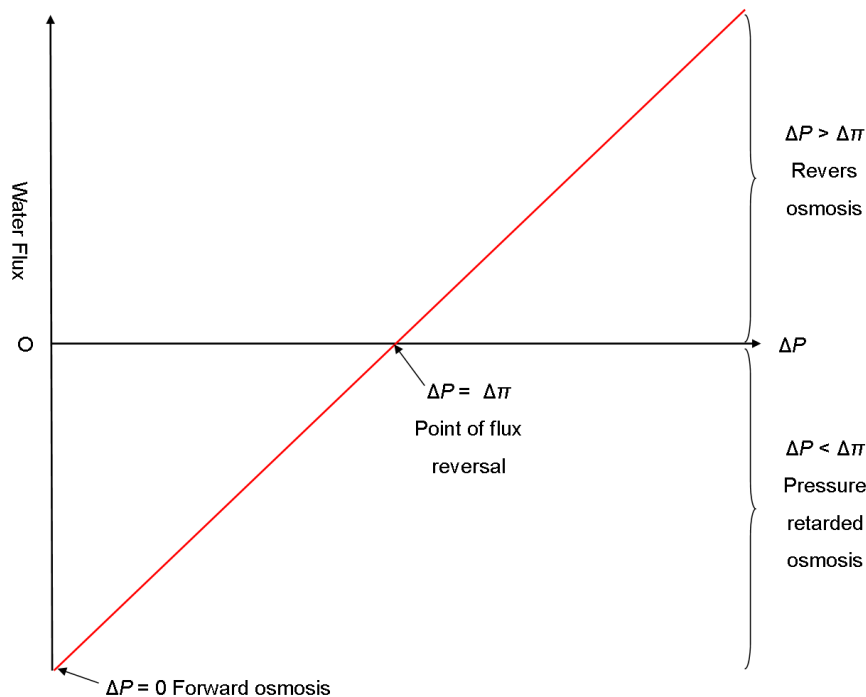

Figure 2-2: Water flux as a function of applied hydraulic pressure. Figure adapted from [13].

The general equation for the water flux (J_w [g m^{-2} h^{-1}]) in osmosis is

$$J_w = A(\sigma \Delta \pi - \Delta P)$$
(2-12)

where A [g m^{-2} bar^{-1} h^{-1}] is the permeability coefficient of water in the membrane and σ is the reflection coefficient of the membrane towards a particular solute [9]. The transport of solute through the membrane can be described by the solute permeability coefficient (B [g m^{-2} h^{-1}]).

$$B = J_w \left(\frac{1 - R_s}{R_s} \right) exp \left(-\frac{J_w}{k} \right)$$
(2-13)

k [g m^{-2} h^{-1}] is the mass transfer coefficient for a certain membrane cell and R_s is the salt rejection [14].

In osmotic processes, the ideal is to have a high water permeability coefficient (A) and a low solute permeability coefficient (B). Typically monovalent draw solutions yield lower osmotic pressures and lower salt rejection than divalent draw solutions [9, 15]. The higher rejection of divalent ions is due to the larger size, which makes transport through the membrane more difficult. For a draw solution of a certain salt, the osmotic pressure increases as the concentration increases [15].

Equation (2-12) gives the water flux in an osmotic process. However, the observed water flux is often lower than expected. The reason for this can be ascribed to concentration polarization (CP) which gives a lower solute concentration difference across the active layer than in the bulk. Thus the driving force is smaller, and consequently so is the water flux. There are two types of external CP. In FO the solute concentration on the permeate side surface of the membrane can be lower than in the bulk because of the water flowing through the membrane. This is called dilutive CP. On the feed side surface of the membrane there can be a buildup of solute. This is called concentrative CP. Both phenomena reduce the effective osmotic pressure and water flux through the membrane. External CP can be reduced by increasing the cross flow velocity of the feed water and draw solution. It is also possible to use a spacer that induces turbulent flow to prevent external CP. In asymmetric or composite membranes it is possible to have internal CP in the porous support layer. If the draw solution faces the active layer the solute concentration can build up in the porous support and concentrate the feed water. This is called internal concentrative CP. If the feed water faces the active layer the draw solution in the porous support will be diluted by the water permeating through the membrane. This is internal dilutive CP. Internal CP cannot be eliminated by increasing cross flow velocity [9].

Fouling is another phenomenon that can reduce a membrane's ability to transport water over time. It can be permanent or reversible. Fouling is defined as a deposition of material on the membrane surface or in the pores [12]. The four types of fouling are bio fouling, colloidal fouling, organic fouling and inorganic fouling [16]. Fouling can be a major problem in processes where porous membranes are used, but less of a problem with dense membranes [12].

7

2.2 The membrane material

Polybenzimidazole was made commercially available in 1983 by Hoechst Celanese [17]. Its thermal stability and chemical resistance against hydrocarbons and oils makes it suitable as a membrane material under harsh conditions such as in gas and oil wells. The structure of the monomer is shown in Figure 2-3.
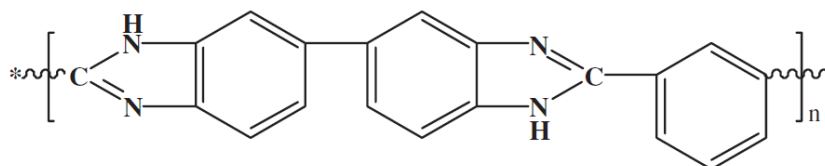

Figure 2-3: The molecular structure of the polybenzimidazole monomer.

The heterocyclic imidazole rings allow for both inter- and intra-molecular hydrogen bonding between PBI molecules. Hence PBI may become self-charged in aqueous solutions, when the neighboring benzene rings delocalize the proton in the imidazole groups. PBI is well suited for water separation, is hydrophilic and has good antifouling properties [18].

2.3 The solubility of hydrocarbons in water

The solubility of normal alkanes in water at room temperature decreases with increasing carbon number. Up to C-11 the decrease is relatively steep. For alkanes larger than C-11 the decrease is lower. Calorimetric data suggests that the heat of solution of normal alkanes in water is a linear function of temperature. The solubility of water in normal alkanes has been reported to not be significantly influenced by increasing carbon number. Calorimetric data suggests that the heat of solution of water in the n-alkanes is independent of temperature [19]. To mix alkanes and water a powerful stirrer has to be employed due to the otherwise rapid phase separation. Alternatively a surfactant can be added to the mix to create an emulsion. In oil and gas wells however the phases are likely not in an emulsion [20].

2.4 The experimental method

The experimental goal is to carry out FO and PRO experiments to measure membrane performance by finding the water and salt permeability under different experimental conditions. To register the water flux through the membrane, the weight change in the draw solution is measured. By plotting the weight (m [g]) against time (t [h]), the slope of the curve can be used to calculate the water flux (J_w) through the membrane on a mass basis:

$$J_w = \frac{C_1}{E}$$

(2-14)

C_1 [g h^{-1}] is the slope constant of the curve and E [m^2] is the membrane area. The water permeability (P_w [mol m m^{-2} h^{-1}]) can be calculated from the water flux and the membrane thickness (s [m]).

$$P_w = J_w s$$

(2-15)

To find the reverse salt flux through the membrane, the conductivity of the feed water is measured. The relation between conductivity and concentration can be found by measuring

the conductivity of dilute salt solutions, at different concentrations. By plotting the concentration of these solutions against their conductivity and finding the equation of the curve, the concentration of salt in the feed water can be calculated. The volume of the feed water decreases as water permeates through the membrane. The current volume (V) can be calculated by

$$V = V_0 - \frac{m}{\rho}$$
(2-16)

where V_0 [L] is the start volume of feed water and ρ [g L^{-1}] is the density of water. The amount of salt (n_s [mol]) that has permeated through the membrane can be calculated from

$$n_s = (dq + e)V$$
(2-17)

where d [mol cm μS^{-1} L^{-1}] and e [mol L^{-1}] are the constants from the calibration curve for the given salt and q [μS cm^{-1}] is the measured conductivity. Calibration curves are presented in Appendix A. The slope constant (C_2 [mol h^{-1}]) of a plot of n versus t can be used to calculate the salt flux (J_s [mol m^{-2} h^{-1}]) through the membrane.

$$J_s = \frac{C_2}{E}$$
(2-18)

The salt permeability (P_s [g m m^{-2} h^{-1}]) can then be calculated from

$$P_s = J_s M_s s$$
(2-19)

where M_s [g mol^{-1}] is the molar mass of the given salt.

2.5 Theoretic osmotic pressure

The theoretic osmotic pressure of different salts has been simulated using the software OLI Analyzer from OLI systems Inc. A comparison of the osmotic pressures of these salts is shown in Figure 2-4. The simulation was done for concentrations from 0 to 6 M solutions except for $MgCl_2$ which reaches saturation at 5 M. The temperature was set to 23 °C. The software uses Equation (2-7) to calculate the osmotic pressure.
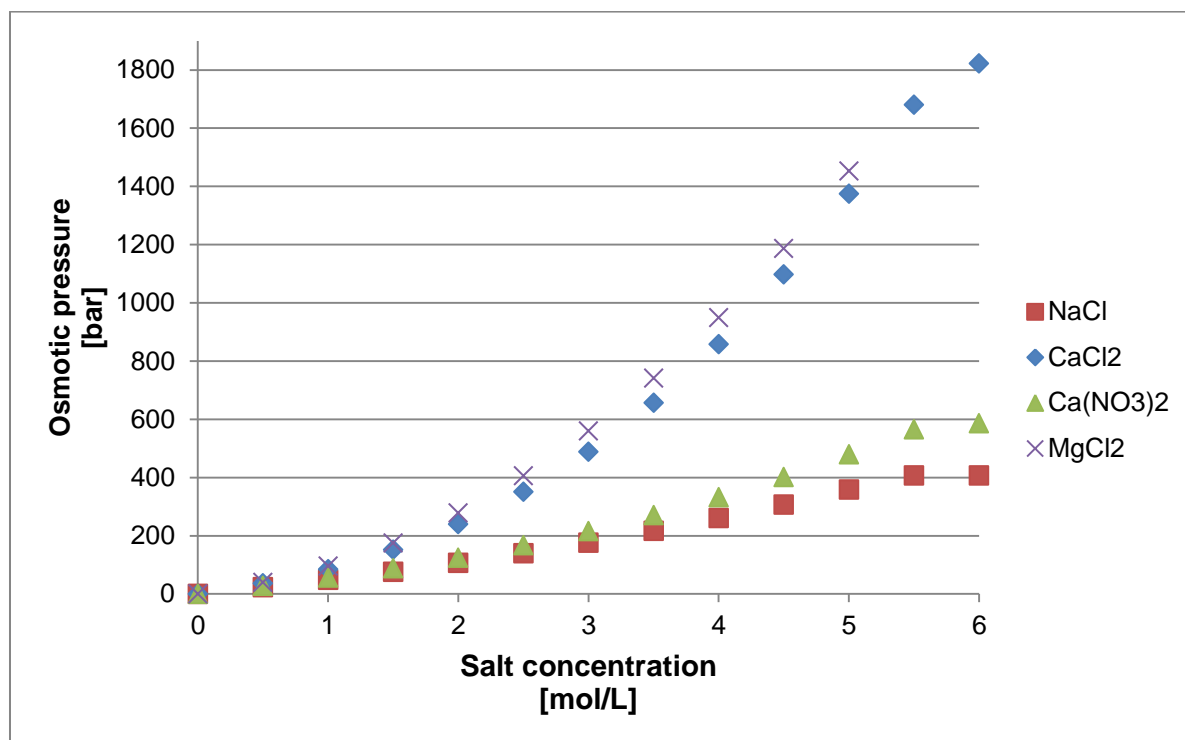

Figure 2-4: Theoretic osmotic pressure of NaCl, CaCl₂, Ca(NO₃)₂ and MgCl₂, versus salt concentration.

The osmotic pressure is the driving force behind the water transport through the membrane in the osmosis experiments. Hence the pressures indicated in Figure 2-4 should give a good indication of the relative permeability of water using different salts as draw solution. This was investigated in the previous student project. In this thesis the experiments are performed using only 5 M NaCl draw solution which has a relatively low osmotic pressure. The reason for this is its relatively low cost and corrosiveness compared to the other salts. A concentration of 5 M is used to make the dissolution of the salt easy. Higher concentrations will make dissolution of the salt more difficult as the concentration approaches the saturation point.

3 Materials and methods

3.1 Investigation of temperature effect in forward osmosis

3.1.1 Materials

The test rig used in the FO experiments is shown in Figure 3-1. The experiments were performed with 5 M NaCl draw solution. NaCl was purchased from Sigma-Aldrich.

The weight used in the experiments is the Mettler Toledo XA1502S, the conductivity meter was the Mettler Toledo SevenEasy, the pumps were Cole Parmer digital gear pumps and the membrane module was a flat sheet module for high pressure use. It was made in the workshop at NTNU.

PBI dope solution was purchased from PBI products Inc. All PBI membranes were prepared under identical conditions, but due to the problem of heating stability, the membranes likely had a slight thickness and separation performance variation. The membrane preparation method is not disclosed in this thesis.
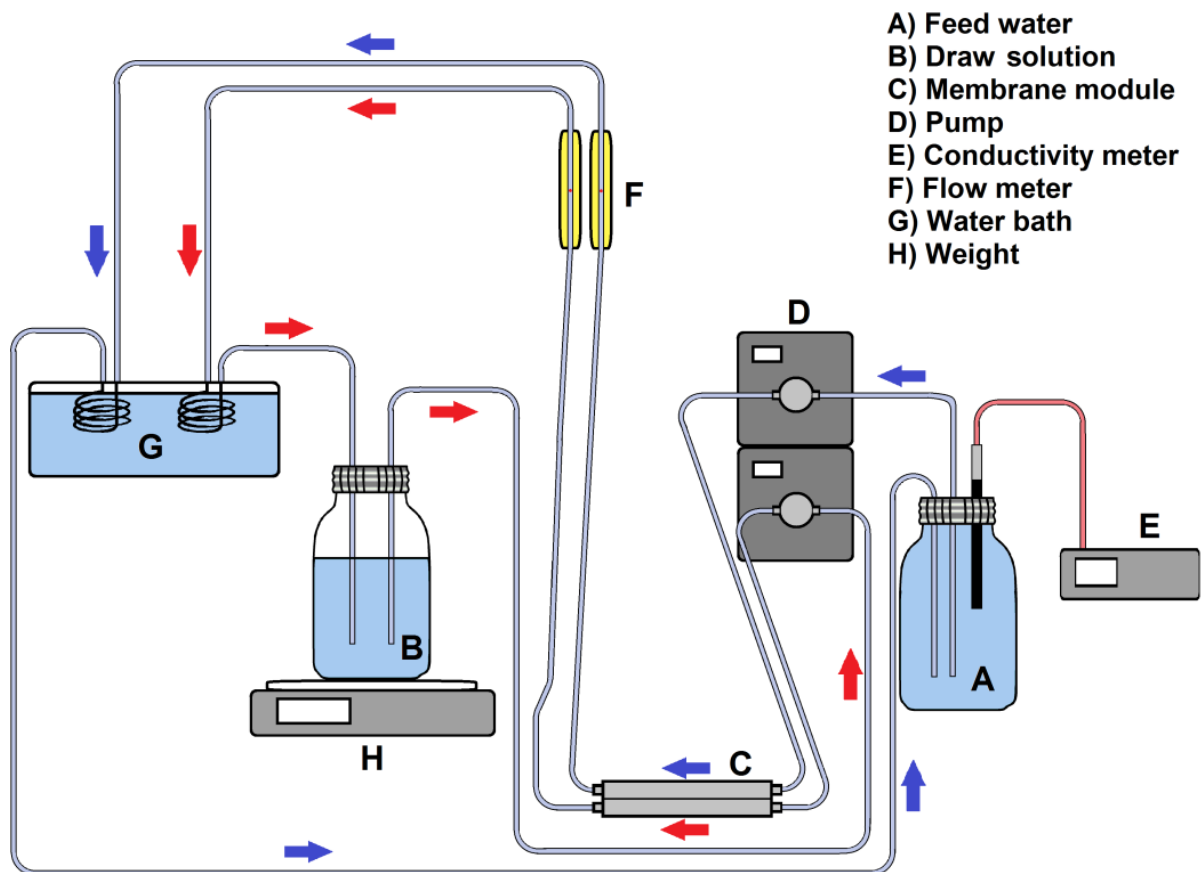

Figure 3-1: Illustration of the test rig used in FO experiments.

3.1.2 Method

The total volume of the tubing and flask of the feed water was pre-measured to be able to calculate concentration of solute in the feed. This is shown in Appendix F.

The membrane was pre-prepared. Before starting tests, the membrane was cut into shape with scissors. The thickness was measured with a micrometer. The membrane was fitted in the flat sheet membrane module before the module was connected to the rig. The water bath temperature was set to the desired temperature. Distilled water was filled in the feed flask and pumped around the circuit until all air bubbles were removed. The conductivity meter was inserted and the flask was filled to the mark where the volume was known. Draw solution was filled into the draw flask. When air bubbles were no longer present, the weight was zeroed. Logging was then started. For the entire duration of the experiments, the change in the weight of the draw solution flask was registered, as well as the conductivity of the feed. The tests were performed at atmospheric pressure and the flow rates for the draw and feed were 0,5 LPM on average. For each temperature one successful test was performed. The temperatures of the tests are listed in Table 3-1. The tests were performed in the order listed in the table. The same membrane was used during these tests and was not removed from the module between the tests. This membrane will be referred to as Membrane A from now on.

Table 3-1: Overview of the tests carried out using Membrane A.

Average temperature [°C]	23	42	62
Test duration [h]	24	21	10

When the three tests were completed dilute solutions of NaCl were prepared. The conductivities of these solutions were measured at the three experimental temperatures listed in Table 3-1. The calibration curves derived from these measurements are presented in Appendix A.

3.2 Evaluation of the membrane preparation method

3.2.1 Materials

The test rig used to evaluate the preparation method of the membranes is shown in Figure 3-1. The tests include the same materials described in chapter 3.1.1. The evaluation of the membrane preparation method is based on reference tests carried out using 4 different membranes. The membranes are referred to as Membrane B, C, D, and G.

3.2.2 Method

The method used is the same as the one described in chapter 3.1.2. They were carried out at room temperature however.

Table 3-2: Overview of the tests used to evaluate the reproducibility of the membrane preparation method.

Membrane	B	C	D	G
Test duration [h]	53	23	23	22

During the testing with Membrane B, C and D black particles could be observed in the feed. It was discovered that these particles were attracted to magnets. This is shown in Figure 3-2. During the HC testing with Membrane D described in chapter 3.3, the feed pump broke

down. When the pump head was disassembled it was discovered that the particles originated from a broken magnet inside the housing. The pump head was replaced and no more black particles were observed during the FO tests using Membrane F and G.
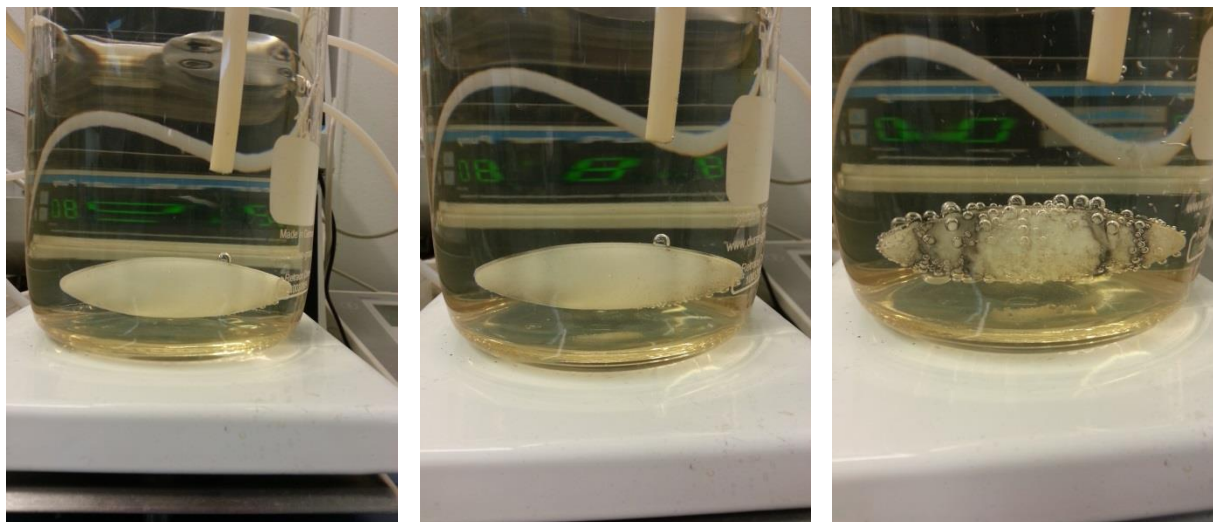

Figure 3-2: Images of the black particles being attracted to a magnet during the testing with Membrane C. The pictures are taken at the start of the experiment, after one hour, and at the end of the experiment respectively.

3.3 Investigation of the effect of hydrocarbons in forward osmosis

3.3.1 Materials

Figure 3-3 shows the test rig used in the FO experiments with hydrocarbons in the feed. The experiments were performed with 5 M NaCl draw solution at room temperature and atmospheric pressure. NaCl was purchased from Sigma-Aldrich. The tests were carried out with different water/hydrocarbon ratios. The hydrocarbon mix prepared consisted of hexane, heptane and octane. Pentane was not included in the mix due to its volatility. The ratios of the hydrocarbon mix are based on the ratios reported from the Åsgard gas condensate field and are shown in Table 3-3. The hydrocarbons were purchased from Merck KGaA.

Table 3-3: The ratio of hexane, heptane and octane in the hydrocarbon mix on a volume basis.

Hydrocarbon	Hexane	Heptane	Octane
Volumetric ratio	0,295	0,374	0,331

The equipment used for the experiments was the same as the equipment described in chapter 3.1.1 but also includes a magnetic stirrer, the IKA RTC basic. This is used to mix the hydrocarbons and water so that both phases enter the feed tube.

FO tests with hydrocarbons were performed with three different membranes. These membranes are referred to as Membrane D, F and G.
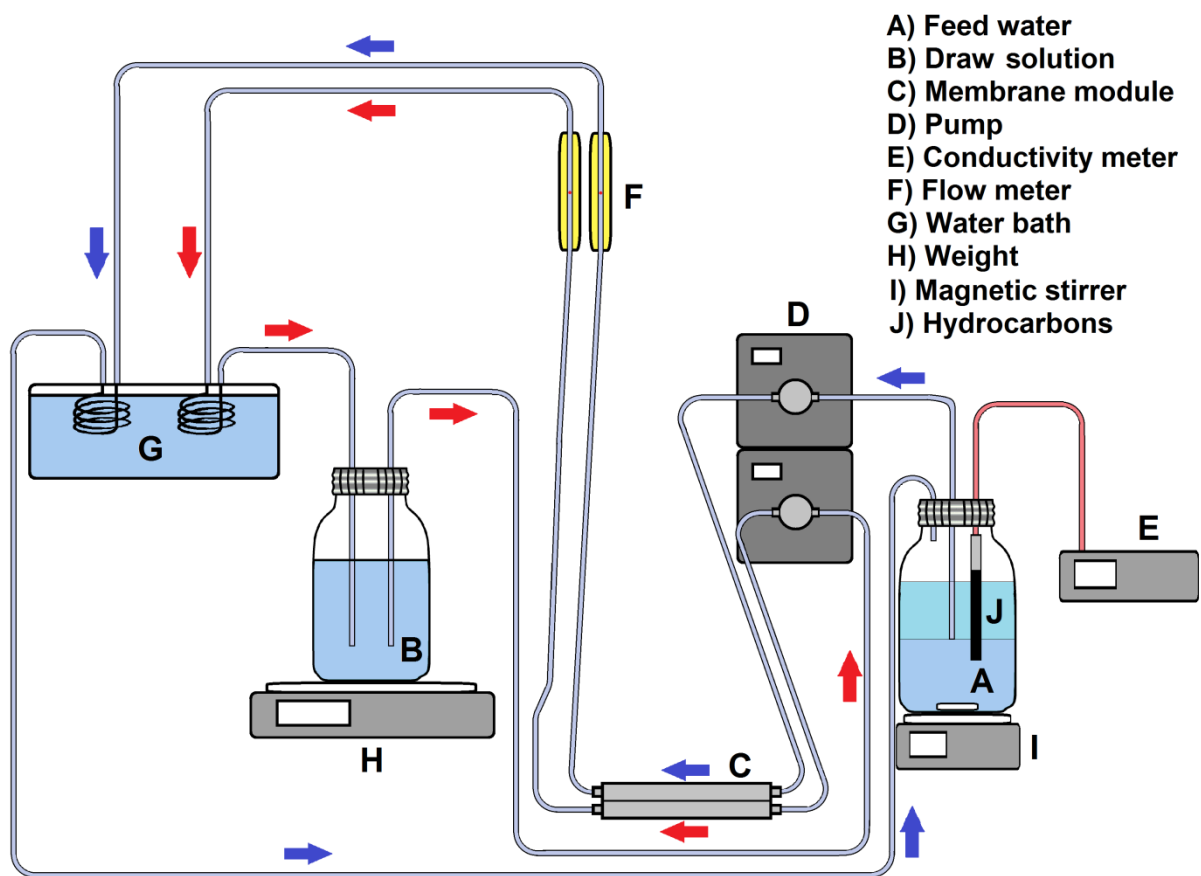
A) Feed water
B) Draw solution
C) Membrane module
D) Pump
E) Conductivity meter
F) Flow meter
G) Water bath
H) Weight
I) Magnetic stirrer
J) Hydrocarbons

Figure 3-3: Illustration of the test rig used in FO experiments with hydrocarbons in the feed water.

3.3.2 Method

Before each test the feed tube and membrane module was emptied of all liquid using compressed air to force the liquid out. It was not cleaned with any solvent, so traces of hydrocarbons from previous tests were likely present in the system. This was done to mimic how the conditions would be in an oil or gas well that has started to produce water. The experiments conducted to investigate the membrane performance with hydrocarbons present can be categorized into two categories: a) Reference tests, in which pure water was used in the feed. b) Tests with hydrocarbons added to the feed water. The method used for reference tests is the same as the method described in chapter 3.1.2. The method used for the tests that included hydrocarbons in the feed is described below.

The feed flask was placed on a weight and the wanted mass ratio of hydrocarbons and water was filled into the bottle. The feed bottle was then placed on the magnetic stirrer and connected to the test rig. To make the liquid enter the pump a Pasteur pipette was used to fill the tube so that the pump could effectively circulate the liquid. A magnet was then inserted into the feed flask and the stirrer turned on. Draw solution was filled into the draw flask. When air bubbles were no longer present, the weight was zeroed. Logging was then started. For the entire duration of the experiments, the change in the weight of the draw solution flask was registered.

The conductivity of the water phase was only measured at the start of the tests and at the end of the tests. Correct measurements of the conductivity were not possible during stirring of the two phases.

The flow rates for the draw and feed were kept at about 0,5 LPM for the reference tests. During the testing with hydrocarbons it was not possible to measure the flow rate of the feed since it was a two phase flow. The surface tension in the interphase between the phases led to increased drag on the flow meter indicator, thus indicating higher flow rates than the actual value. This is shown in Figure 3-4. Consequently the pump was kept at the same speed as for the reference tests.

Figure 3-4: Picture of the flow meter showing the two phase flow.

A presentation of the experiments carried out with Membrane D is shown in Table 3-4.

Table 3-4: Forward osmosis experiments carried out with Membrane D in chronological order.

Hydrocarbon ratio [%]	Duration [h]	Weight feed water [g]	Weight HC in feed [g]
0	23	1230	0
20	23	800	200
100	23	0	400
50	21	400	400
80	16	137,5	550

Table 3-5: Forward osmosis experiments carried out with Membrane F in chronological order.

Hydrocarbon ratio [%]	Duration [h]	Weight feed water [g]	Weight HC in feed [g]
0	23	1243	0
20	24	350	87,5
50	91	200	200

The FO experiments performed with Membrane F and G is shown in Table 3-5 and Table 3-6 respectively.

Table 3-6: Forward osmosis experiments carried out with Membrane G in chronological order.

Hydrocarbon ratio [%]	Duration [h]	Weight feed water [g]	Weight HC in feed [g]
0	22	1243	0
20	22	350	87,5
0	18	1243	0
50	23	200	200
0	22	1243	0
80	23	75	300
0	23	1243	0
80	41	75	300
0	58	1243	0
50	27	200	200
0	23	1243	0
20	33	350	87,5
0	35	1243	0

The experiments carried out with Membrane D and F were conducted with the membrane module in an angled position to improve the contact of water with the membrane. This is illustrated in Figure 3-5.
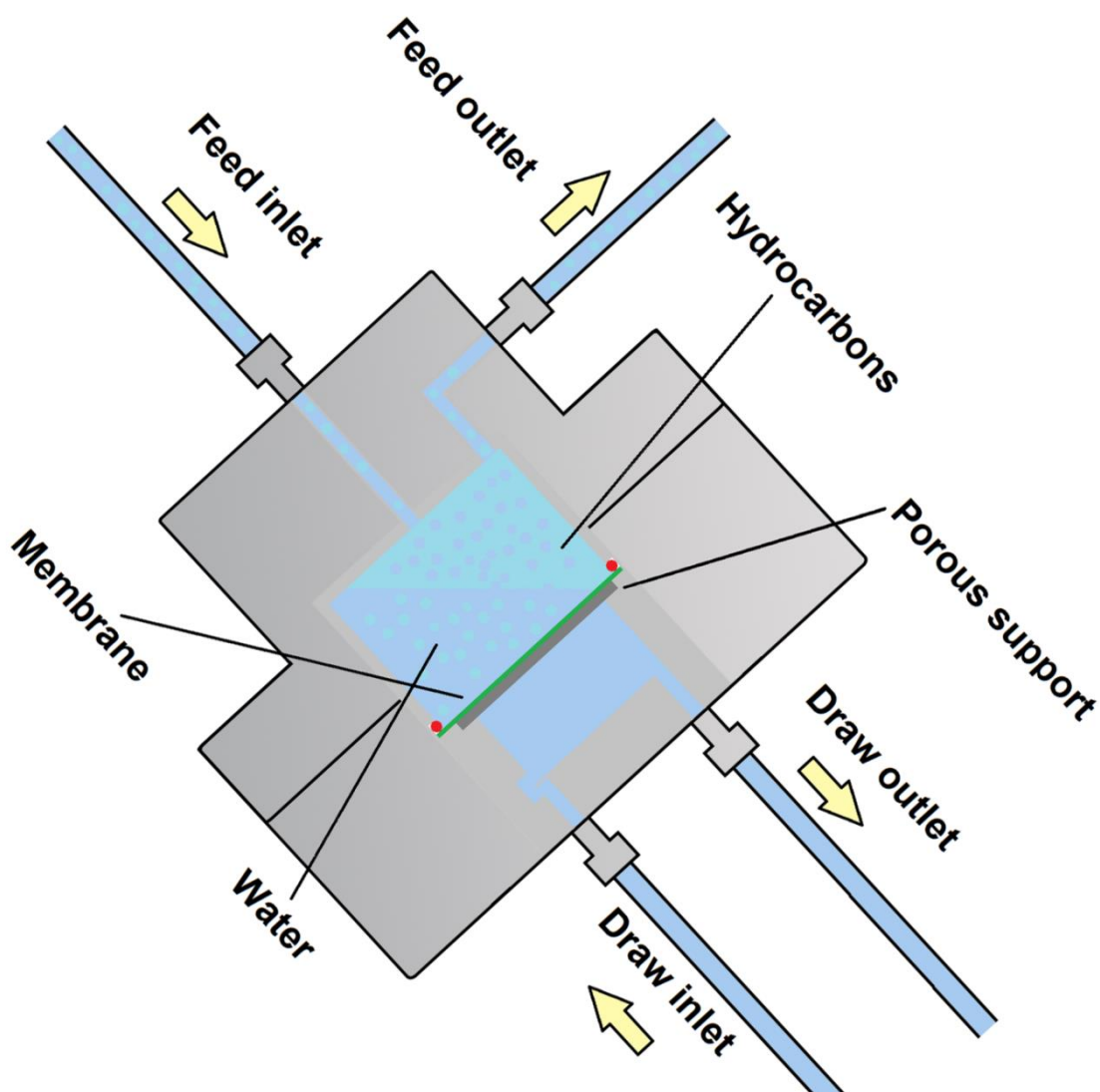
Figure 3-5: An illustration of the cross section of the membrane module during FO tests performed with Membrane D and F.

After reviewing the results of the test conducted with Membrane D and F a decision was made to position the module so that the membrane was in a vertical position for the tests using Membrane G. This is shown in Figure 3-6. The tube was also fixed into position using tape to make sure it did not move in the feed flask during experiments. During the tests using Membrane D and F the conductivity of the feed water was not registered. However for the tests using Membrane G the start and finish conductivities in the water phase was measured except for the first 80 % HC test.
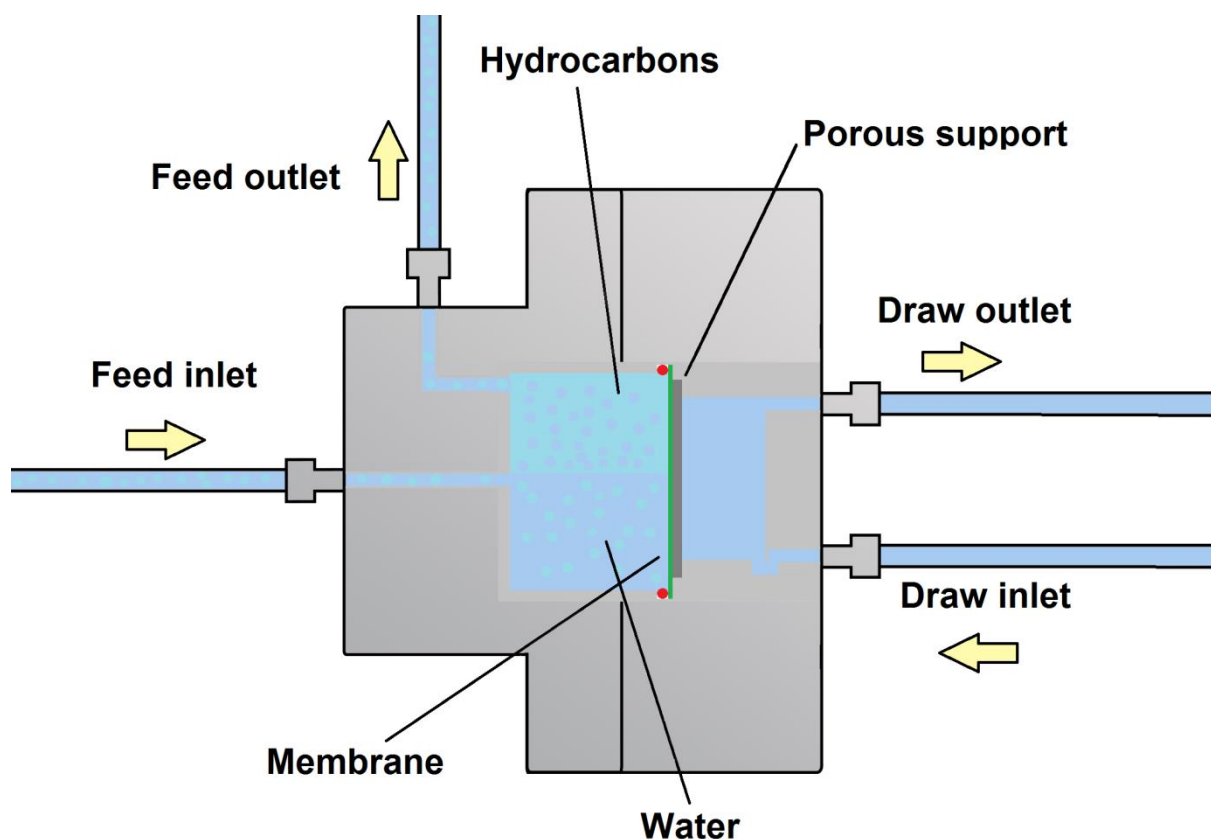
Figure 3-6: An illustration of the cross section of the membrane module during FO tests performed with Membrane G.

Membrane D and G had not been previously used when the test cycle with these membranes were started. Membrane F however had previously been used in PRO experiments as described in chapter 3.5. After completing the test with 50 % hydrocarbons the membrane started leaking. Thus it was not tested for 80 %.

3.4 Investigation of membrane performance in PRO

3.4.1 Materials

The PRO experiments were conducted using the setup shown in Figure 3-7. The experiment was performed with 5 M NaCl draw solution. NaCl was purchased from Sigma-Aldrich. The membrane used in the experiment had not previously been used and is referred to as Membrane E.

The weight used was a Sartorius AX6202, the conductivity meter was the Mettler Toledo SevenCompact. The pumps heads used were Cat Pumps model 2SF05SEEL with 0,75 kW motors made by Shin Myung Electric Mfg. The valves including the safety valve, tubes and pressure regulator was made by Swagelok. The flow meters were the Processmaster 300 electromagnetic flow meters from ABB. The pressure sensors were UniTrans Universal Pressure Transmitters from WIKA and the water bath was a VWB 18 from VWR. The membrane module was a flat sheet module for high pressure use. The same used in the FO experiments.
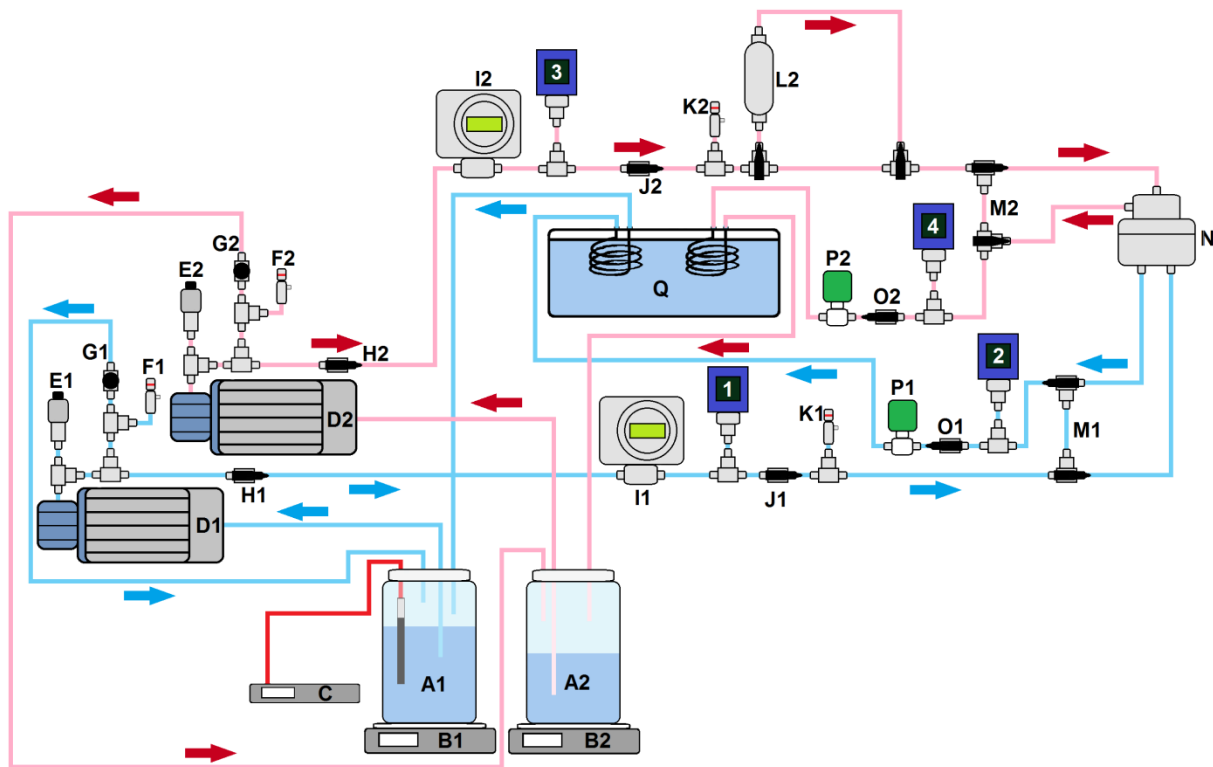
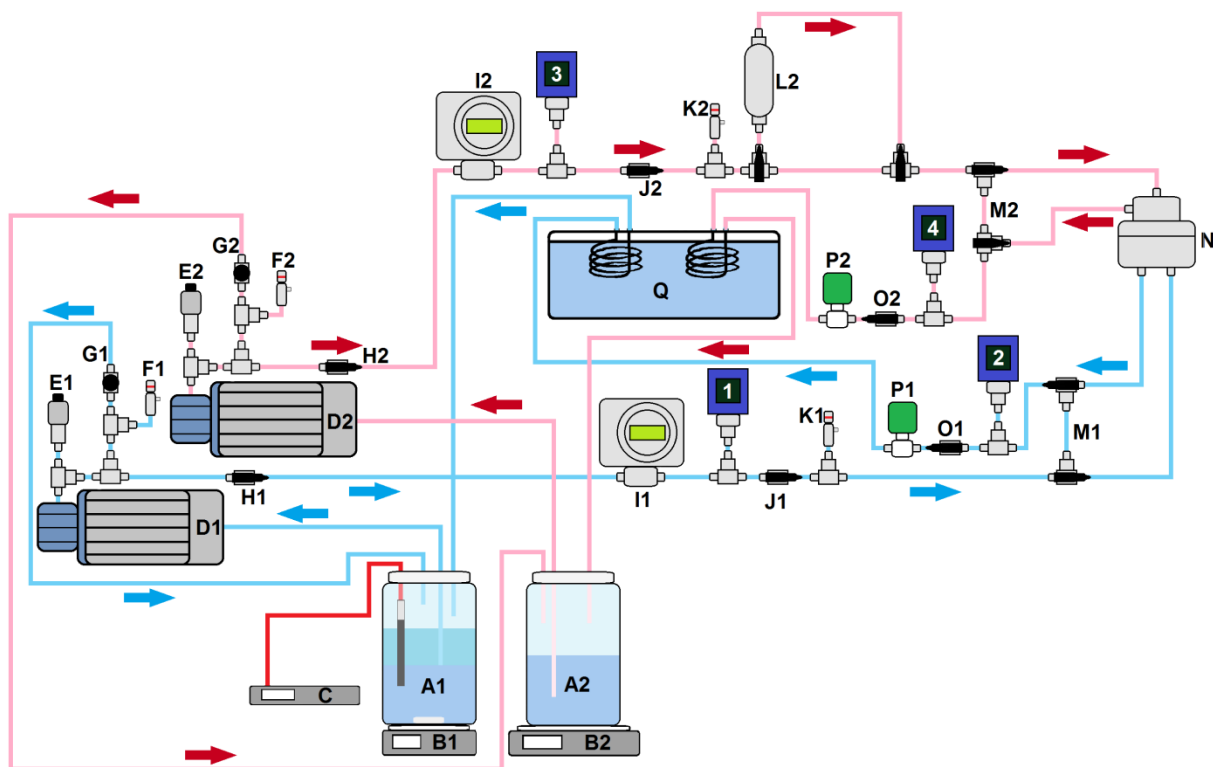**Figure 3-7: Illustration of the setup used for the PRO experiments. 1, 2, 3 and 4 indicate pressure and temperature sensors. A1: Feed water container, A2: Draw solution container, B: Weight, C: Conductivity meter, D: Pump, E: Vibration dampener, F: Safety release valve, G: Bypass valve, H: Ball valve, I: Flow meter, J: Check valve, K: Safety release valve, L: Dampener, M: Membrane module bypass, N: Membrane module, O: Ball valve, P: Pressure regulator, Q: Water Bath.**

3.4.2 Method

Before the experiment was performed the system was cleaned and tested using distilled water in both the feed and draw circuits.

Draw solution was filled in the draw solution container (A2) and distilled water was filled in the feed water container (A1). The pump (D2) was started and the bypass valve (G2) was opened and closed multiple times to remove air bubbles. The pump (D2) was left running for about 30 minutes. The bypass valve (G2) was closed before pressurizing the system to about 5 bar using the regulator (P2). The membrane was only supported on the bottom side due to the module's (N) design. This is shown in Figure 3-8. To avoid the membrane being pushed out of position by pressure from the bottom, an overpressure in the draw loop had to be maintained at all times. The pump (D1) could now be started. The bypass valve (G1) was used to remove air from the feed loop. The system was left running for a few hours to remove the remaining air. When the flow rate readouts on the flow meters (I1 and I2) had stabilized, the experiment was started.

The weight (B1) was zeroed and logging initiated. The experiment was left running for about 17 hours with a pressure difference of 8,0 bar on average between pressure indicator 4 and 2.

The regulator (P2) was used to adjust the pressure so that an average pressure difference of about 1,4 bar was maintained. The weight was zeroed and the experiment was left running another 31 hours.

The pressure was now adjusted to maintain an average pressure difference of 12,8 bar. The experiment was left running for 19 additional hours. At this point the membrane started leaking. The experiment was then stopped.

The leak was caused by the porous support plate which had been bent by the high pressure. The sharp edge of the plate was then bent upwards causing it to cut the membrane.

The average temperature in the system during the experiment was 32 °C. The indicated flow rates during the experiment can be seen in Figure 8-72 in Appendix D.
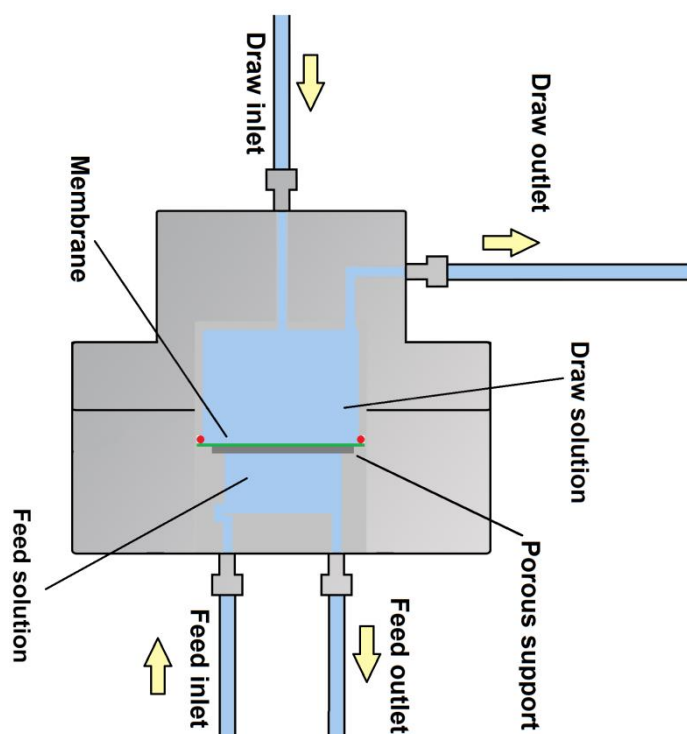
Figure 3-8: Illustration of the membrane orientation in PRO.

3.5 The effect of hydrocarbons on the generated pressure in PRO

3.5.1 Materials
The PRO experiments with hydrocarbons present in the feed water were conducted using the setup shown in Figure 3-9. The reference test was performed using the setup as shown in Figure 3-7. The experiments were performed with 5 M NaCl draw solution. NaCl was purchased from Sigma-Aldrich. The hydrocarbon mix used in the experiments is presented in Table 3-3. The membrane used in the experiments was new and replaced Membrane E upon its destruction. It is referred to as Membrane F, the same membrane later used in some of the FO experiments described in chapter 3.3. Before installing the new membrane the weakened porous support plate was replaced by a slightly thicker and stronger plate.

The equipment used was the same as in chapter 3.4.1 except for the addition of a magnetic stirrer, the IKA RH digital KT/C.

Figure 3-9: Illustration of the setup used for the PRO experiments with hydrocarbons in the feed. 1, 2, 3 and 4 indicate pressure and temperature sensors. A1: Feed container, A2: Draw solution container, B1: Magnetic stirrer, B2: Weight, C: Conductivity meter, D: Pump, E: Vibration dampener, F: Safety release valve, G: Bypass valve, H: Ball valve, I: Flow meter, J: Check valve, K: Safety release valve, L: Dampener, M: Membrane module bypass, N: Membrane module, O: Ball valve, P: Pressure regulator, Q: Water Bath.

3.5.2 Method

Before hydrocarbons where introduced a reference test was performed as follows.

Draw solution was filled in the draw solution container (A2) and distilled water was filled in the feed water container (A1). The pump (D2) was started and the bypass valve (G2) was opened and closed multiple times to remove air bubbles. The pump (D2) was left running for about 40 minutes. The bypass valve (G2) was closed before pressurizing the system to about 5 bar using the regulator (P2). The feed pump (D1) could now be started. The bypass valve (G1) was used to remove air from the feed loop. The system was left running for a few hours to remove the remaining air. When the flow rate readouts on the flow meters (I1 and I2) had stabilized the weight (B1) was zeroed and logging was started. The experiment was left running about 24 hours with an average pressure difference and temperature of 3,1 bar and 32 °C respectively. The system was cleaned with distilled water in both the feed and draw loop after the test.

The method for the main experiments where the rate of generated pressure was measured is described below.

The start of the experiments was conducted in the same manner as the reference test except that the amount of feed water and hydrocarbons added were measured on the weight to get the correct ratio. The feed container was also placed on a magnetic stirrer (B1) instead of the weight and a magnet was added to the container (A1). This is shown in Figure 3-9. When all air had been removed from the system by the methods described in the previous section, the

valves (J2, O2) were closed and the draw pump (D2) was switched off. All three actions were performed simultaneously. Logging was now started. The initial pressure difference between sensor 4 and 2 was noted. The readout on sensor 4 gradually increased. When it reached almost 30 bar the logging was stopped and the pressure released by opening the valves (J2, O2). The feed pump (D1) was then stopped. An overview of the hydrocarbon ratios tested is shown in Table 3-7.

The last 80 % HC test was performed after a 20 hour pause where the system was left with the pumps off. As can be seen in the table, the duration of the second 80 % HC test is much longer due to a slower pressure generation rate. The pressure was unable to reach 30 bar due to a small leak in the system, which after a certain time had reached a higher rate than the osmotic pressure generation rate. This caused the pressure difference to drop below the initial value.

A final test to measure the leak rate was performed using pure HC in the feed.

Table 3-7: Experiments carried out to measure the rate of generated osmotic pressure

Hydrocarbon ratio [%]	Duration [min]	Weight feed water [g]	Weight HC in feed [g]	Initial pressure difference [bar]
0	30	697	0	4,7
20	36	697	174	6,7
50	27	697	697	5,6
50	41	697	697	7,4
80	32	321	1283	7,1
80	1120	321	1283	7,0
100	60	0	1283	13,0

The indicated flow rates during the experiments can be found in Appendix D.b. For the tests using hydrocarbons in the system the indicated flow rates are not correct as the flow was a two phase flow. The pump speed was however kept constant for all the tests.

3.6 Characterization

3.6.1 Investigation of the effect of hydrocarbons on the membrane thickness
Membrane F was used for this experiment. The membrane was immersed in water. After one week it was taken out and the thickness of the membrane was measured with a micrometer. The membrane was then immersed in pure hydrocarbon for one week. The thickness was again measured. The membrane was finally immersed in 50 % water and 50 % hydrocarbons for a week before a final thickness measurement was conducted.

3.6.2 Thermogravimetric analysis
A dry membrane sample was put in an oven and dried for about 20 hours. The sample was cut in to small pieces to fit the sample pan of the TGA. The sample was heated to 120 °C and kept there for 30 minutes to remove any remaining moisture in the sample. The temperature was then gradually increased to 570 °C. The weight of the sample was monitored and logged during the course of the experiment. When the experiment was finished the sample was examined. The sample had darkened by the high temperature as can be seen in Figure 3-10.

The TGA used in the experiment was the Q500 from TA Instruments.
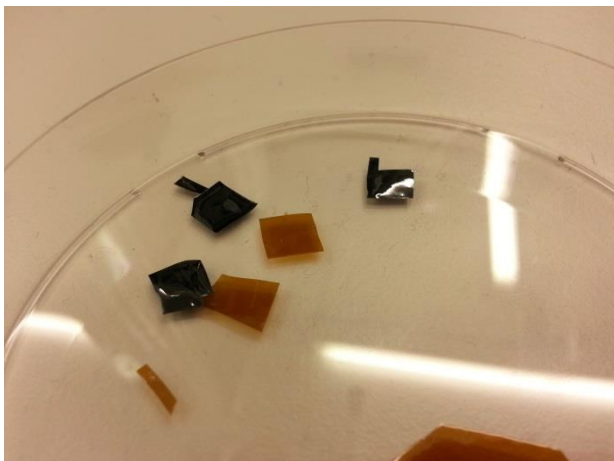
Figure 3-10: Color comparison of the TGA sample after the experiment and a fresh sample.

3.6.3 Contact angle measurements

Attempts were made to measure the contact angle of water on the membrane surface using the Theta optical tensiometer from Attension. However it proved impossible to get good measurements due to the twisting and swelling of the membrane when in contact with water. The hydrophilic properties of the membrane were however clearly demonstrated, as the membrane would start to lift from the surface when the water drop was hanging above it.

3.6.4 SEM morphology investigation

The samples were cleaned in 75 % ethanol and put in an oven to dry for about 24 hours. The sample for cross section investigation was frozen in liquid nitrogen and split, to get a clean cross section cut. It was then coated with carbon in a carbon coater to reduce charging. The sample was photographed with the voltage set to 10 kV and the current to 1 µA.

The sample for surface investigation was coated with gold in a sputter coater to reduce charging. This sample was photographed with the voltage set to 15 kV and current to 5 µA, and again with the voltage set to 20 kV and current to 7 µA.

The microscope used for investigation is a Hitachi S-5500 SEM.

4 Results

4.1 Membrane thickness and area measurements

The measured membrane thickness and area for all membranes are shown in Table 4-1. The data for the measurements can be found in Appendix E.

Table 4-1: Measurements of the membranes used in the experiments.

Membrane	Membrane thickness [μm]	Membrane area [cm^2]
A	-	27,9
B	45,1	27,9
C	43,8	27,9
D	43,5	27,9
E	69,3	27,9
F	45,9	27,9
G	49,7	27,9

4.2 Investigation of temperature effect in forward osmosis

The results for the FO experiments using 5 M NaCl as draw solution are shown in Table 4-2. Plots of the water and salt flux are shown in Figure 4-1 and Figure 4-2 respectively. Raw data and calculation examples can be found in Appendix B.

Table 4-2: Results of the FO test at different temperatures with 5 M NaCl draw solution.

Temperature [°C]	Water flux [g m^{-2} h^{-1}]	Salt flux [mg m^{-2} h^{-1}]
23	284	176
42	455	256
62	570	384
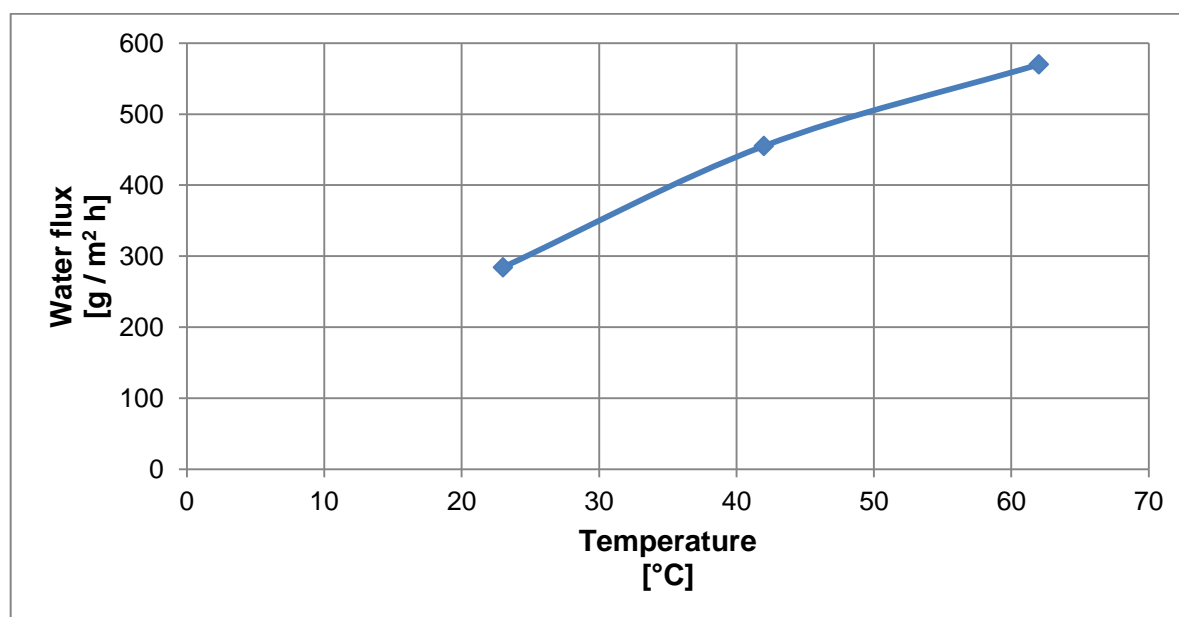
Figure 4-1: Water flux as a function of temperature.
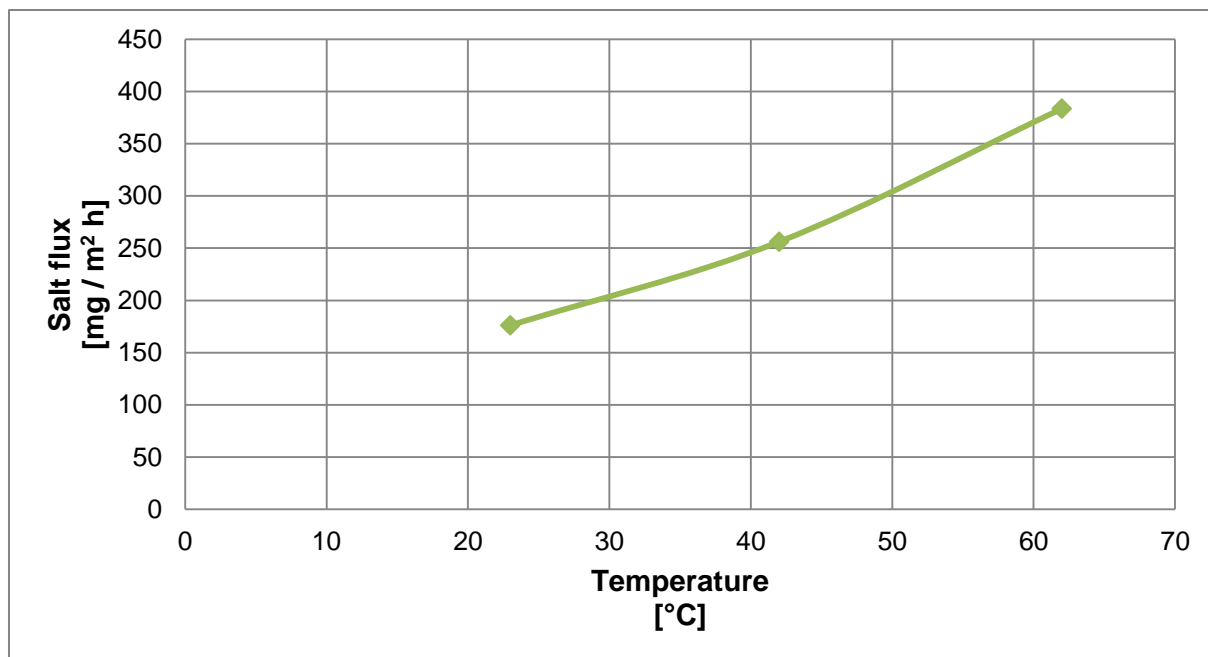
Figure 4-2: Salt flux as a function temperature.

4.3 Evaluation of the membrane preparation method

Table 4-3 shows the results for the first FO experiment carried out with each membrane. A comparison of the water and salt fluxes of the virgin membranes are respectively shown in Figure 4-3 and Figure 4-4. Raw data and calculation examples can be found in Appendix C.

Table 4-3: Results of the FO reference tests carried out with Membrane B, C, D and G.

Membrane	Thickness [μm]	Water flux [g m^{-2} h^{-1}]	Water permeability [g mm m^{-2} h^{-1}]	Salt permeability [mg mm m^{-2} h^{-1}]
B	45,1	470	21,2	46,1
C	43,7	537	23,5	53,9
D	43,5	593	25,8	32,7
G	49,7	551	27,4	38,9
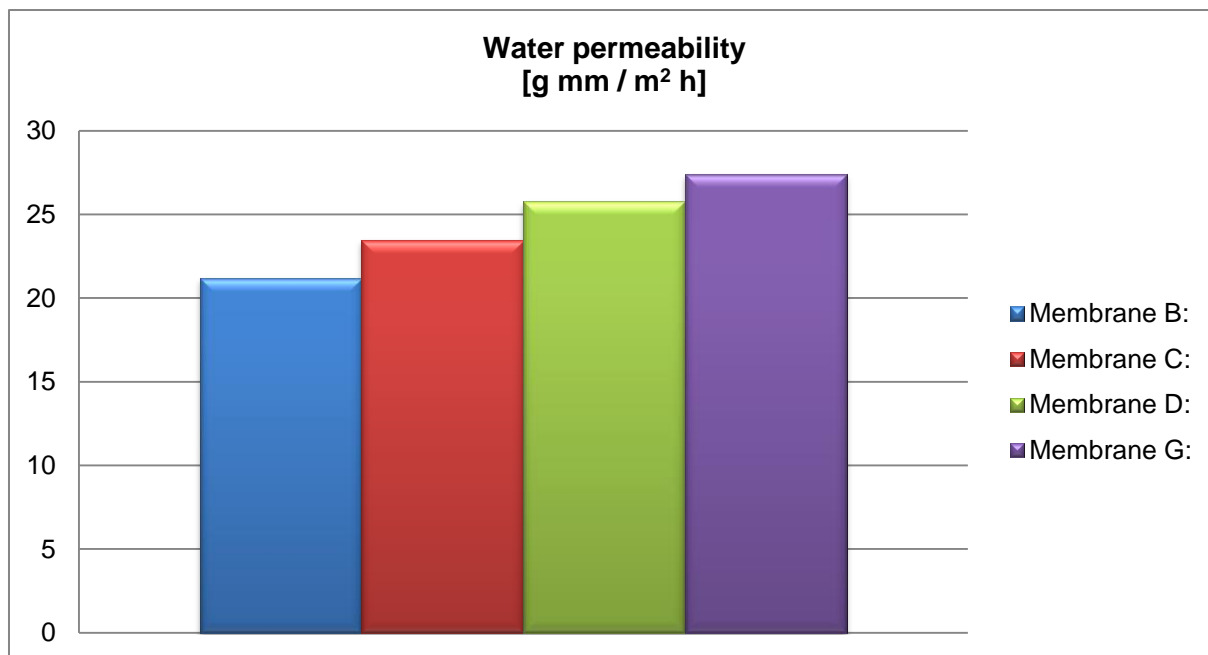
Figure 4-3: A comparison of the water permeability of the Membrane B, C, D and G.
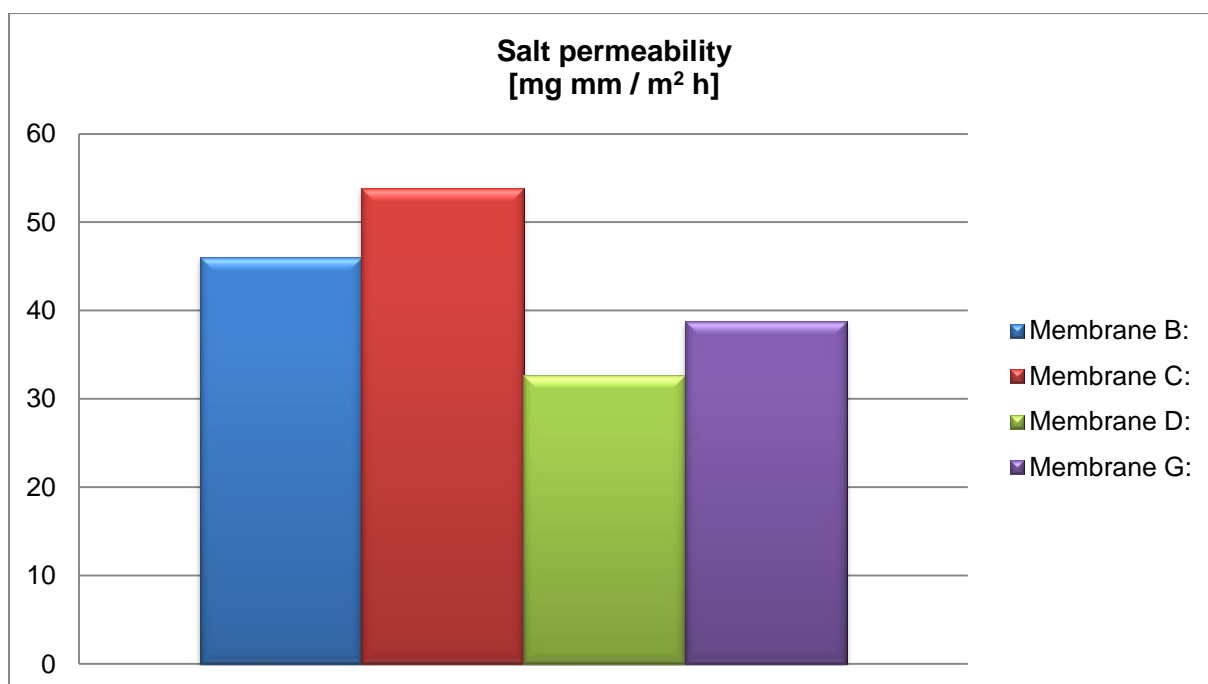
Figure 4-4: A comparison of the salt permeability of the Membrane B, C, D and G.

4.4 Investigation of the effect of hydrocarbons in forward osmosis

The results for the experiments carried out with hydrocarbons using Membrane D is presented in Table 4-4. An illustration of the water permeability versus the hydrocarbon ratio is shown in Figure 4-5. Raw data and calculation examples can be found in Appendix C.

Table 4-4: Results of the FO experiments carried out with Membrane D.

Hydrocarbon ratio [%]	Water flux [g m^{-2} h^{-1}]	Water permeability [g mm m^{-2} h^{-1}]
0	592	25,8
20	406	17,7
100	0	0
50	587	25,5
80	610	26,5
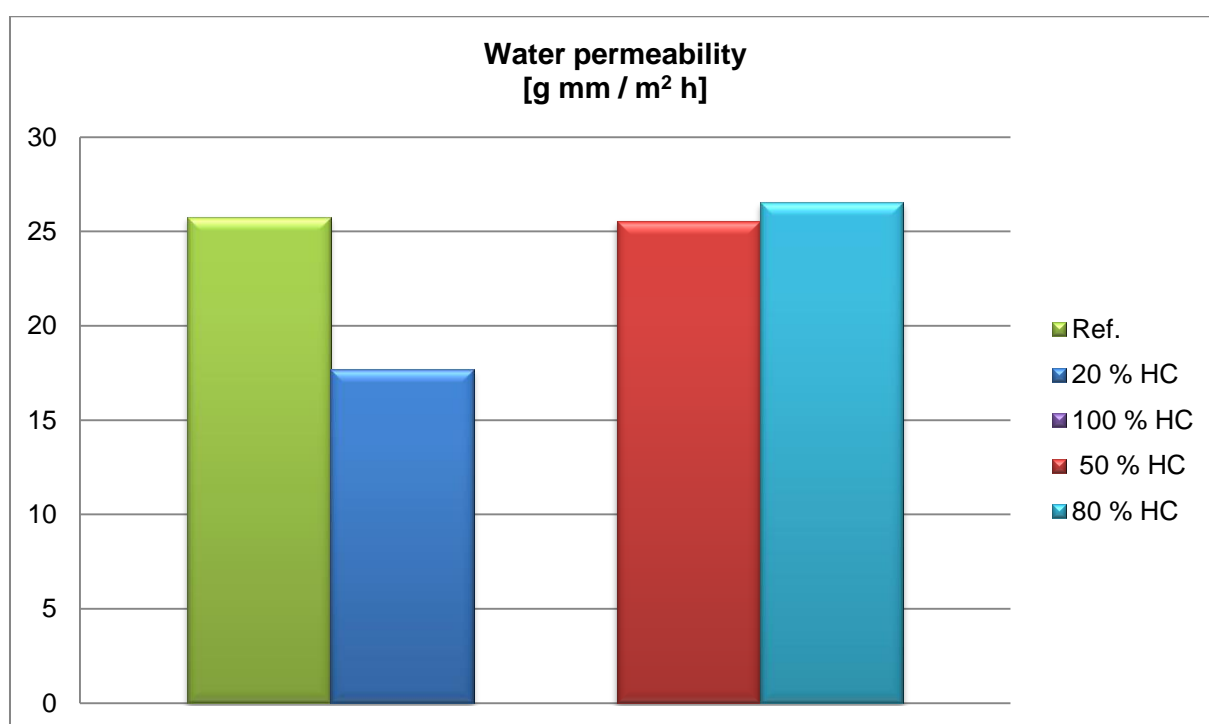
Figure 4-5: A visualization of the water permeability results for Membrane D in chronological order.

The results for the FO experiments using Membrane F is shown in Table 4-5.

Table 4-5: Results of the FO experiments carried out with Membrane F.

Hydrocarbon ratio [%]	Water flux [g m^{-2} h^{-1}]	Water permeability [g mm m^{-2} h^{-1}]
0	268	12,3
20	312	14,3
50	59,5	2,73

In Figure 4-6 an illustration of the water permeability for each tested hydrocarbon ratio is presented.
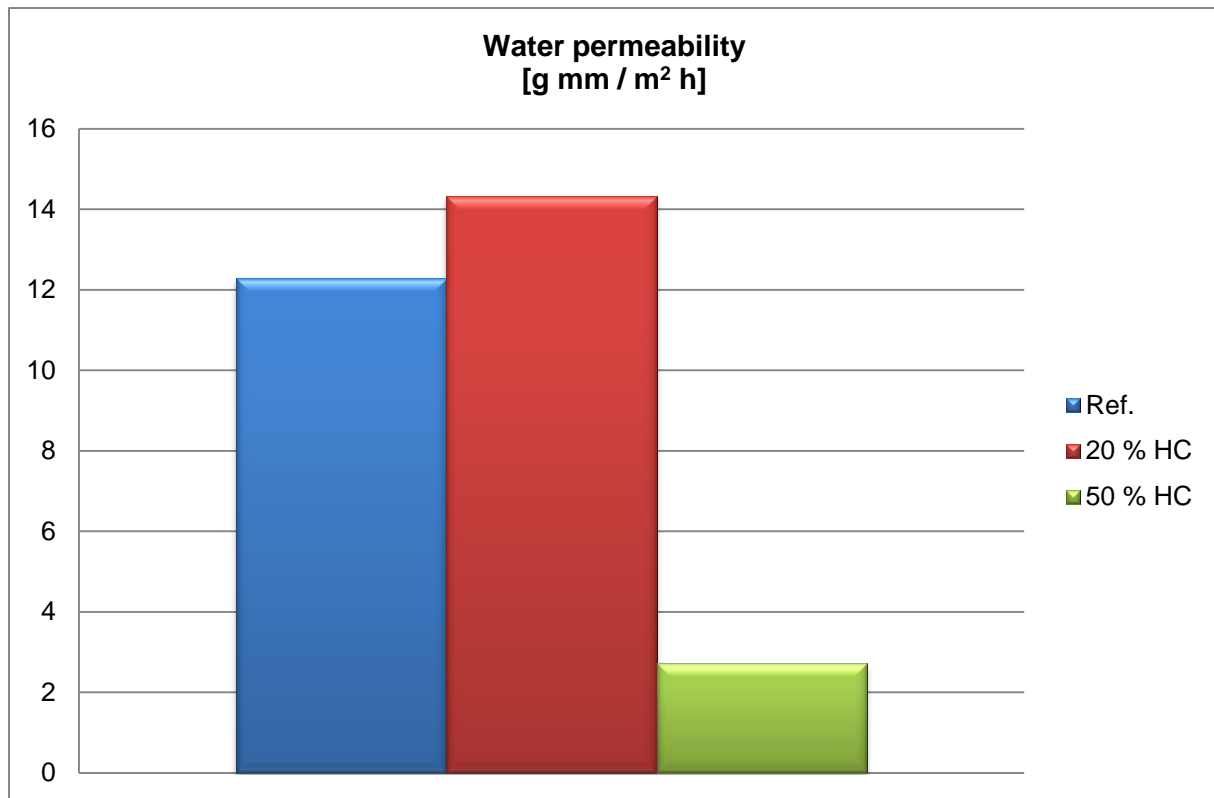
Figure 4-6: A visualization of the water permeability results for Membrane F in chronological order.

The results for the experiments using Membrane G is shown in Table 4-6.

Table 4-6: Results of the FO experiments carried out with Membrane G.

Hydrocarbon ratio [%]	Water flux [g m^{-2} h^{-1}]	Water permeability [g mm m^{-2} h^{-1}]	Salt permeability [mg mm m^{-2} h^{-1}]
0	551	27,4	38,9
20	150	7,44	14,2
0	360	17,9	14,7
50	133	6,60	22,1
0	406	20,2	17,1
80	122	6,05	-
0	384	19,1	14,6
80	77,4	3,85	4,71
0	323	16,1	13,1
50	133	6,63	7,92
0	306	15,2	12,8
20	92,5	4,60	6,73
0	301	15,0	13,0

Figure 4-7 and Figure 4-8. is a graphic visualization of the water and salt permeability results respectively for Membrane G.
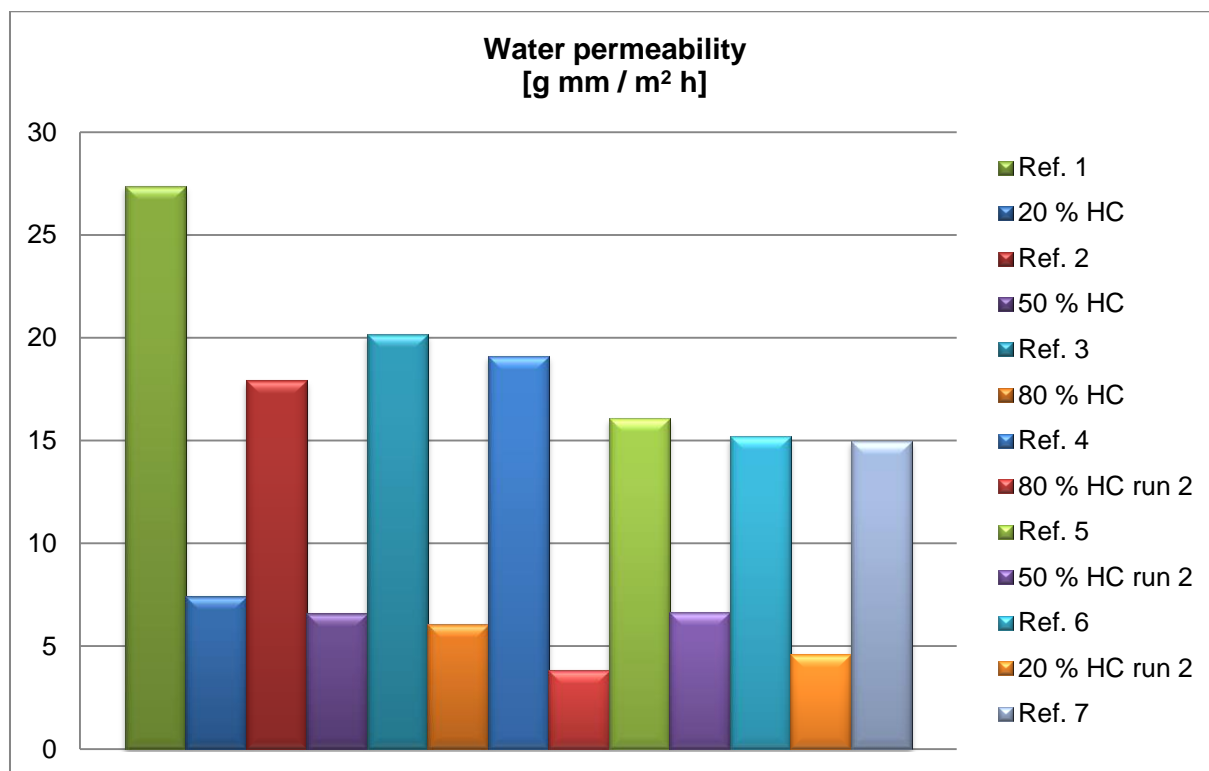
Figure 4-7: A visualization of the water permeability results for Membrane G in chronological order.
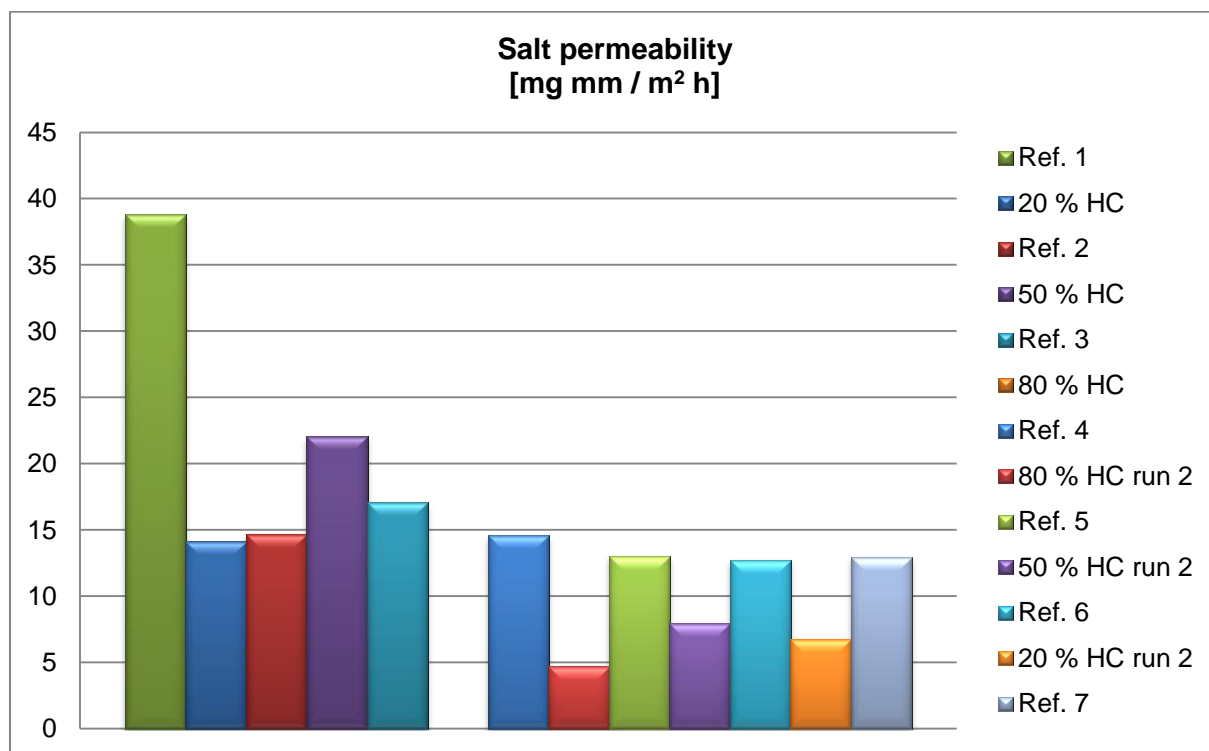
Figure 4-8: A visualization of the salt permeability results for Membrane G in chronological order.

4.5 Investigation of membrane performance in PRO

In Table 4-7 the results for the PRO experiment is shown. In Figure 4-9 the results for the flow rate is plotted versus the pressure difference. Raw data can be found in Appendix D.

Table 4-7: The results of the PRO experiment.

Pressure difference [bar]	Water flux [g m^{-2} h^{-1}]
1,4	744
8,0	874
12,8	480
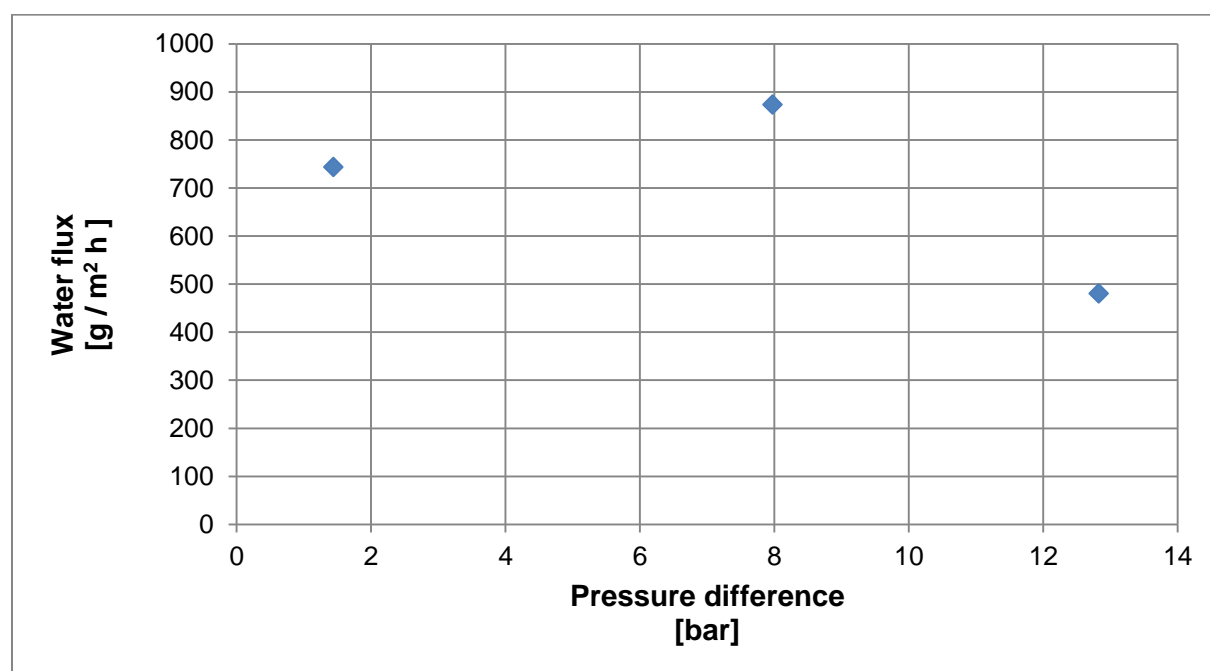
Figure 4-9: The results for the flow rate plotted versus the pressure difference.

4.6 The effect of hydrocarbons on the generated pressure in PRO

The result of the reference test is presented in Table 4-8. The result for the pressure generation tests is presented in Table 4-9. The continuously measured draw side pressures minus the average pressures on the feed side are presented in Figure 4-10, Figure 4-11, Figure 4-13, and Figure 4-14. In the second test with 80 % HC and the test with 100 % HC the pressure did not increase. Raw data can be found in Appendix D.

Table 4-8: The result of the PRO reference test.

Pressure difference [bar]	Water flux [g m^{-2} h^{-1}]
3,1	1098

Table 4-9: The results presented as average pressure increase rate between 8 and 23 bar.

HC ratio [%]	Time 8-23 bar [minutes]	Average rate 8-23 bar [bar min^{-1}]
0	14,6	1,03
20	24,2	0,62
50	18,0	0,83
50	21,4	0,70
80	22,6	0,66
80	-	-
100	-	-
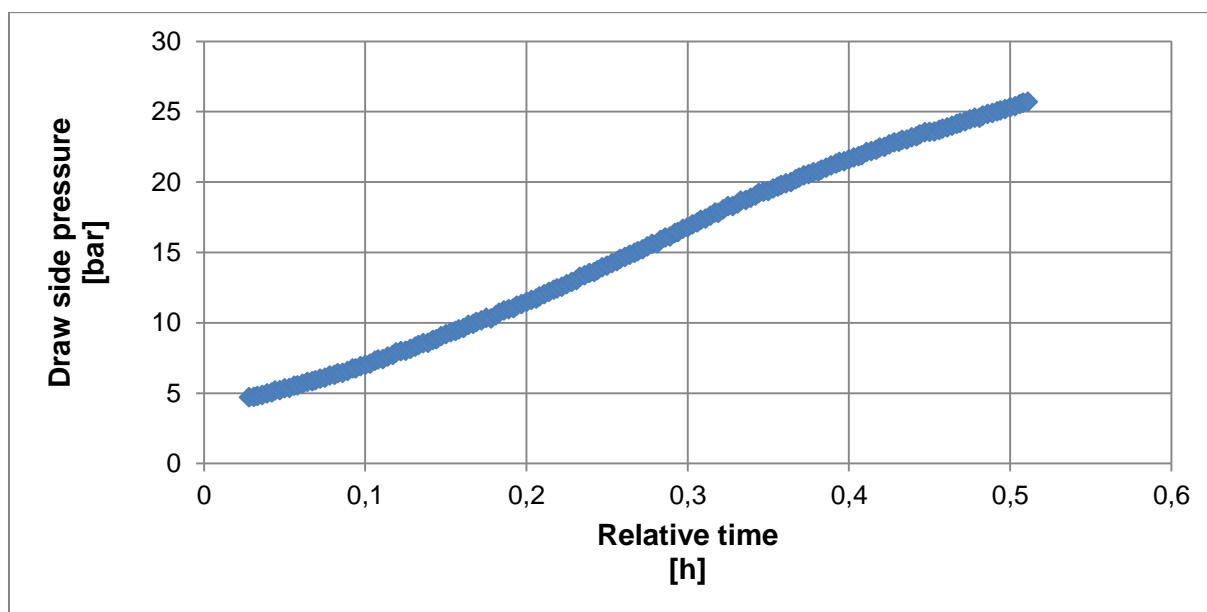
Figure 4-10: The measured pressure of the feed minus the average pressure in the draw when 0 % HC in the feed.
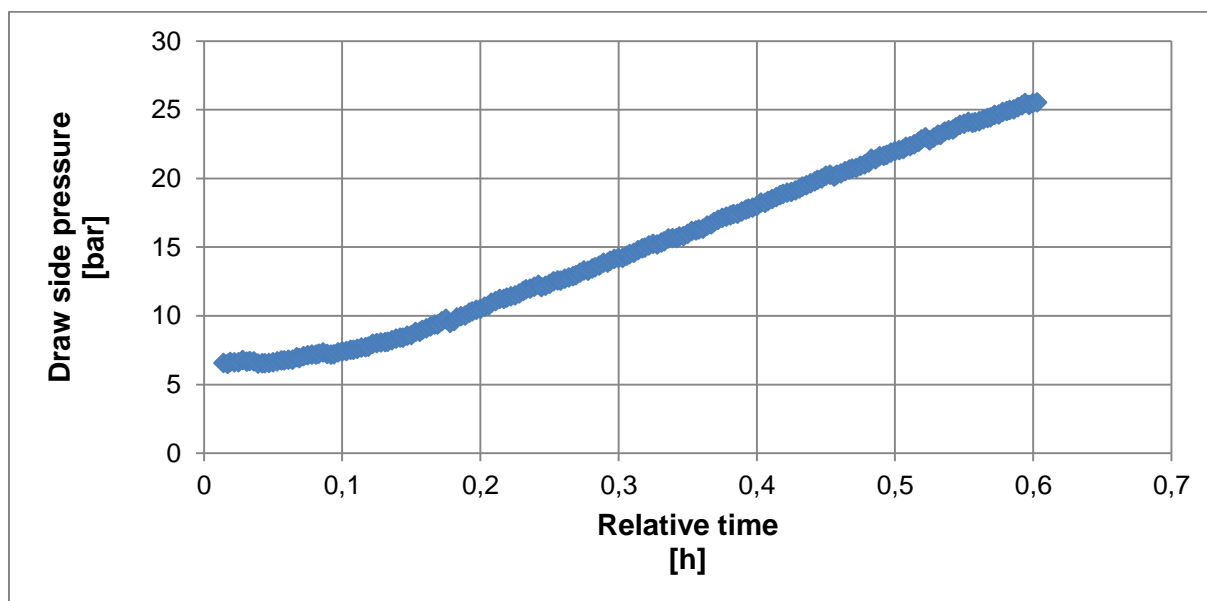
Figure 4-11: The measured pressure of the feed minus the average pressure in the draw when 20 % HC in the feed.
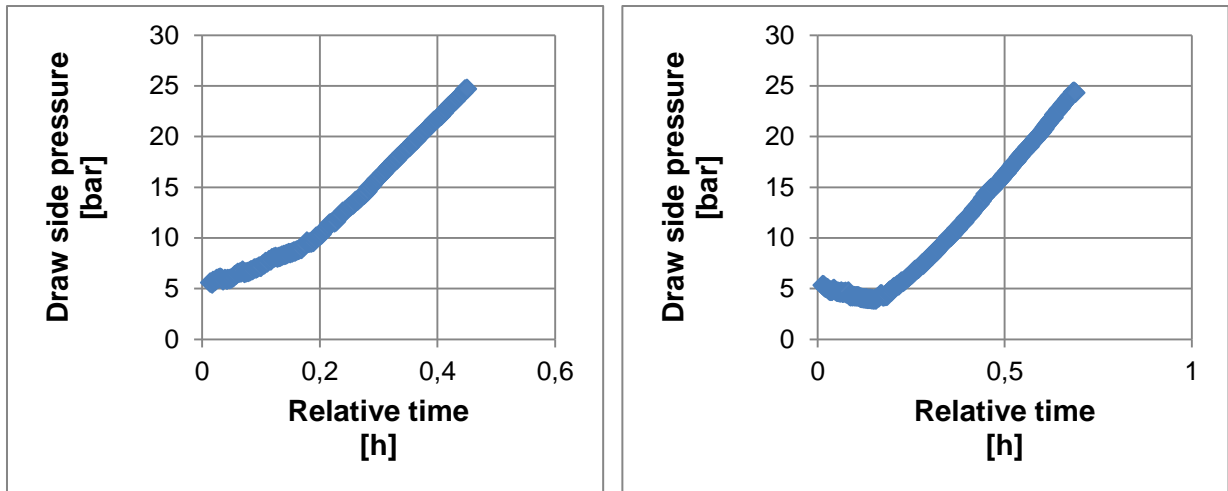
Figure 4-12: The measured pressure of the feed minus the average pressure in the draw when 50 % HC in the feed. First test left second test right.
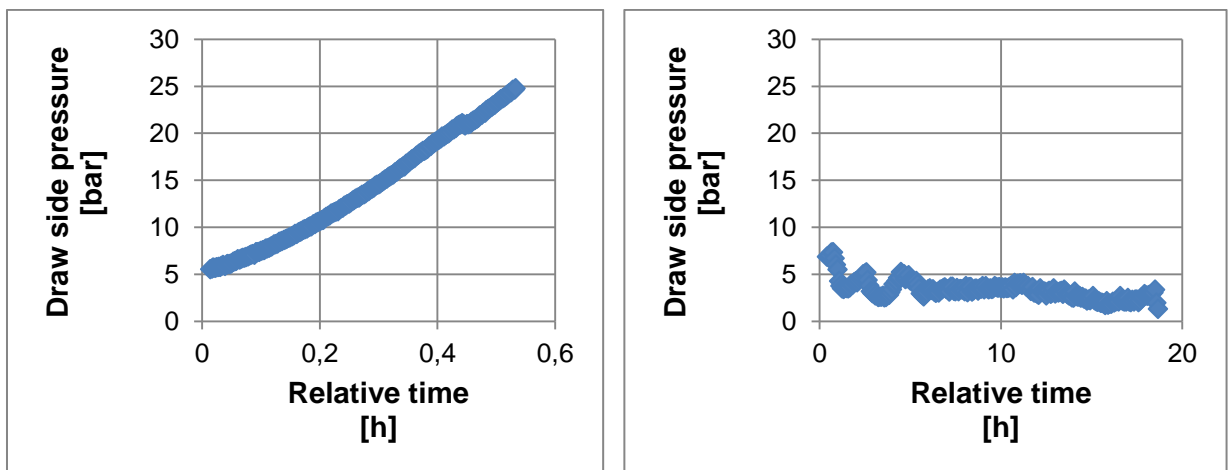
Figure 4-13: The measured pressure of the feed minus the average pressure in the draw when 80 % HC in the feed. First test left second test right.
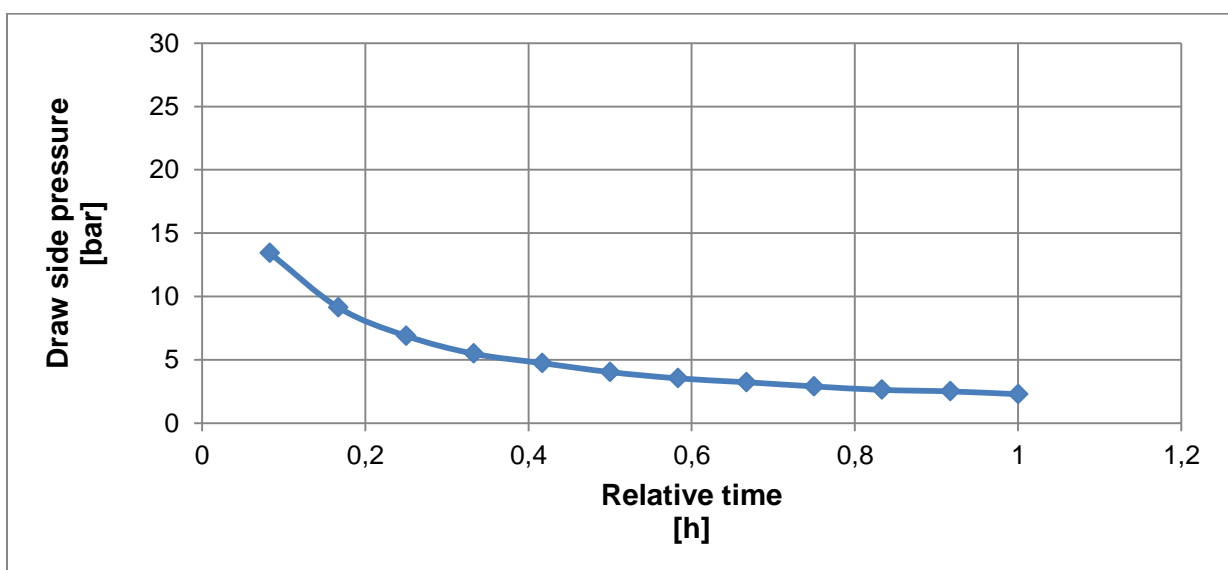
Figure 4-14: The measured pressure of the feed minus the average pressure in the draw when 100 % HC in the feed.

4.7 Characterization

4.7.1 Investigation of the effect of hydrocarbons on the membrane thickness

The results of the thickness measurements of the membrane are shown in Table 4-10.The data for the measurements can be found in Appendix E.

Table 4-10: Average thickness measurements of Membrane F.

	New	1 week in water	1 week in HC	1 week in water + HC
Thickness [µm]	46	53	55	59

4.7.2 Thermogravimetric analysis

In Figure 4-15 sample weight is plotted versus the temperature. Figure 4-16 shows the rate of weight change of the sample versus the temperature during the experiment.
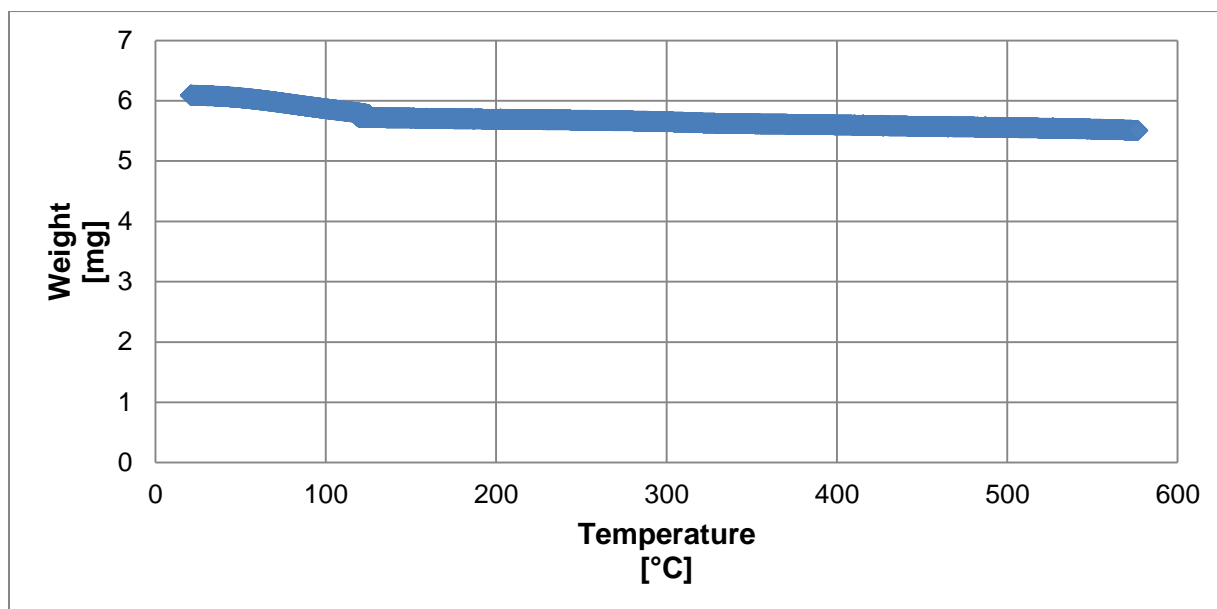
Figure 4-15: The measured weight of the sample plotted versus temperature.
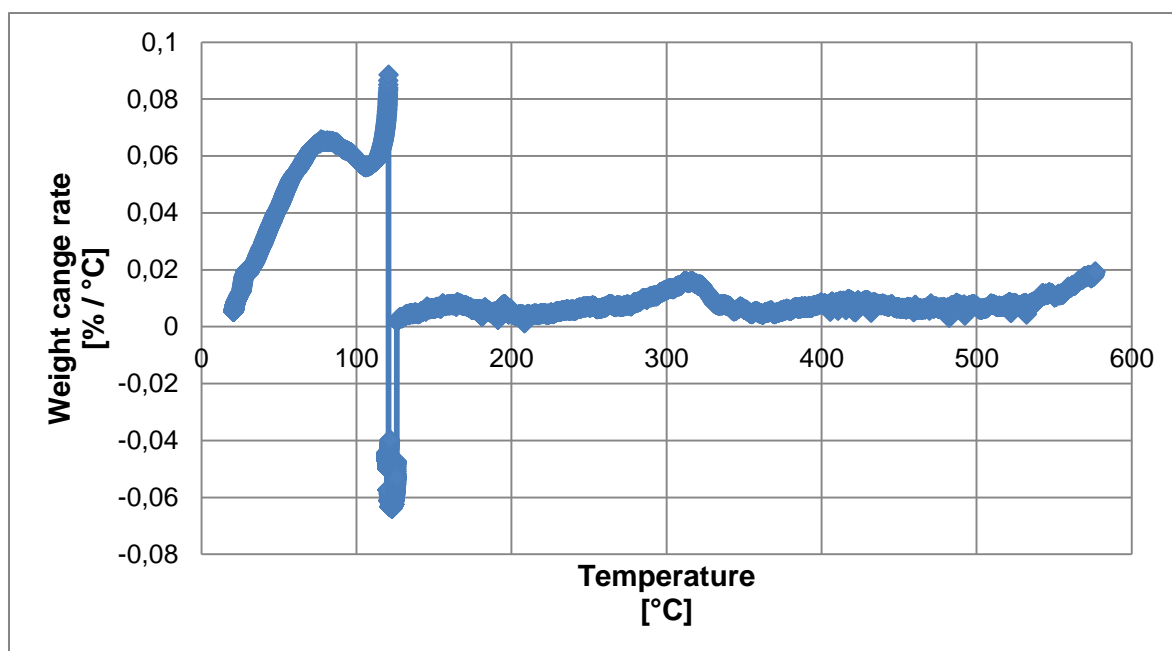
Figure 4-16: The rate of weight change of the sample plotted versus temperature.

4.7.3 Contact angle measurements

The measurement of the contact angle between water and the membrane was not successful, due to the swelling and twisting of the membrane. In Figure 4-17 the swelling of the membrane can be seen.

Figure 4-17: Water drop on membrane surface 1, 7, 11 and 30 seconds after drop impact. It can be seen how the membrane rises above the baseline. Pictures are placed side by side for easier comparison.

4.7.4 SEM micrograph of the membrane
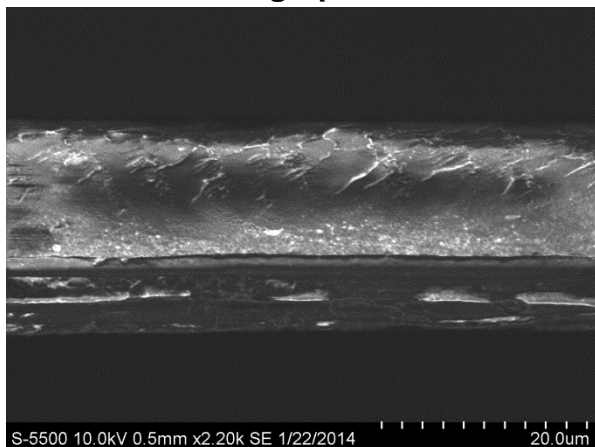
Figure 4-18: SEM micrograph of the cross section of the membrane.
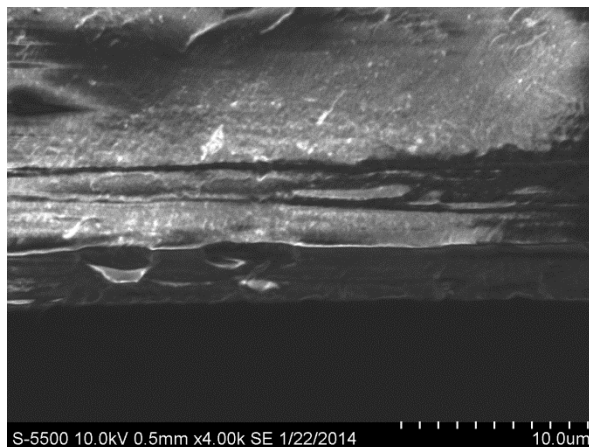
Figure 4-19: SEM micrograph of the lower part cross section of the membrane.

Figure 4-18, Figure 4-19 and Figure 4-20 show the cross section of the membrane. Figure 4-21 and Figure 4-22 show the membrane surface.
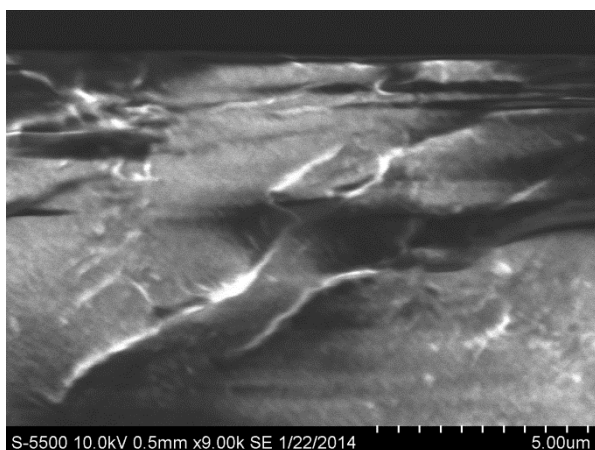
Figure 4-20: SEM micrograph of the upper part cross section of the membrane.
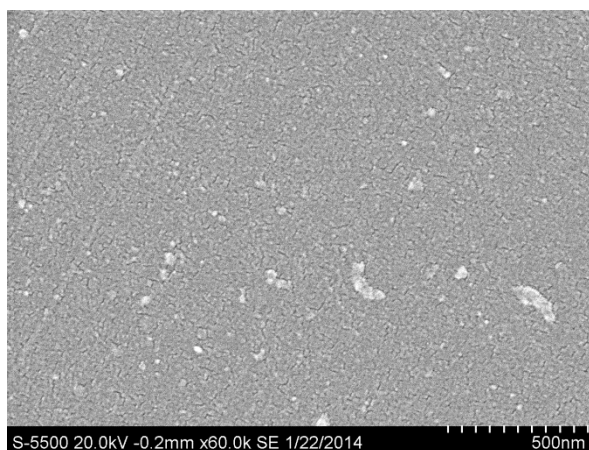
Figure 4-21: SEM micrograph of the membrane surface.
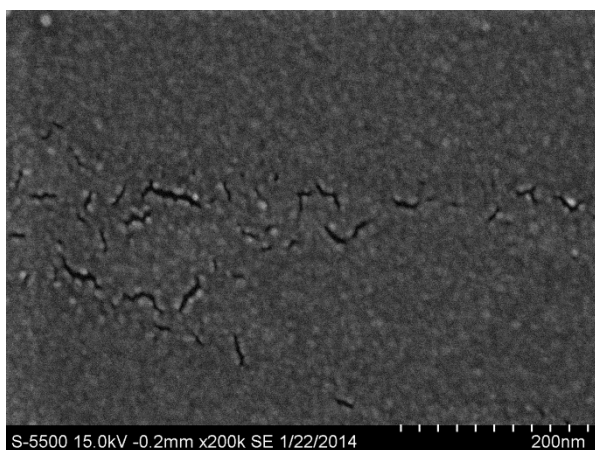
Figure 4-22: SEM micrograph of the membrane surface. The Cracks are about 1-15 nm across.

35

5   Discussion

5.1   Temperature effect on the flux

Figure 4-1 and Figure 4-2 indicate that both the water and salt flux increase with temperature in the temperature range tested. This is in accordance with other studies [15, 21-23]. The increase in the flux is possibly caused by swelling of the membrane as the temperature increases. The increased temperature may also lead to increased diffusivity of water and salt which again contributes to increased osmotic pressure and thus the increased flux.

5.2   Evaluation of the membrane preparation method

The water permeabilities compared in Figure 4-3 and salt permeabilities compared in Figure 4-4 are relatively similar. This indicates that the membranes are quite uniform and that the preparation method used is good. The membranes should perform equally. The small differences between the membranes may be influenced by small differences in the experimental conditions. The tests performed with Membrane B, C and D may be influenced by the failing feed pump which led to the magnet shavings being present in the feed loop. When these membranes were tested hydrocarbons had not yet been used in the apparatus. When the test with Membrane G was conducted residue of hydrocarbons used in previous experiments may have been present on the surface of the tubes and the membrane module, and thus affecting the water and salt fluxes. Another factor is possibly the orientation of the membrane module. Membrane G was tested with the membrane in a vertical position as shown in Figure 3-6. The other membranes were tested with the membrane in an angled position as shown in Figure 3-5. This may have led to changed flow conditions over the membrane surface and consequently so the external CP.

5.3   The effect of hydrocarbons

In Figure 5-1 the results for the water permeabilities of Membrane D, F and G are shown. For Membrane G only the first test of each HC ratio is included. As can be seen from the figure the results are not conclusive. In the tests using Membrane D the water permeability for 0 %, 50 % and 80 % HC was virtually the same. There is even a small increase in the water permeability for 80 % HC compared to 0 % HC. For the 20 % HC test however, the water permeability is lower. There are many possible factors that may contribute to this result. The first may be that the ratio of HC that is being pumped into the tubes may not be the same as the ratio in the flask. Since the mixing of water and HC is not perfect, the ratio of HC that gets pumped into the tube depends on the position of the tube. A surplus of water is likely to be in the bottom of the flask while in the top there will be a surplus of HC. Attempts were made to keep the tube in a position where the distance from the top of the liquid to the tip of the tube was equal to the distance to the bottom of the flask as shown in Figure 5-2. However the tube could easily move when affected by the stirring. Thus it is possible that a HC ratio lower than the target entered the tube during the tests. When the HC ratio was 20 % the mixing appeared to be much better than for the higher HC ratios, which may have affected the result. It was also the first time hydrocarbons were introduced into the system. For this reason a large amount of magnet residue was released into the flow due to the dissolving effect of the hydrocarbons. This residue may have led to temporary fouling of the membrane and consequently caused the reduced performance. It is possible that when the 50 and 80 % HC was conducted there was a decreasing amount of fouling in the system. This might have led to the increased performance for these tests. For the 100 % HC test the weight change of

the draw flask was 0,00 g. This result shows that hydrocarbons will not permeate through the membrane.
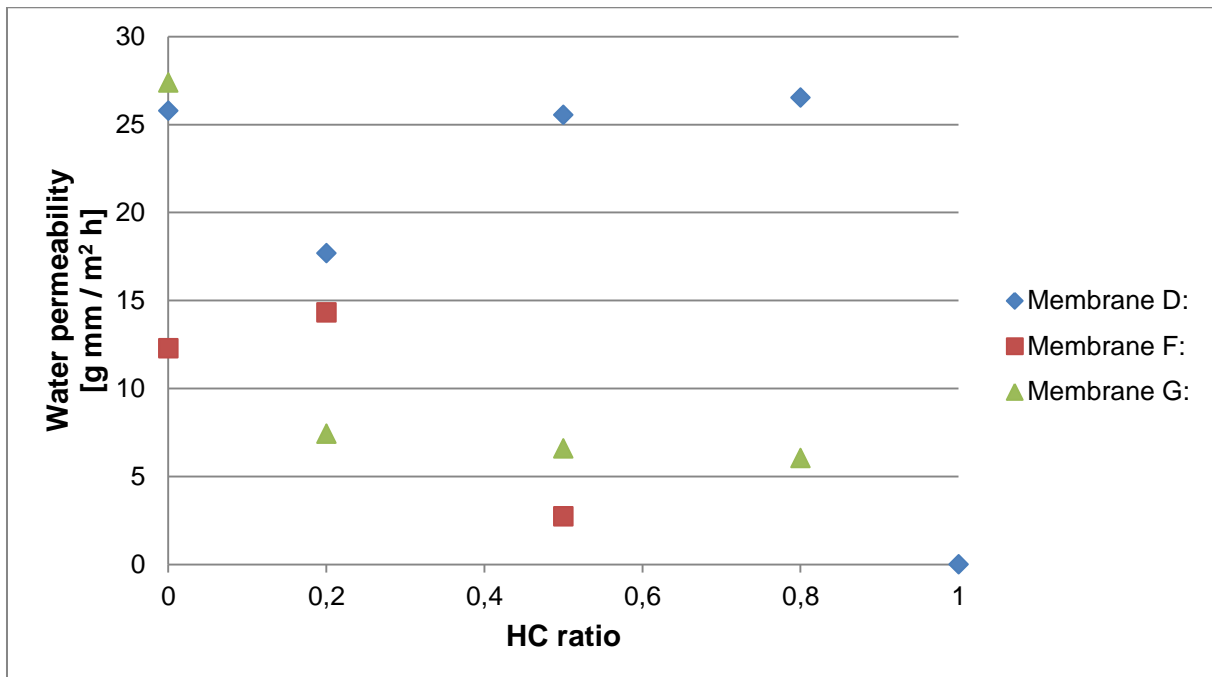

Figure 5-1: Comparison of the results for the water permeability at different HC ratios for Membrane D, F and the first results for Membrane G.

Membrane F had previously been used in PRO experiments. Thus it was likely suffering from fouling. It may also have been compressed by the high pressure in PRO, which would make it more dense than the others. These two factors may explain why the water permeability for the 0 % HC test was much lower than for the two other membranes. For the 20 % HC test there is an increase in the water permeability. The hydrocarbons are non-polar solvents. It is possible that they work as a cleaning agent, thus removing some of the fouling on the membrane surface. It is also possible that the hydrocarbons caused the membrane to swell, which made it less dense. The thickness measurements presented in chapter 4.7.1 indicates that hydrocarbons do cause swelling of the membrane when in an environment with a mix of water and hydrocarbons. Both phenomena are possible explanations for the increased water permeability. The 50 % HC test gave low water permeability. Again the likely cause could be the tube position which would lead to a different HC ratio than what was aimed for.

When water and HC enter the membrane module the two phases will likely separate. This may cause a surplus of water on the bottom and a surplus of HC on the top. For the tests with Membrane D and F the membrane was oriented in an angled position. This may have caused a situation as illustrated in Figure 3-5. In this situation the contact of water and the membrane would not reflect the targeted HC ratio for the experiments. This may also explain the inconclusive results for Membrane D and F.
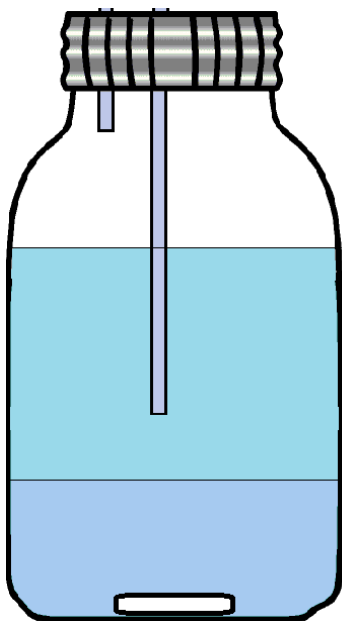
Figure 5-2: Illustration of the tube position in the feed flask.

For the tests with Membrane G the orientation of the membrane was changed to a vertical position. This would possibly give the situation illustrated in Figure 3-6 where the water membrane contact better reflects the HC ratio. The tube was also fixed into position using tape to make sure the tube did not move. For the 20 % test the water permeability dropped significantly compared to the first 0 % HC test. Unlike the Membrane D and F tests the water permeability decreased with the HC ratio for the first test with 20, 50 and 80 % HC. This is likely due to repositioning of the membrane module and the fixing of the feed tube. As can be seen in Figure 4-7 the water permeability for the reference test 2 dropped after introducing the membrane to hydrocarbons. For reference test 3 however it increased compared to the previous reference test. Possibly this is because the membrane now has had time to swell and is thus less dense leading to the increased water permeability. For the subsequent reference tests the permeability drops quite steadily which likely depicts increased fouling effect on the membrane. For the second test with 80 and 50 % HC the water permeability results show the same trend as the first. It increases as the HC ratio decreases. The last test with 20 % HC does not follow this trend. However this is may be a consequence of membrane degradation or the tube being out of position.

As can be seen in Figure 4-8 the salt permeability also drops significantly once the membrane has been introduced to hydrocarbons. From the second through the seventh reference tests the salt permeability is less than half of the first. This indicates that hydrocarbons may increase the salt retention. For the two first tests with 20 and 50 % HC, the salt permeability results do not show the same trend as the water permeability, and there was no result in the first 80 % HC test. The last three HC experiments seem to follow the same pattern as the water permeability result for these tests. This could indicate that the water and salt permeability are related.

The results of the PRO pressure generation tests presented in chapter 4.6 show no conclusive evidence that the HC ratio affects the pressure generation rate. In the test with

pure water in the feed, the pressure generation rate is the highest. The results for the 20, 50 and the first 80 % HC tests are quite similar. However, when the system was left overnight with 80 % HC inside, the pressure generation rate became so low that it was unmeasurable due to the apparatus having a small leak. A possible explanation for this originates in the way the module was installed in the PRO setup. In PRO the feed was facing towards the porous support plate as illustrated in Figure 3-8. This is opposite of the way it was mounted in FO where the draw solution was facing the support. When the first four HC tests were conducted, the pores in the plate were probably pre-filled with water from the reference test. Since the experiments were conducted in a short period of time, the pores did not get filled with HC in the correct ratio. However when left overnight the HC displaced the water, since it is less dense. When the next test was performed there was not enough water in contact with the membrane to generate sufficient pressure. Since the plate was in the ceiling of the chamber, the water was probably unable to reenter the pores as it is the heavier phase. However, the 100 % HC pressure test shows that there was quite a significant leak in the system contributing to the inconclusiveness of the results.

From the FO and PRO results it can be concluded that the ratio of hydrocarbons may not be the most important factor to the water permeation through the membrane. Since water and hydrocarbons will separate into two phases, contact between the water and the membrane seems to be an important factor. Thus an oil or gas well may not need to produce much water before it triggers the osmotic actuator. It may depend more on the positioning of the actuator in the drainage pipe and the design of the actuator itself. For instance, it could make a big difference whether the membranes are composed of flat or hollow fibers.

5.4   The membrane performance in PRO

Figure 4-9 indicates that there is no linear relationship between the water flux and the pressure difference. This is in accordance with other studies [24-26]. However there are also studies that have found a linear relationship [15, 27].

5.5   Concentration polarization and fouling

Concentration polarization possibly had an effect on the results in both FO and PRO experiments. The porous support plate may have limited the mass transfer from the bulk to the membrane surface thus causing internal CP. In the FO experiments the porous support was facing the draw solution as illustrated in Figure 5-3. In the PRO experiments it was facing the feed as illustrated in Figure 5-4.
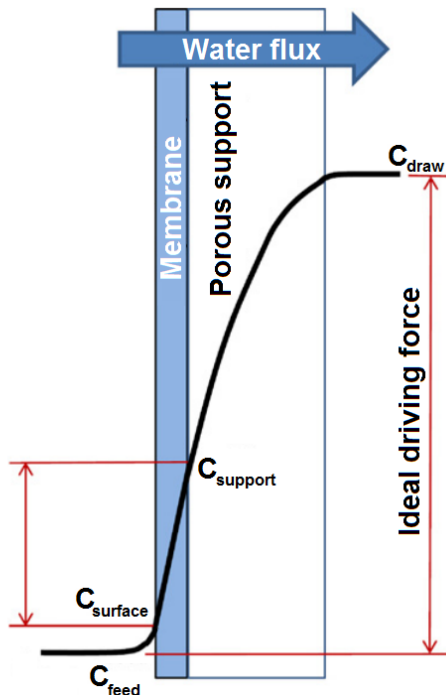
Figure 5-3: Concentration profile with the support facing the draw. Dilutive CP. Adapted from [13].
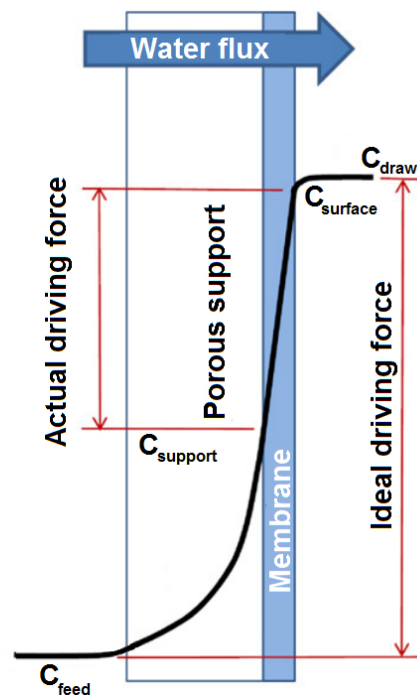
Figure 5-4: Concentration profile with the support facing the feed. Concentrative CP. Adapted from [13].

CP increases as the water flux through the membrane increases [27]. The dense PBI membranes have relatively slow water flux rates. Consequently the effect of CP is likely limited, yet still present. As can be seen from the figures the actual driving force is affected by the membrane orientation. Other studies have found that the water flux is higher under otherwise equal conditions when the membrane faces the draw side [15, 21]. This is due to the higher actual driving force as can be seen in Figure 5-3 and Figure 5-4. For this thesis this was not investigated under comparable conditions.

Figure 5-5 shows the water flux results from the reference tests performed with Membrane G. The decrease in the water flux over time is likely caused by fouling.
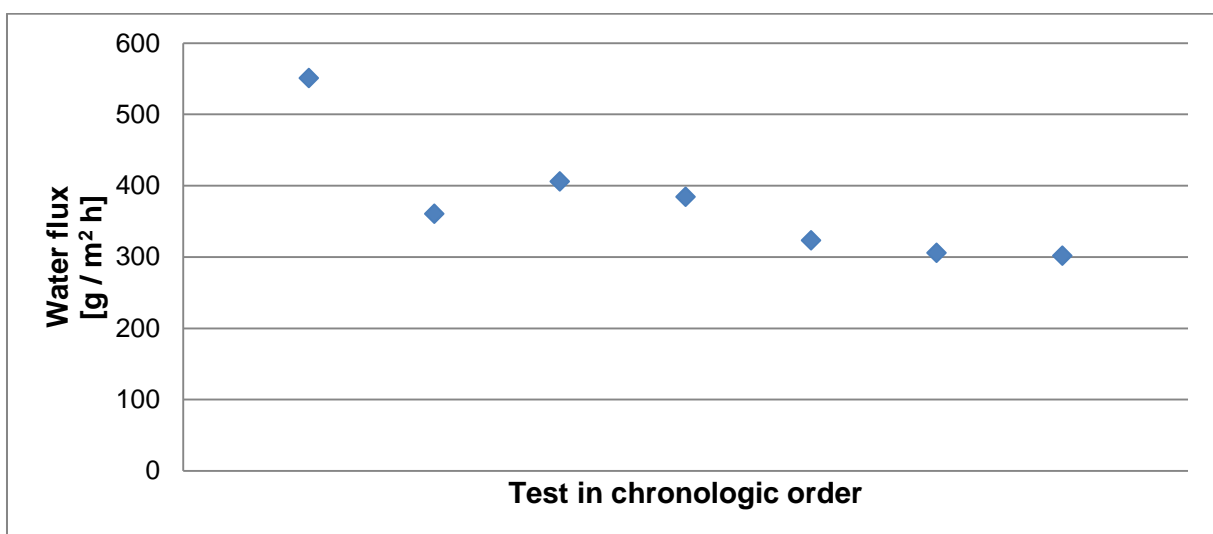
Figure 5-5: The water flux results for Membrane G using only distilled water in the feed.

For future experiments it is suggested to use two separate pumps for the hydrocarbons and water as shown in Figure 5-6. Phase separation is rapid, thus it is possible to pump the liquid from each liquid layer, then mixing them after the pumps. This should improve the ability to control the water and hydrocarbon ratio by adjusting pump speeds. It is also suggested to investigate the use of hollow fiber membranes. These would possibly be less sensitive to membrane orientation in relation to the gravitational field.
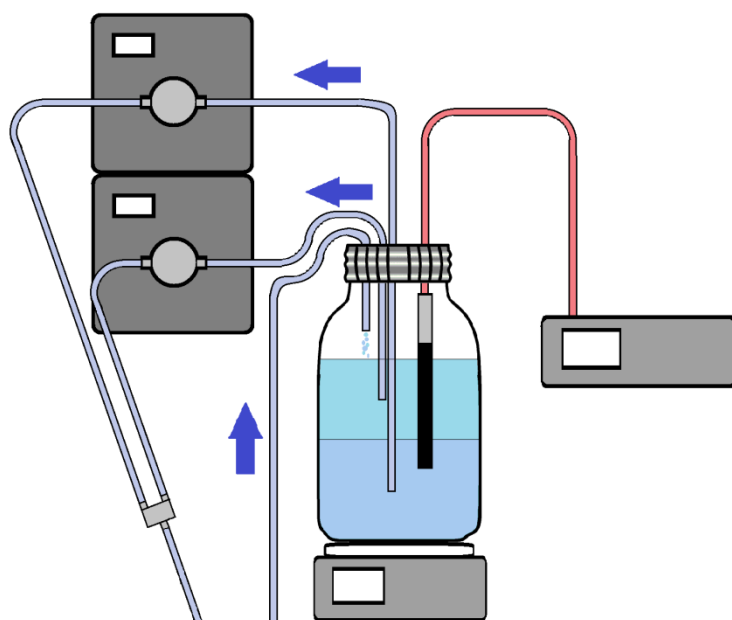
Figure 5-6: Suggested feed setup employing separate pumps for the water and hydrocarbons.

5.6 Characterization

The SEM sample membrane seems to have three layers, as seen in Figure 4-18, Figure 4-19 and Figure 4-20. This could be caused by the heat plate in the oven used during the membrane preparation. The heat seems to have created a relatively thick crust-like layer on the side of the membrane that faced the plate. Figure 4-18 and Figure 4-20 shows that the crust-like layer on the top part of the membrane is not as thick as the lower layer, since it was not facing the heat plate.

The membrane was only about 20 μm thick. This is thinner than the measurements of the wet membrane used in the FO tests (about 50 μm). This indicates that the membrane shrinks when dried. This supports the findings in the attempted contact angle measurements, where the membrane would start swelling in contact with water (Figure 4-17). In Figure 4-22, cracks in the membrane surface are seen. The cracks are assumed to be caused by the drying of the membrane. After preparation, the membranes are always kept wet in a bath of distilled water, to prevent them from drying when not used in experiments. If cracks were present during the FO testing, the salt flux would probably have been higher.

The thermogravimetric analysis of the membrane shows that the membrane material is very thermally stable. Figure 4-15 shows weight decrease in the beginning of the experiment. This is probably water absorbed from the air due to its hydrophilicity. After the period of constant temperature of 120 °C, the weight decrease is very low, as can be seen in Figure 4-16. Pure PBI has a decomposition temperature of 600 °C or above and a glass transition temperature

of around 400 °C [28, 29]. This is well above the temperatures reported from the Åsgard field, which should be no higher than 165 °C [30]. The membranes should not thermally decompose under these conditions short term. However, studies have indicated that PBI may decompose when exposed to high temperatures under oxidative conditions for long periods of time [29].

The membrane's chemical stability in contact with HC appears to be good. Hydrocarbons do not dissolve the membrane. However, the thickness measurements presented in chapter 4.7.1 indicate that the hydrocarbon water mix may cause swelling of the membrane. Other studies have found that hydrocarbons may cause swelling in polymeric membranes [31, 32].

6 Conclusion

The PBI membrane's thermal stability was investigated using thermogravimetric analysis. It was heated to temperatures just short of 600 °C with very little loss of mass. This indicates that the membrane is thermally stable and should be able to withstand the temperatures in oil and gas fields short term. It should however be further investigated whether the PBI membrane can endure high temperatures for long periods of time. FO experiments were carried out to test the effect of temperature on the trans-membrane water and salt flux. It was found that both water and salt flux increase with temperature. FO and PRO experiments with different hydrocarbon ratios mixed into the feed water were performed. The membranes performed well under these conditions. The results did not conclusively indicate that there is a relationship between the hydrocarbon ratio and the water or salt permeability. Instead it appeared that the contact between the water and the membrane surface is the most important factor contributing to water permeation. However, this needs to be investigated further. After being exposed to hydrocarbons, the membrane's salt retention seemingly increased. It was also found that hydrocarbons possibly cause swelling of the membrane. This was done by measuring thickness before and after exposure under different circumstances. In PRO mode, pressure was generated on the draw side when hydrocarbons were mixed together with water in the feed. PRO experiments using pure water in the feed were performed. The results showed no linear relationship between water flux and pressure difference. By comparing the FO results of different virgin membranes, it was found that the preparation method used gives little variation in membrane performance. The membrane morphology was characterized by SEM, and its hydrophilic properties demonstrated by attempted contact angle measurements. It was discovered that the SEM sample membrane had a crust-like layer in its bottom part of the cross section. It was also found that the membranes shrink considerably when dried.

7 References

[1] M.B. Hägg, OMPA - Development of an Osmotic Membrane Pressure Actuator for Enhanced Oil & Gas Recovery, in, 2010, pp. 1-11.

[2] H. Aakre, Method for operating actuator and an actuator device for use in drainage pipe used for producing oil and/or gas, in, Google Patents, 2010.

[3] S.S. Bach, F.P. Brodersen, J. Campbell, E. Garland, A. Glickman, G. Indrebø, S. Johnsen, J.P. Ray, J. Smith, M. Tangveld, T.I.R. Utvik, B. De Vals, W. Veerkamp, Fate and effects of naturally occurring substances in produced water on the marine environment, in, International Association of Oil & Gas Producers, London, UK, 2005.

[4] J. Glater, The early history of reverse osmosis membrane development, Desalination, 117 (1998) 297-309.

[5] J.A. Nollet, Lecons de physique experimentale, Hippolyte-Louis Guerin and Louis-Francios Dela-tour, Paris, 1948.

[6] M. Traube, Physiologie und Wisserschlaftliche Medicin, Archiv fur Anatomic, (1867).

[7] S. Loeb, The Loeb-Sourirajan Membrane - How It Came About, Abstr Pap Am Chem S, 180 (1980) 1-Cell.

[8] I.L. Alsvik, M.B. Hagg, Pressure Retarded Osmosis and Forward Osmosis Membranes: Materials and Methods, Polymers-Basel, 5 (2013) 303-327.

[9] T.Y. Cath, A.E. Childress, M. Elimelech, Forward osmosis: Principles, applications, and recent developments, J Membrane Sci, 281 (2006) 70-87.

[10] R.J. Aaberg, Osmotic power: A new and powerful renewable energy source?, Refocus, 4 (2003) 48-50.

[11] L.C. Sawyer, R.S. Jones, Observations on the Structure of 1st Generation Polybenzimidazole Reverse-Osmosis Membranes, J Membrane Sci, 20 (1984) 147-166.

[12] M. Mulder, Basic principles of membrane technology, 2nd ed., Kluwer Academic, Dordrecht ; Boston, 1996.

[13] K.L. Lee, R.W. Baker, H.K. Lonsdale, Membranes for Power-Generation by Pressure-Retarded Osmosis, J Membrane Sci, 8 (1981) 141-171.

[14] A. Tiraferri, N.Y. Yip, W.A. Phillip, J.D. Schiffman, M. Elimelech, Relating performance of thin-film composite forward osmosis membranes to support layer formation and structure, J Membrane Sci, 367 (2011) 340-352.

[15] K.Y. Wang, T.S. Chung, J.J. Qin, Polybenzimidazole (PBI) nanofiltration hollow fiber membranes applied in forward osmosis process, J Membrane Sci, 300 (2007) 6-12.

[16] G. Amy, Fundamental understanding of organic matter fouling of membranes, Desalination, 231 (2008) 44-51.

[17] O. Olabisi, Handbook of thermoplastics, Marcel Dekker, New York, 1997.

[18] K.Y. Wang, Q. Yang, T.S. Chung, R. Rajagopalan, Enhanced forward osmosis from chemically modified polybenzimidazole (PBI) nanofiltration hollow fiber membranes with a thin wall, Chem Eng Sci, 64 (2009) 1577-1584.

[19] C. Tsonopoulos, Thermodynamic analysis of the mutual solubilities of normal alkanes and water, Fluid Phase Equilibr, 156 (1999) 21-33.

[20] M. Muskat, R. Wycokoff, An approximate theory of water-coning in oil production, Transactions of the AIME, 114 (1935) 144-163.

[21] E.R. Cornelissen, D. Harmsen, K.F. de Korte, C.J. Ruiken, J.J. Qin, H. Oo, L.P. Wessels, Membrane fouling and process performance of forward osmosis membranes on activated sludge, J Membrane Sci, 319 (2008) 158-168.

[22] M.F.A. Goosen, S.S. Sablani, S.S. Al-Maskari, R.H. Al-Belushi, M. Wilf, Effect of feed temperature on permeate flux and mass transfer coefficient in spiral-wound reverse osmosis systems, Desalination, 144 (2002) 367-372.

[23] M. Manttari, A. Pihlajamaki, E. Kaipainen, M. Nystrom, Effect of temperature and membrane pre-treatment by pressure on the filtration properties of nanofiltration membranes, Desalination, 145 (2002) 81-86.

[24] G. Han, T.S. Chung, Robust and High Performance Pressure Retarded Osmosis Hollow Fiber Membranes for Osmotic Power Generation, Aiche J, 60 (2014) 1107-1119.

[25] S.R. Chou, R. Wang, A.G. Fane, Robust and High performance hollow fiber membranes for energy harvesting from salinity gradients by pressure retarded osmosis, J Membrane Sci, 448 (2013) 44-54.

[26] A. Achilli, T.Y. Cath, A.E. Childress, Power generation with pressure retarded osmosis: An experimental and theoretical investigation, J Membrane Sci, 343 (2009) 42-52.

[27] Y. Xu, X.Y. Peng, C.Y.Y. Tang, Q.S.A. Fu, S.Z. Nie, Effect of draw solution concentration and operating conditions on forward osmosis and pressure retarded osmosis performance in a spiral wound module, J Membrane Sci, 348 (2010) 298-309.

[28] S.M.J. Zaidi, Preparation and characterization of composite membranes using blends of SPEEK/PBI with boron phosphate, Electrochim Acta, 50 (2005) 4771-4777.

[29] M. Jaffe, M.I. Haider, J. Menczel, J. Rafalko, Thermal Characterization of High-Performance Pbi and 6f Polymers and Their Alloys, Polym Eng Sci, 32 (1992) 1236-1241.

[30] P. Nice, A. Kopliku, L. Scoppio, Materials selection testing for the Åsgard field well tubulars, Stainless steel world, 9 (1997) 33-38.

[31] K. Okamoto, H.Y. Wang, T. Ijyuin, S. Fujiwara, K. Tanaka, H. Kita, Pervaporation of aromatic/non-aromatic hydrocarbon mixtures through crosslinked membranes of polyimide with pendant phosphonate ester groups, J Membrane Sci, 157 (1999) 97-105.

[32] S.B. Harogoppad, T.M. Aminabhavi, R.H. Balundgi, Swelling Characteristics of Polymer Membranes in the Presence of Aromatic Hydrocarbon Liquids, J Appl Polym Sci, 44 (1992) 1687-1694.

8 Appendix

A Calibration curves

Table 8-1 shows the measured conductivity for dilute NaCl solutions at 62 °C. Figure 8-1 shows the curve derived from these values and the equation for the curve. The equation gives the relation between conductivity and concentration, and is used to calculate the amount of salt that has permeated through the membrane.

Table 8-1: Measured calibration data for dilute NaCl solutions at 62 °C.

Concentration [mol/L]	Conductivity [µS/cm]	Temp [°C]
0,01	1322	62
0,0005	72,4	62
0,00025	38,3	62
0,0001	16,36	62
0	2,16	62
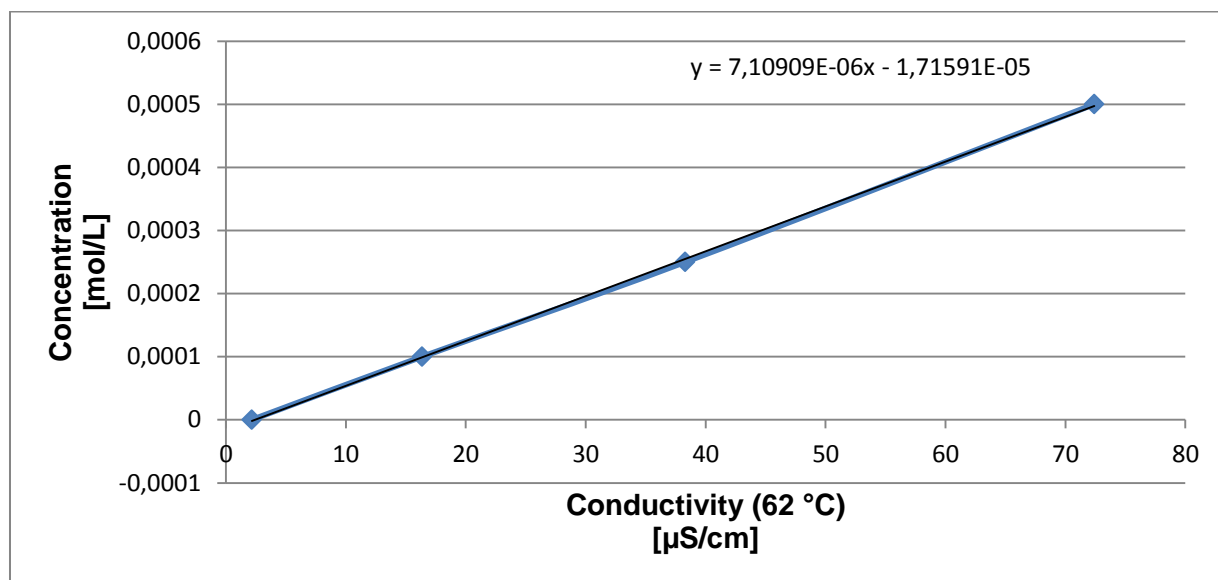
Figure 8-1: NaCl concentration plotted versus the conductivity of the solutions at 62 °C.

Table 8-2 shows the measured conductivity for dilute NaCl solutions at 42 °C. Figure 8-2 shows the curve derived from these values and the equation for the curve.

Table 8-2: Measured calibration data for dilute NaCl solutions at 42 °C.

Concentration [mol/L]	Conductivity [µS/cm]	Temp [*C]
0,01	996	42
0,0005	70,4	42
0,00025	36,3	42
0,0001	15,84	42
0	2,15	42
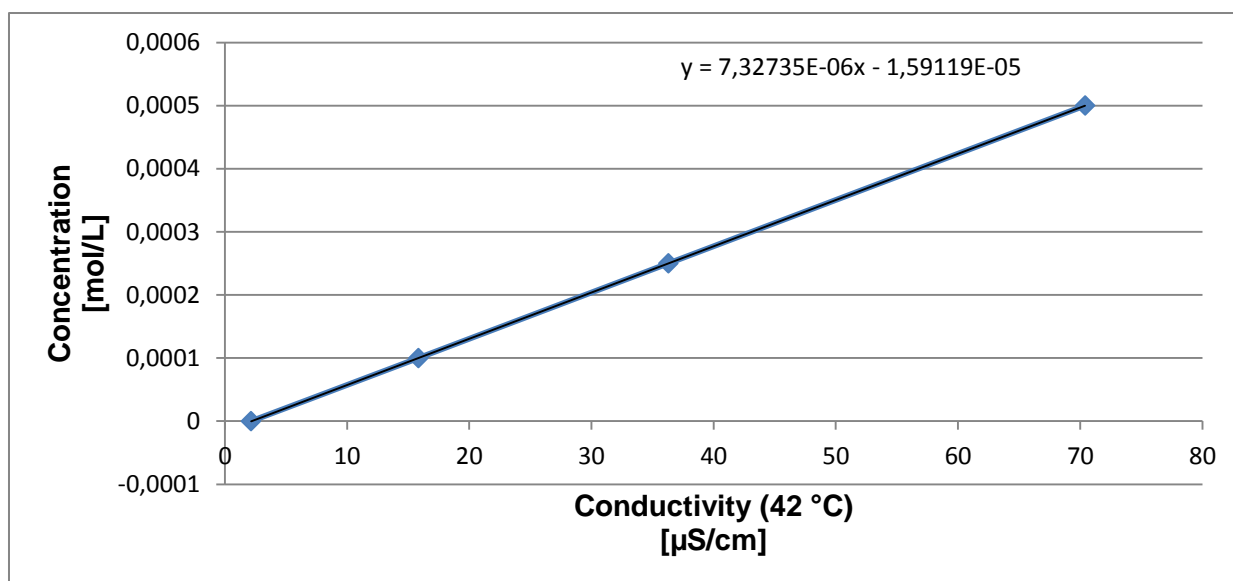
Figure 8-2: NaCl concentration plotted versus the conductivity of the solutions at 42 °C.

In Table 8-3, the measured conductivity of different dilute NaCl solutions at 23 °C are shown. Figure 8-3 shows the curve generated from these values and the curve's equation.

Table 8-3: Measured calibration data for dilute NaCl solutions at 23 °C.

Concentration [mol/L]	Conductivity [µS/cm]	Temp [*C]
0,001	129,9	23
0,0005	67	23
0,00025	34,9	23
0,0001	14,87	23
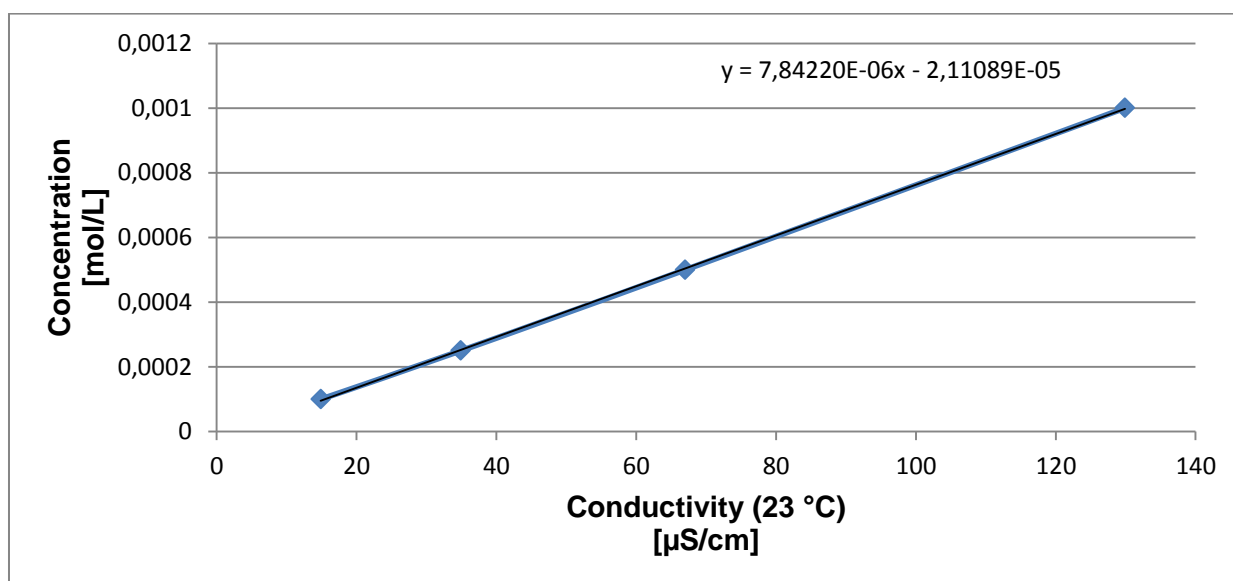
Figure 8-3: NaCl concentration plotted versus the conductivity of the solutions at 23 °C.

B   Data and calculations for the temperature dependence experiments

In this chapter, the measured data of the temperature dependence experiments performed with Membrane A presented.

B.a   23 ⁰C experiment with example calculations

The measured values of weight plotted versus time is shown in Figure 8-4 The plot is based on 223 points of data.
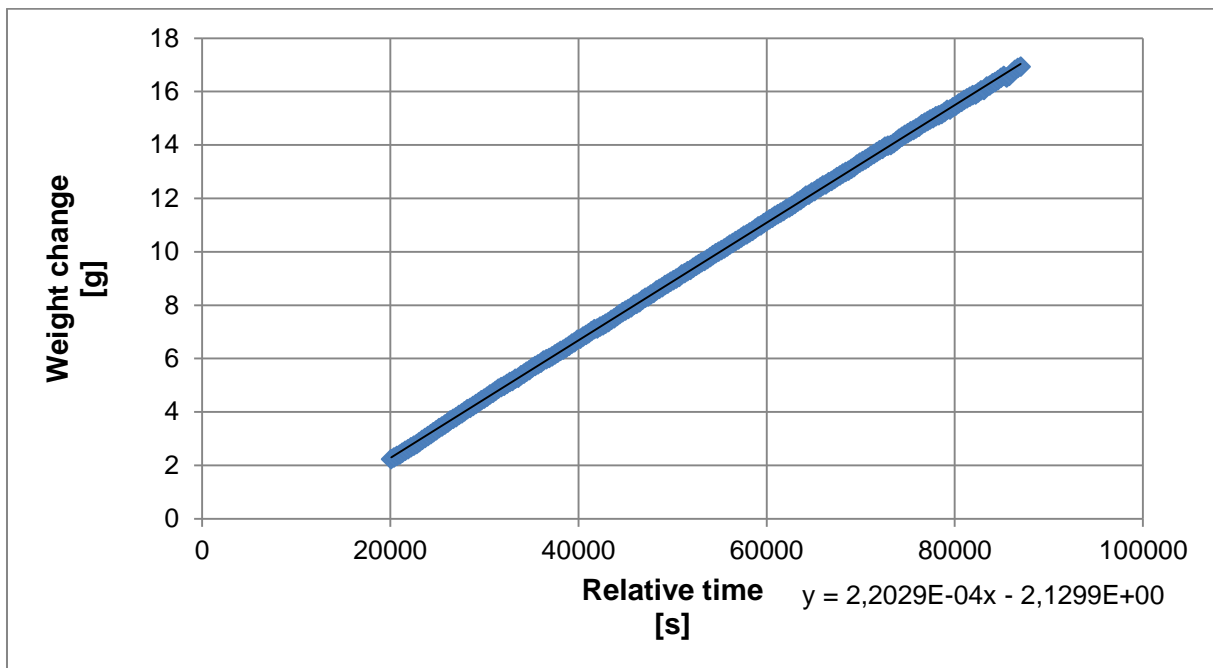
Figure 8-4: Plot of weight versus time for the 23⁰C experiment.

The water flux through the membrane is then calculated using Equation (2-14). C_1 is the slope of the curve shown in Figure 8-4. An example of this calculation:

$$J_w = \frac{C_1}{E} = \frac{0{,}00022029 \, \frac{g}{s} * 3600 \, \frac{s}{h}}{0{,}00279 \, \text{m}^2} = 284 \frac{g}{\text{m}^2\text{h}}$$

The volume in the feed flask is calculated using Equation (2-16):

$$V = V_0 - \frac{m}{\rho}$$

An example of this calculation is shown in cell F2 in Table 8-4. The starting volume is 1248,98 ml.

Table 8-4: Example calculations from the Excel sheet for the 23 ⁰C experiment.

	C	D	E	F	G
1	Time [s]	Weight [g]	Conductivity [µS/cm]	Feed volume [ml]	Salt to feed [mol]
2	300	0,00	2,18	=1248,98-D2/0,9975	= (0,0000078422*E2 - 0,0000211089)*F2/1000

To calculate the amount of salt that has permeated through the membrane to the feed, Equation (2-17), which includes the equation form from the calibration curve in Figure 8-3, is used:

$$n = (dq + e)V$$

A demonstration of this calculation can be seen in cell G2 in Table 8-4. Figure 8-5 shows the measured conductivity plotted versus time.shows the calculated amount of salt plotted versus time. The plots are based on 83 data points.
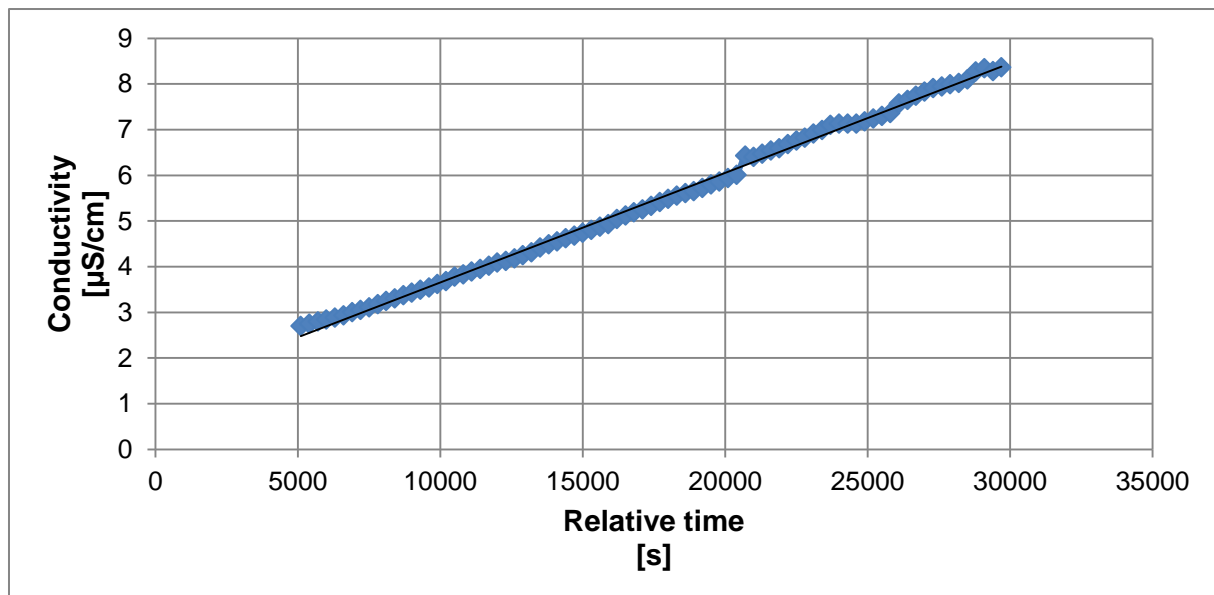
Figure 8-5: Plot of conductivity versus time for the 23 ⁰C experiment.
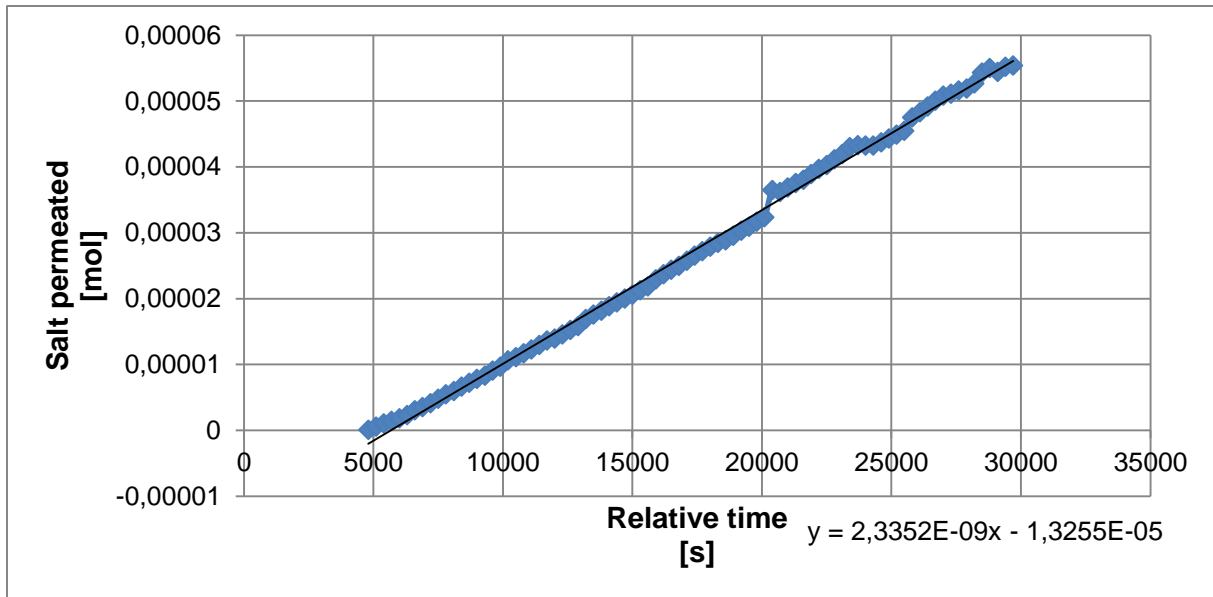
Figure 8-6: Plot of the amount of salt that has permeated to the feed, versus time for 23 ⁰C experiment.

The salt flux through the membrane is calculated from Equation (2-18). C_2 is the slope of the curve shown in Figure 8-6. Example:

$$J_s = \frac{C_2}{E} = \frac{2,3352 * 10^{-9}\frac{mol}{s} * 3600\frac{s}{h}}{0,00279 \text{ m}^2} = 3,01 * 10^{-3}\frac{mol}{m^2h}$$

B.b   42 ⁰C experiment

Figure 8-7 shows the measured values of weight plotted versus time, as well as the equation for calculating the water flux. The plot is based on 107 data points.
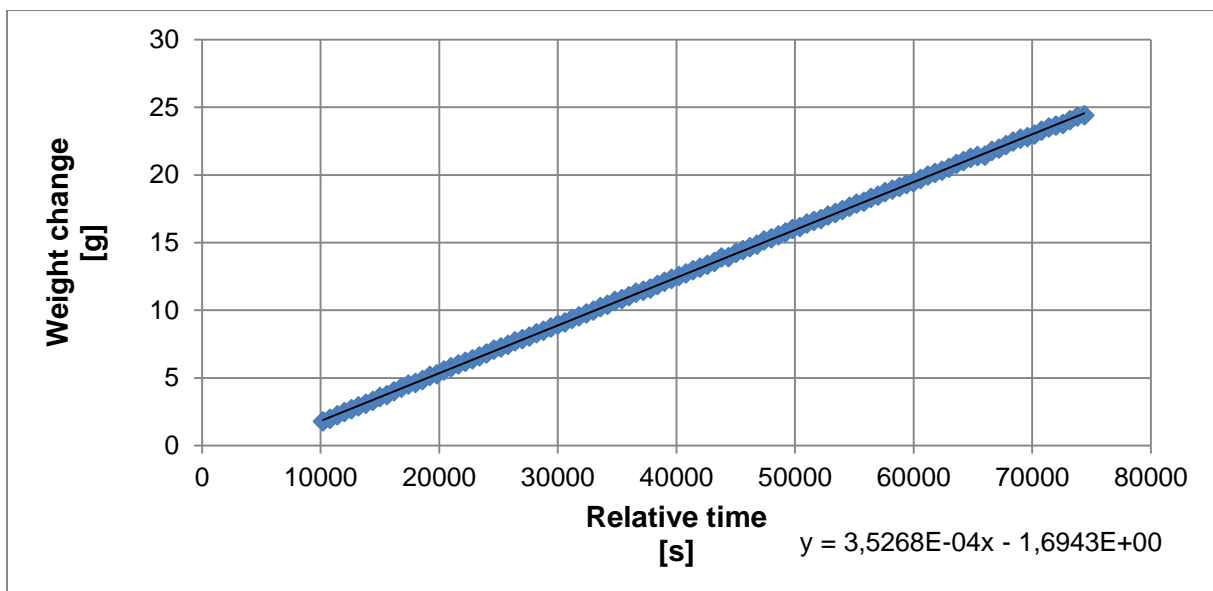
Figure 8-7: Plot of weight versus time for the 42 ⁰C experiment.

In Figure 8-8 the measured conductivity is plotted versus time is shown. The plot is based on 107 data points. These points are used to calculate the amount of salt permeated.
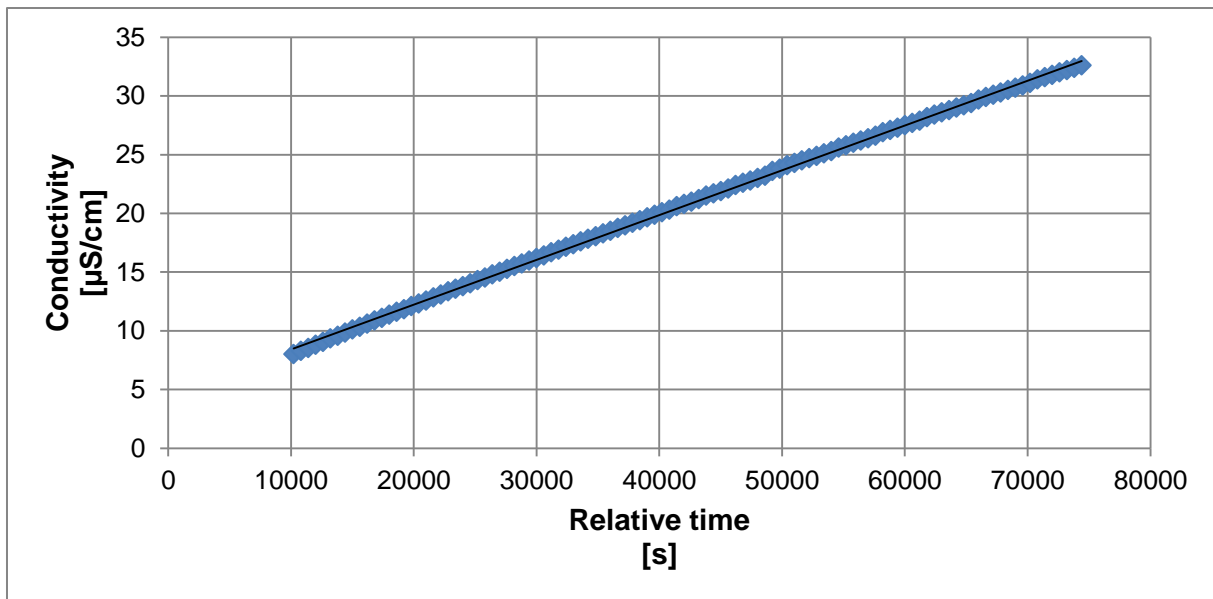
Figure 8-8: Plot of conductivity versus time for the 42 ⁰C experiment.

In Figure 8-9 the calculated amount of salt permeated is plotted versus time.

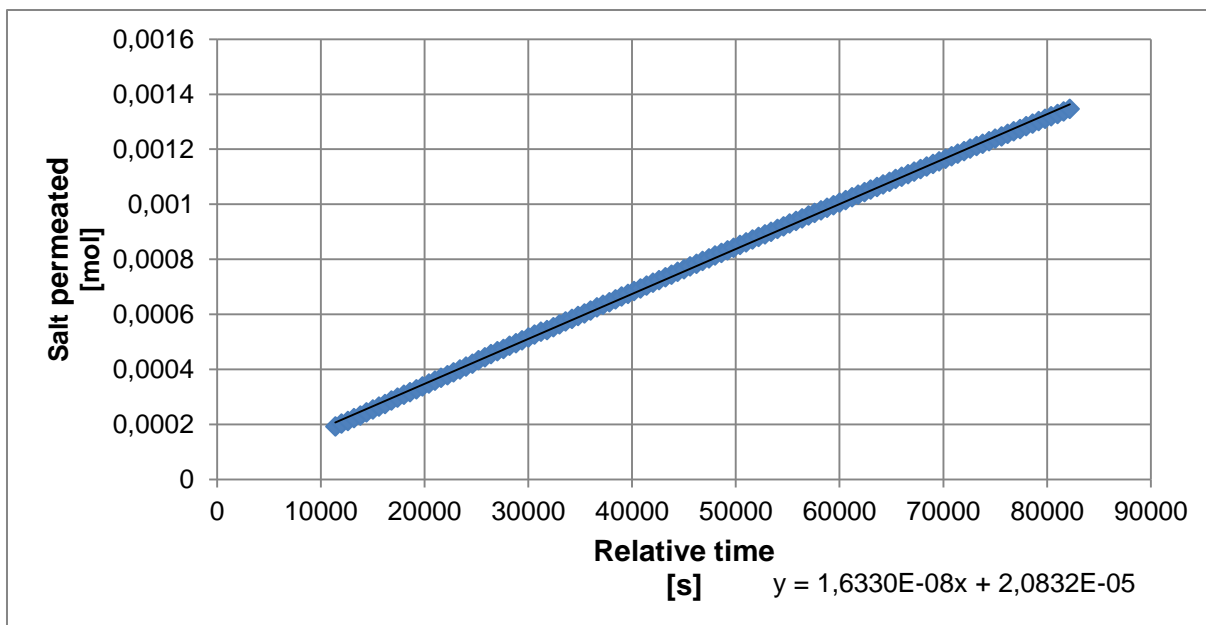$$y = 3,3961E\text{-}09x + 2,3757E\text{-}05$$
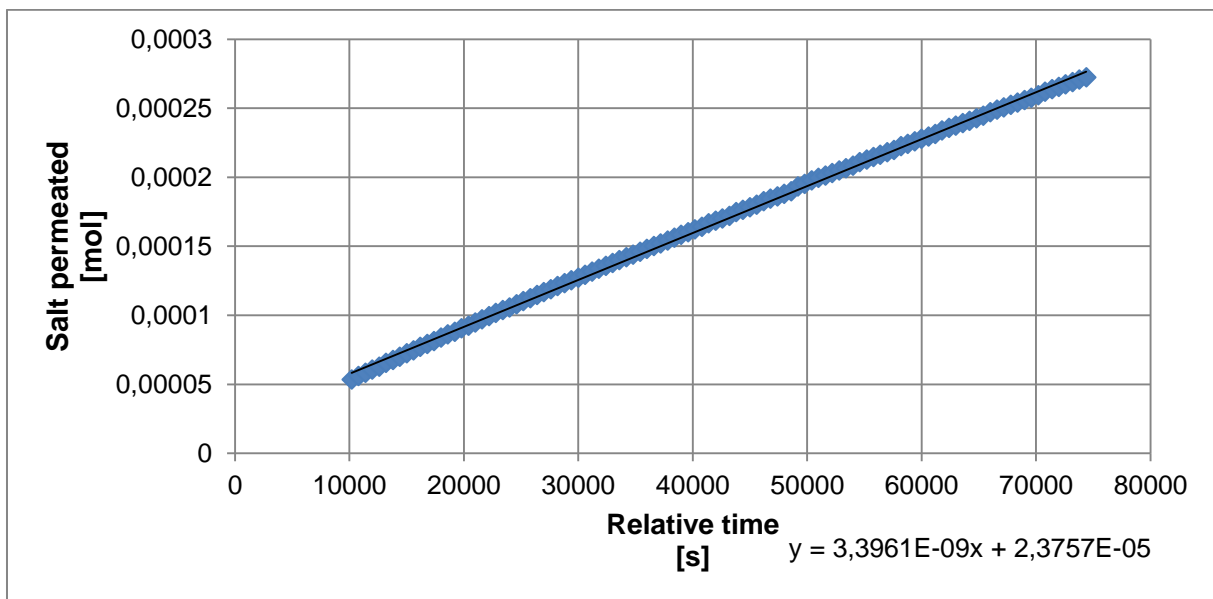
Figure 8-9: Plot of the amount of salt that has permeated to the feed, versus time for 42 ⁰C experiment.

B.c   62 ⁰C experiment

The measured values of weight plotted versus time, is shown in Figure 8-10. The plot is based on 52 data points.
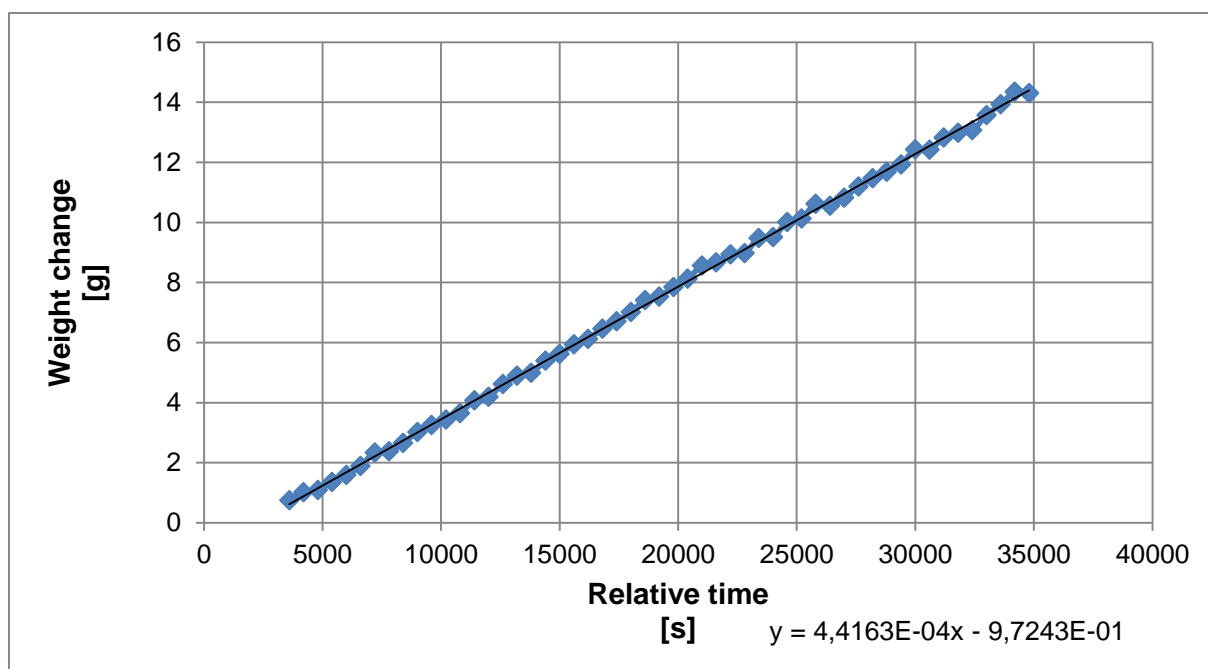
Figure 8-10: Plot of weight versus time for the 62 ⁰C experiment.

Figure 8-11 shows the measured conductivity plotted versus time. The plot is based on 52 points of data, which are used in the calculation of permeated salt.
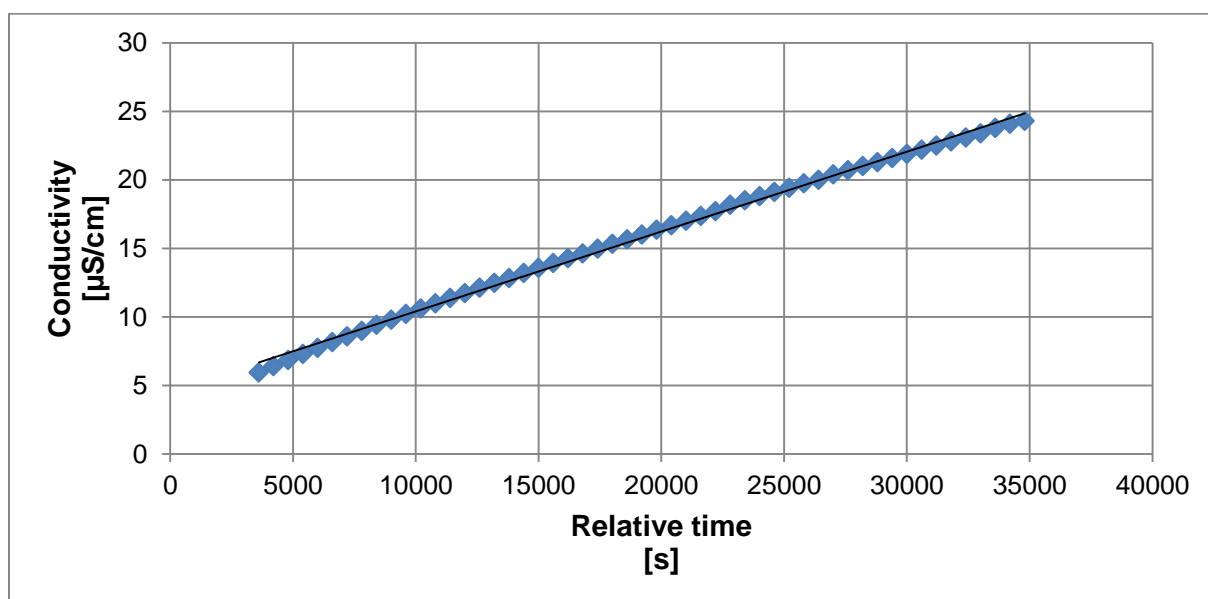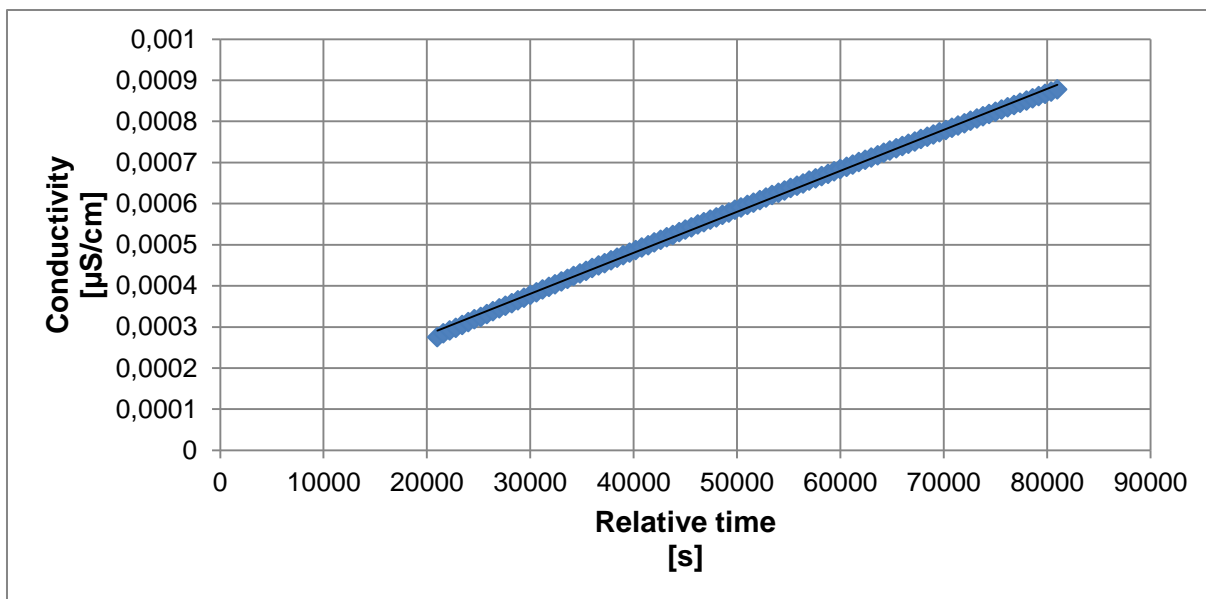

Figure 8-11: Plot of conductivity versus time for the 62 ⁰C experiment.
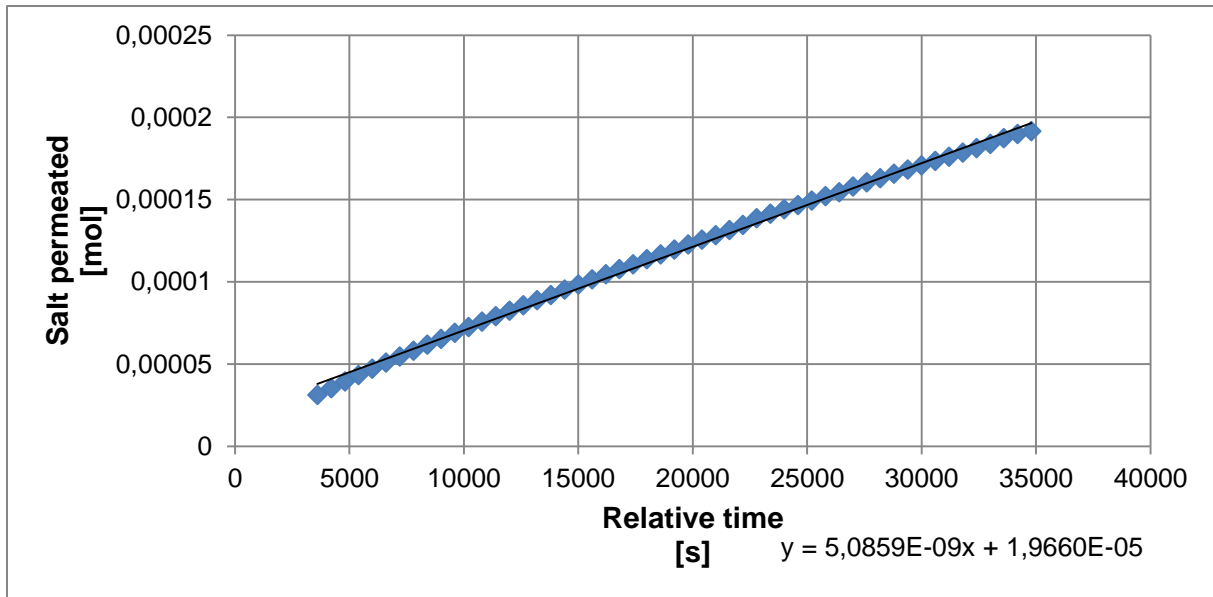
Figure 8-12: Plot of the amount of salt that has permeated to the feed, versus time for 62 ⁰C experiment.

In Figure 8-12 the calculated amount of salt permeated is plotted versus time.

C   Data and calculations for the forward osmosis experiments
In this chapter, the measured data of the remaining FO experiments are presented.

C.a   Membrane B reference test with example calculations
The measured values of weight plotted versus time, is shown in Figure 8-13. The plot consists of 130 data points.
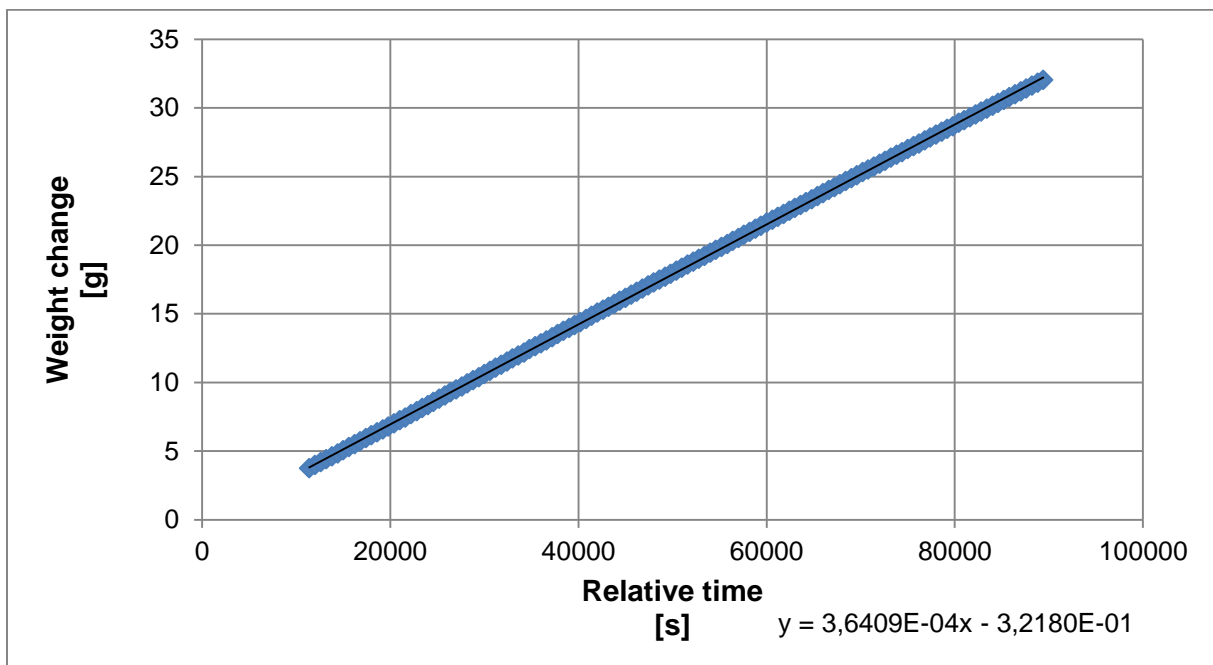
Figure 8-13: Plot of weight versus time for the Membrane B reference test.

The water flux through the membrane is then calculated using Equation (2-14). C_1 is the slope of the curve shown in Figure 8-13. An example of this calculation:

$$J_w = \frac{C_1}{E} = \frac{0,00036409 \frac{g}{s} * 3600 \frac{s}{h}}{0,00279 \text{ m}^2} = 470 \frac{g}{m^2 h}$$

The water permeability is calculated by Equation (2-15). Example:

$$P_w = J_w s = 470 \frac{g}{m^2 h} * 0,0451 \text{ mm} = 21,2 \text{ g} \frac{m}{m^2 h}$$

The volume in the feed flask is calculated using Equation (2-16):

$$V = V_0 - \frac{m}{\rho}$$

An example of this calculation is shown in cell F2 in Table 8-5. The starting volume, is 1233,13 ml.

Table 8-5: Example calculations from the Excel sheet for the Membrane B reference test.

	C	D	E	F	G
1	Time [s]	Weight [g]	Conductivity [µS/cm]	Feed volume [ml]	Salt to feed [mol]
2	600	0,00	6,16	=1233,13-D2/0,998	= (0,0000078422*E2 - 0,0000211089)*F2/1000

To calculate the amount of salt that has permeated through the membrane to the feed, Equation (2-17), which includes the equation form from the calibration curve in Figure 8-3, is used:

$$n = (dq + e)V$$

A demonstration of this calculation can be seen in cell G2 in Table 8-5. Figure 8-14 shows the measured conductivity plotted versus time, and Figure 8-15 shows the calculated amount of salt plotted versus time. The plots are based on 130 data points.
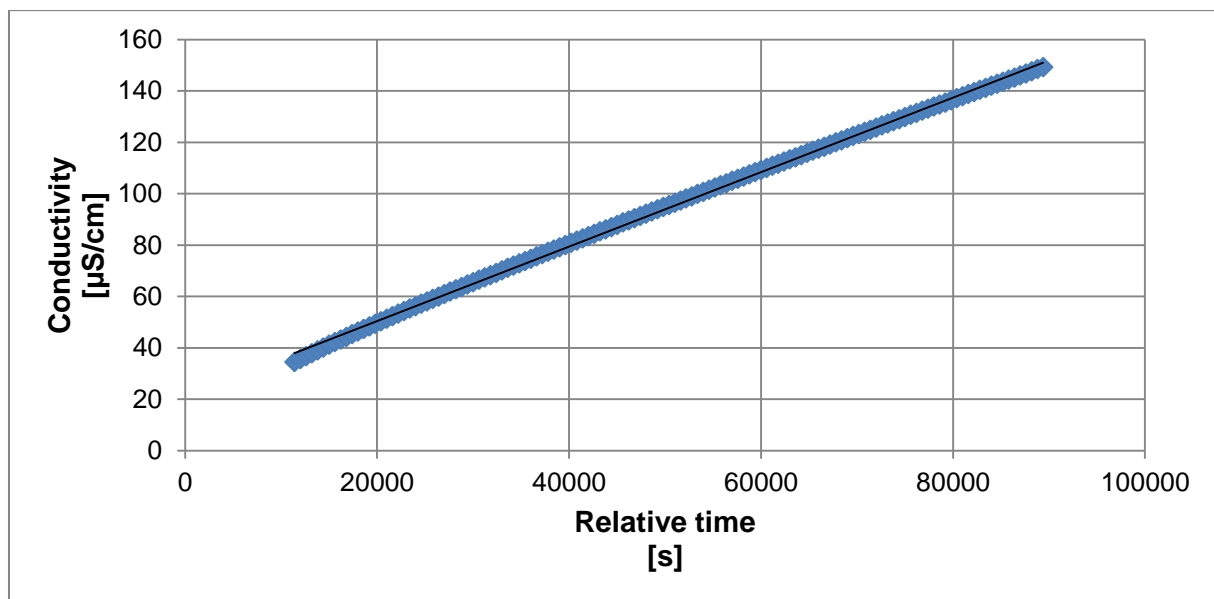
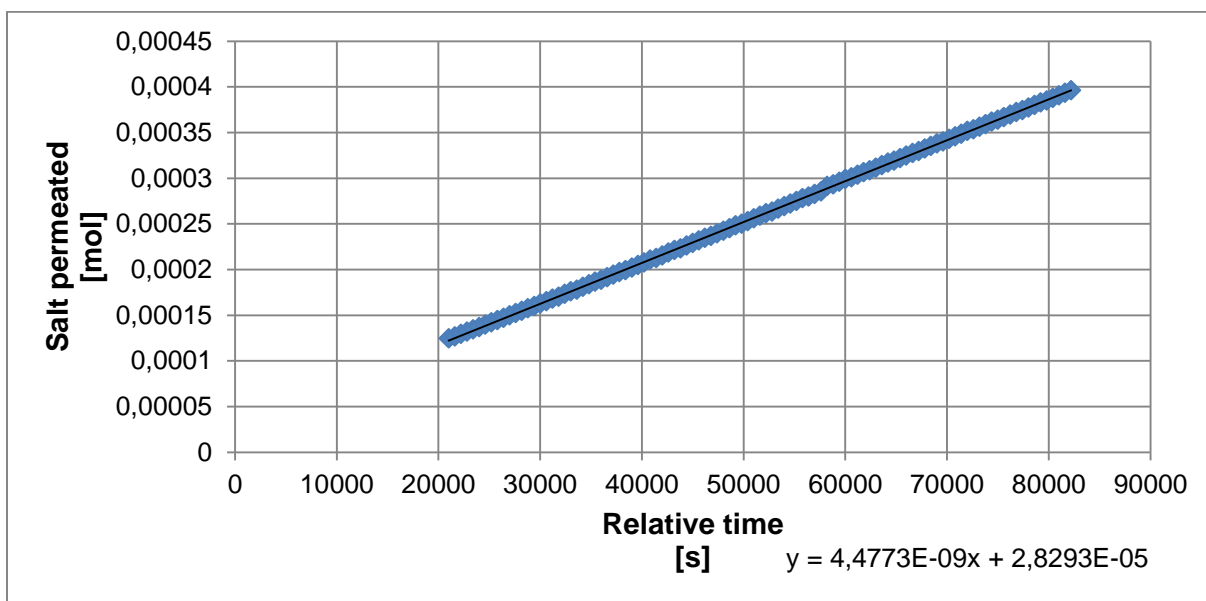**Figure 8-14: Plot of conductivity versus time for the Membrane B reference test.**
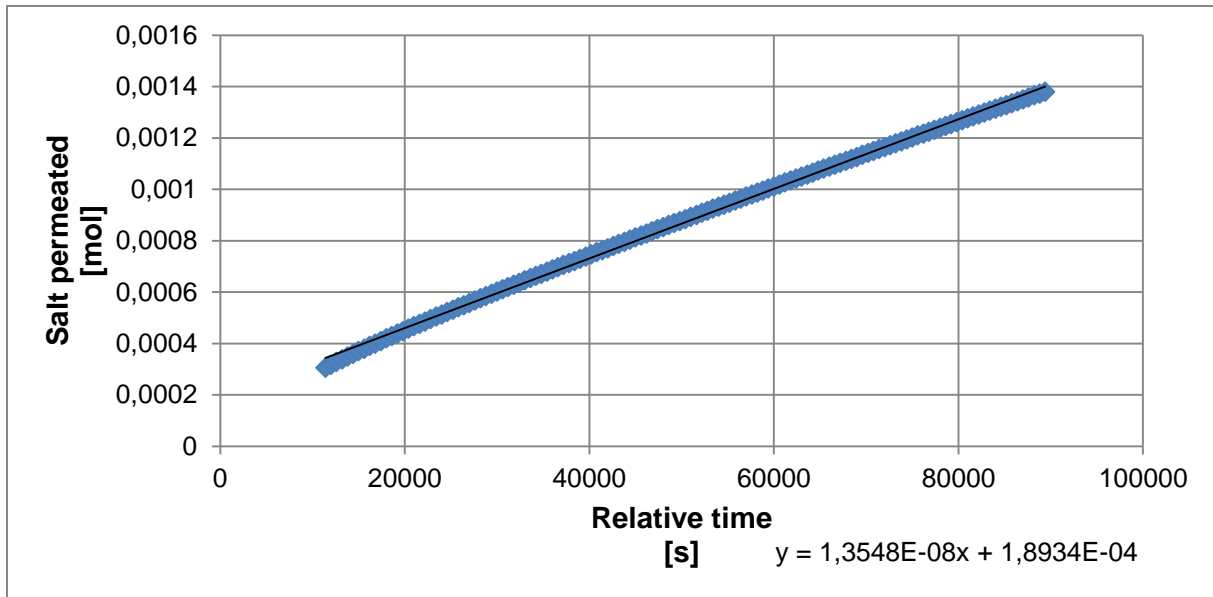
Figure 8-15: Plot of the amount of salt that has permeated to the feed, versus time for the Membrane B reference test.

The salt flux through the membrane is calculated from Equation (2-18). C_2 is the slope of the curve shown in Figure 8-15. Example:

$$J_s = \frac{C_2}{E} = \frac{1{,}3548 * 10^{-8}\frac{\text{mol}}{\text{s}} * 3600\frac{\text{s}}{\text{h}}}{0{,}00279 \text{ m}^2} = 17{,}5 * 10^{-3}\frac{\text{mol}}{\text{m}^2\text{h}}$$

The salt permeability is calculated using Equation (2-19). An example of this calculation:

$$P_s = J_s M_s s = 17{,}5 * 10^{-3}\frac{\text{mol}}{\text{m}^2\text{h}} * 58{,}44\frac{\text{g}}{\text{mol}} * 0{,}0451 \text{ mm} = 46{,}1 * 10^{-3} \text{ g}\frac{\text{mm}}{\text{m}^2\text{h}}$$

C.b   Membrane C reference test

Figure 8-16 shows the measured values of weight plotted versus time. The plot is based on 118 data points.

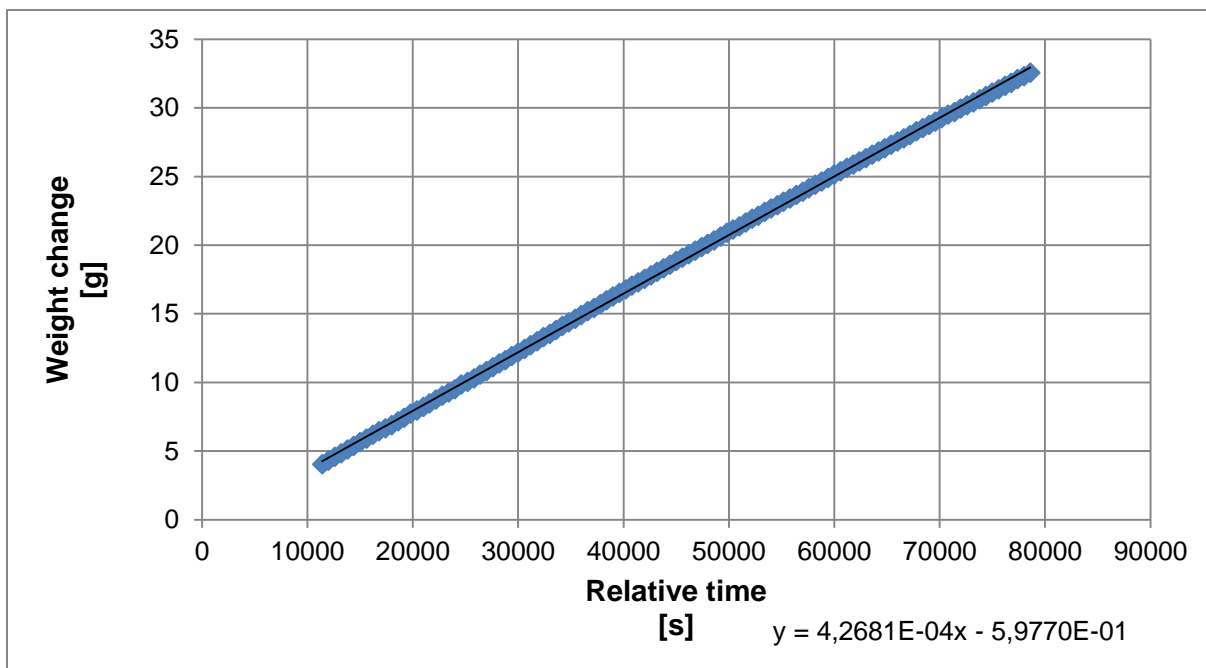$$y = 4,1607\text{E-}04x - 8,0815\text{E-}01$$
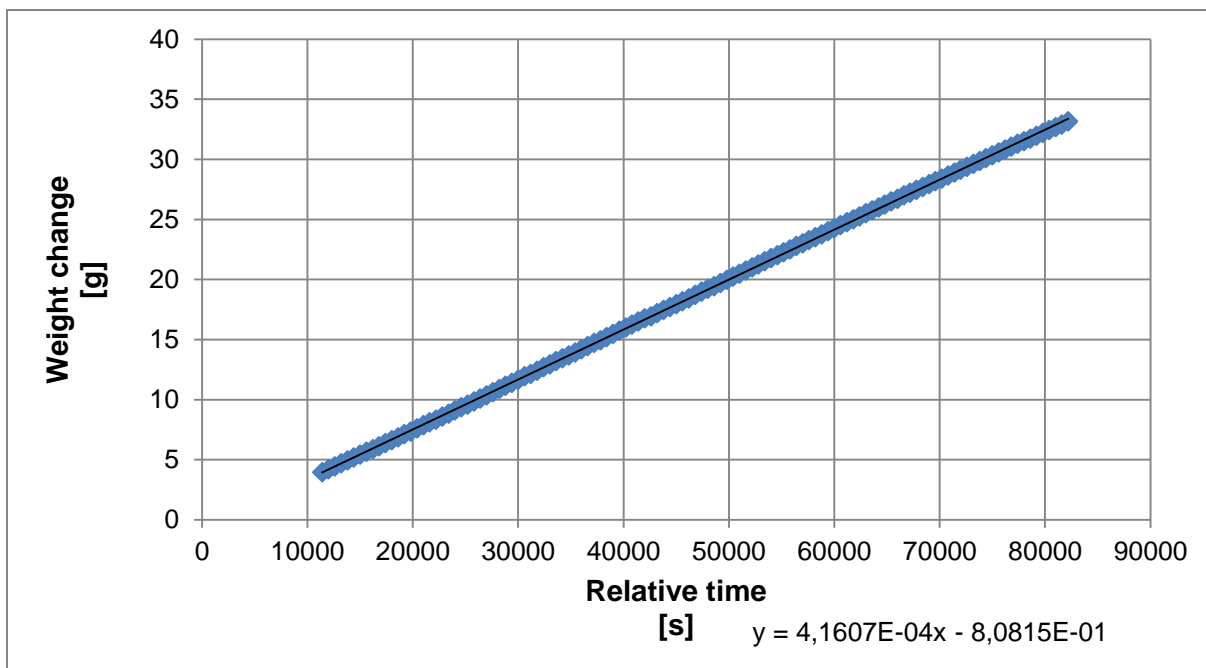
Figure 8-16: Plot of weight versus time for the Membrane C reference test.

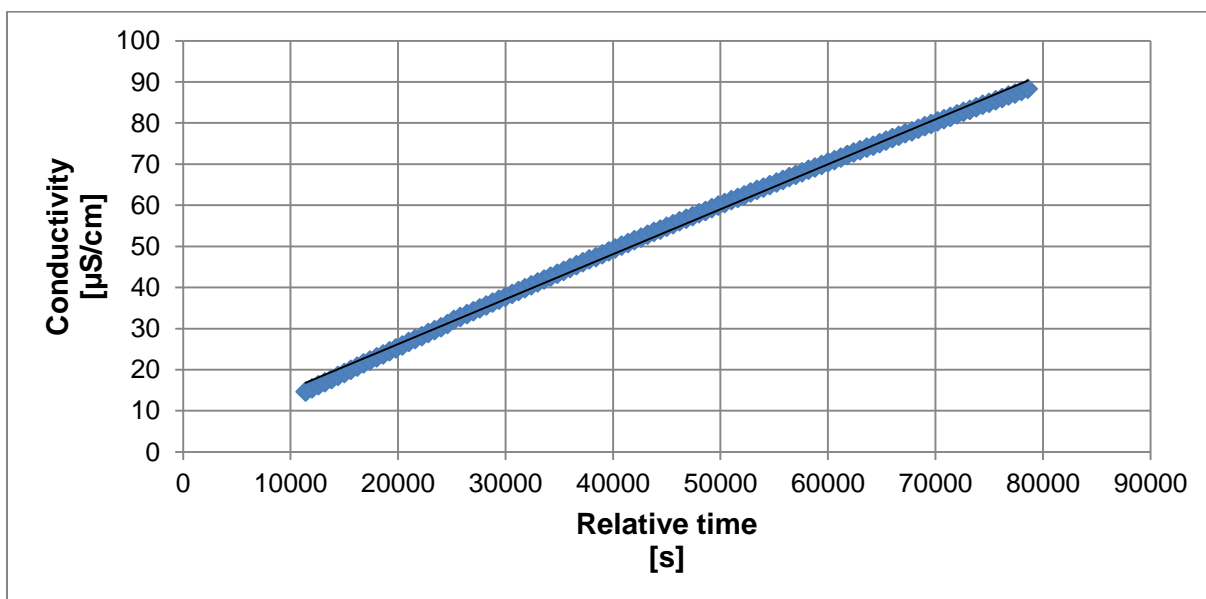In Figure 8-17 the measured conductivity is plotted versus time. The plot is based on 118 data points. These points are used to calculate the amount of salt permeated.
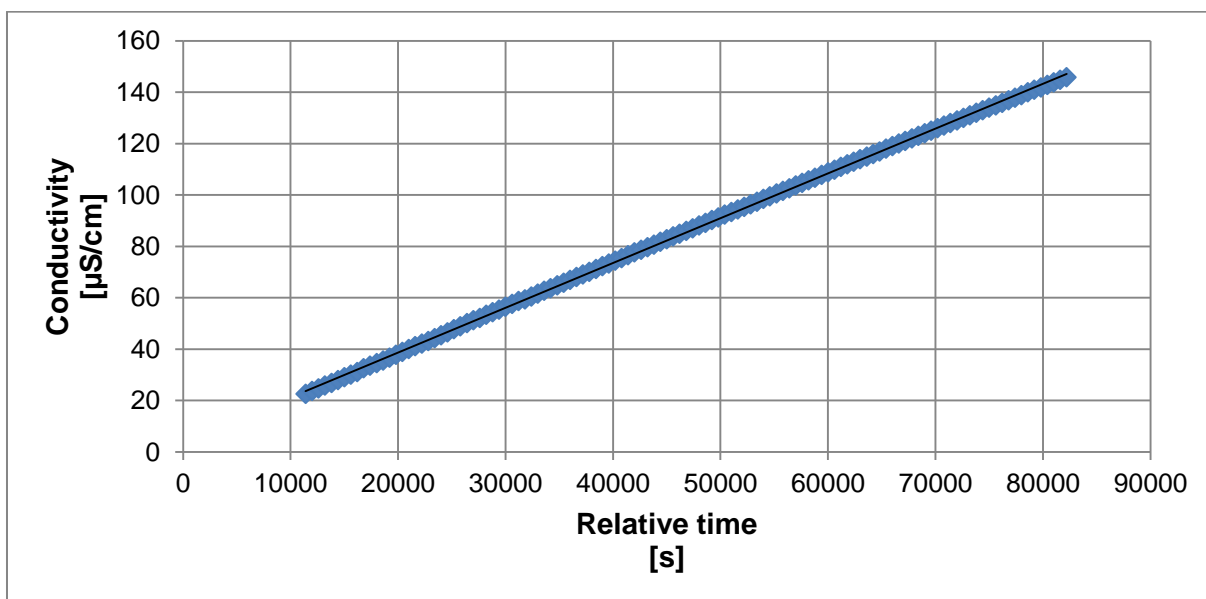
Figure 8-17: Plot of conductivity versus time for the Membrane C reference test.

In Figure 8-18 the calculated amount of salt permeated is plotted versus time.

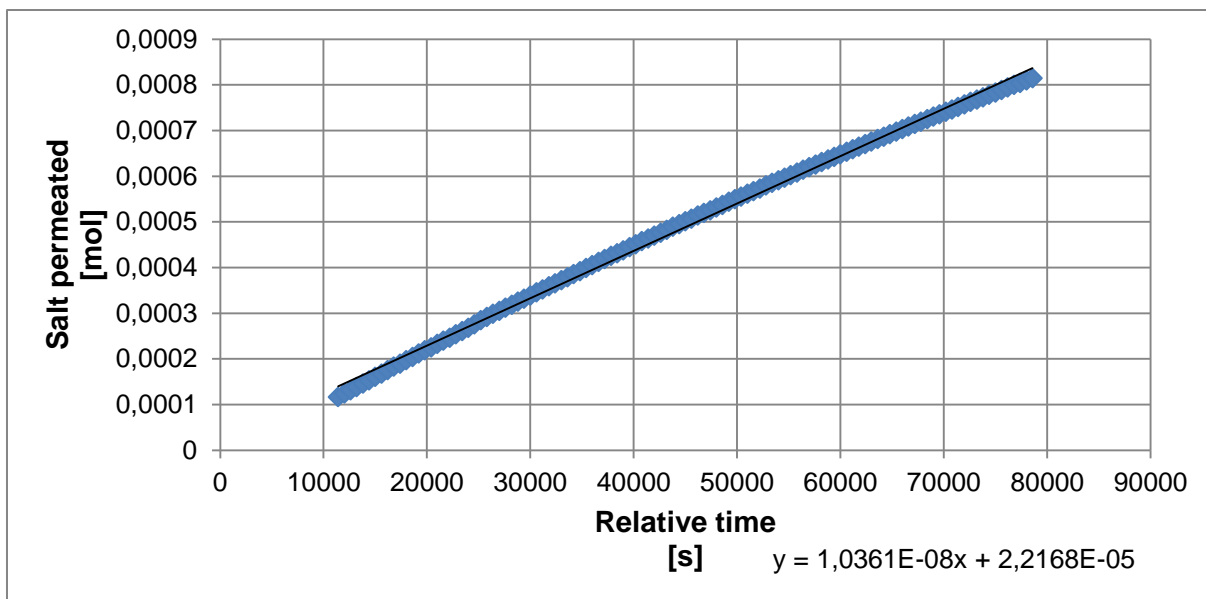**Figure 8-18: Plot of the amount of salt that has permeated to the feed, versus time for the Membrane C reference test.**

C.c   Membrane D reference test

The measured values of weight plotted versus time, is shown in Figure 8-19. The plot consists of 100 data points.
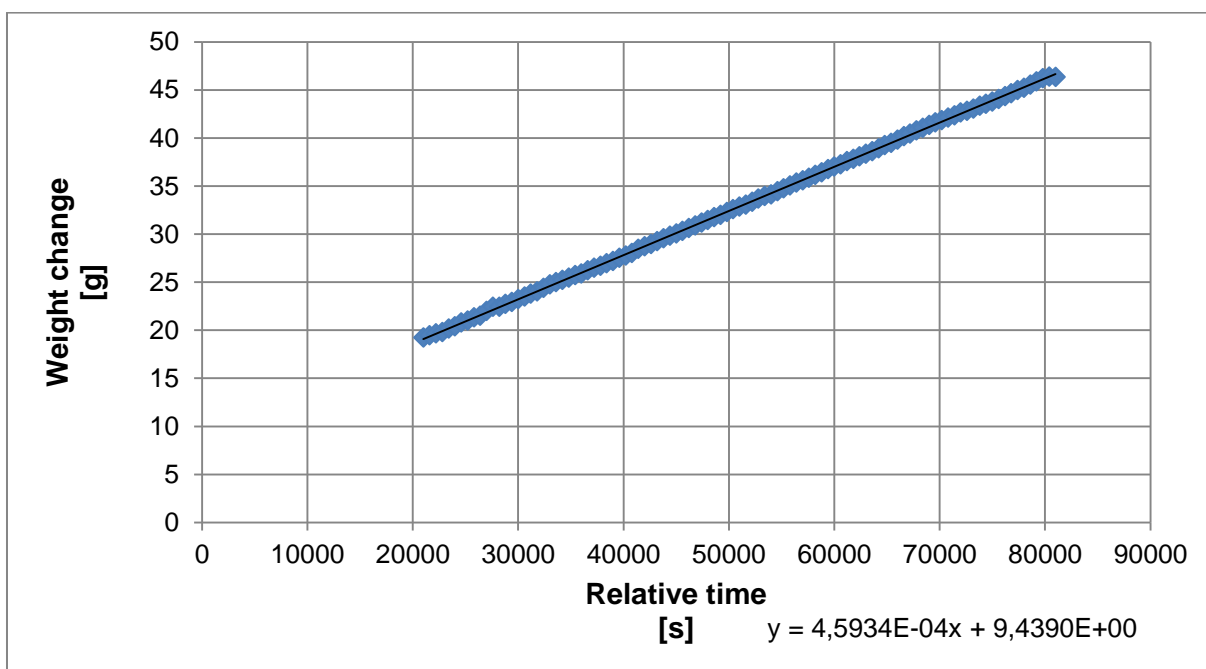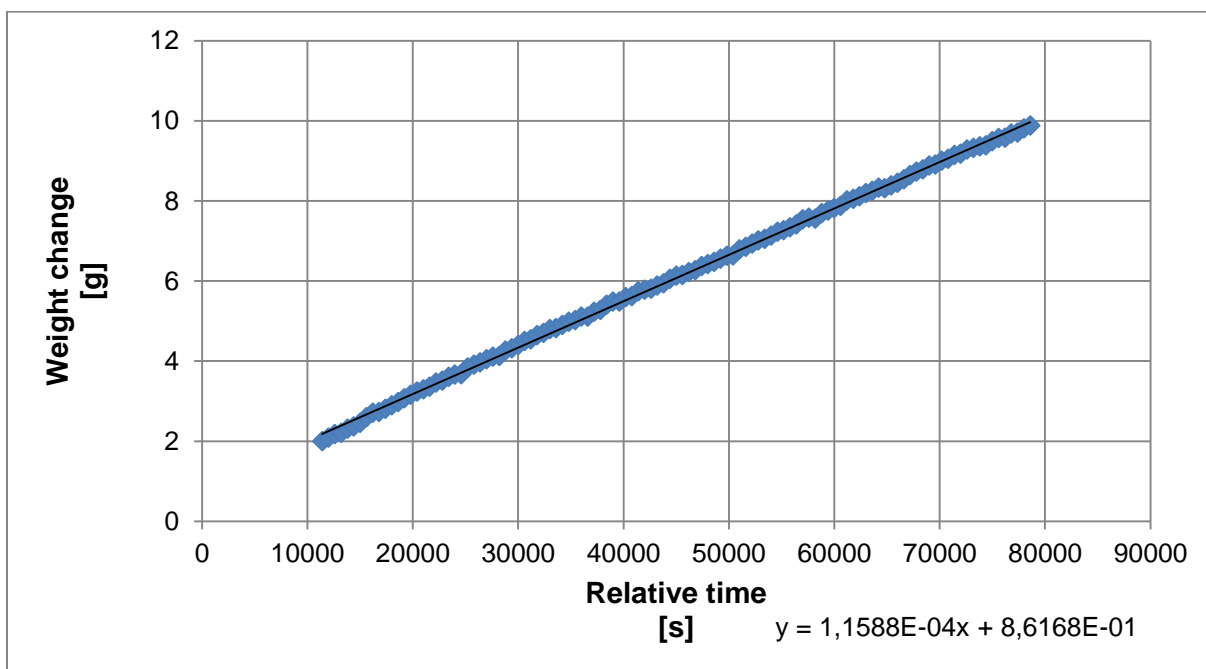

Figure 8-19: Plot of weight versus time for the Membrane D reference test.

Figure 8-20 shows the measured conductivity is plotted versus time. The plot consists of 100 points of data. These points are used in the calculation of permeated salt.

Figure 8-20: Plot of conductivity versus time for the Membrane D reference test.

Figure 8-21 shows the calculated amount of salt plotted versus time.

$y = 9{,}9658E\text{-}09x + 8{,}1656E\text{-}05$
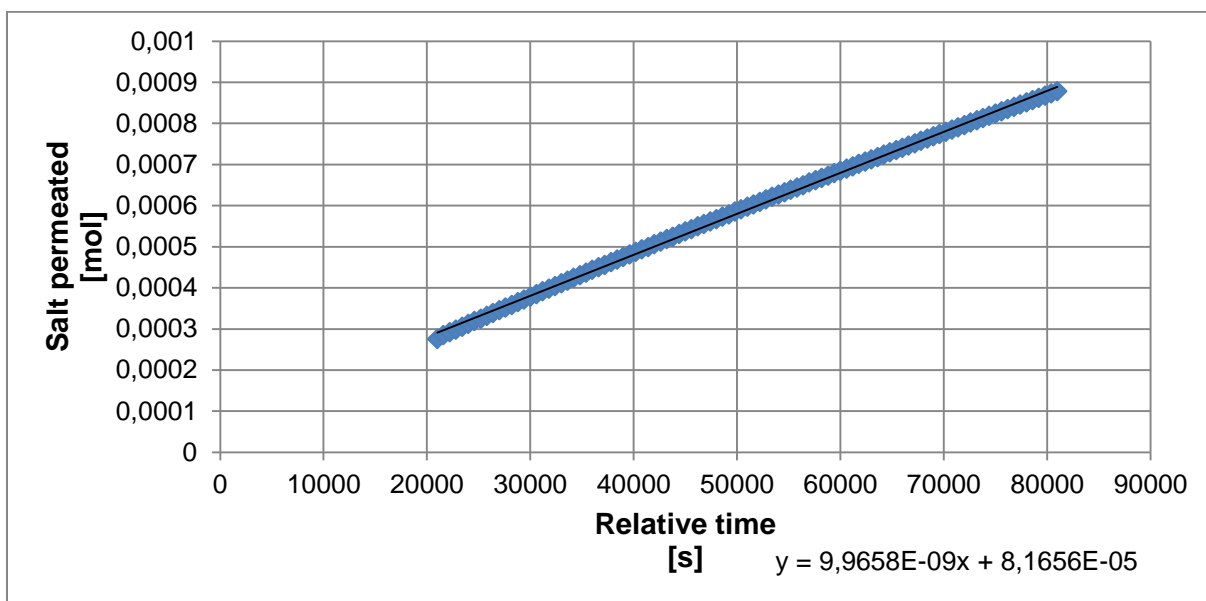
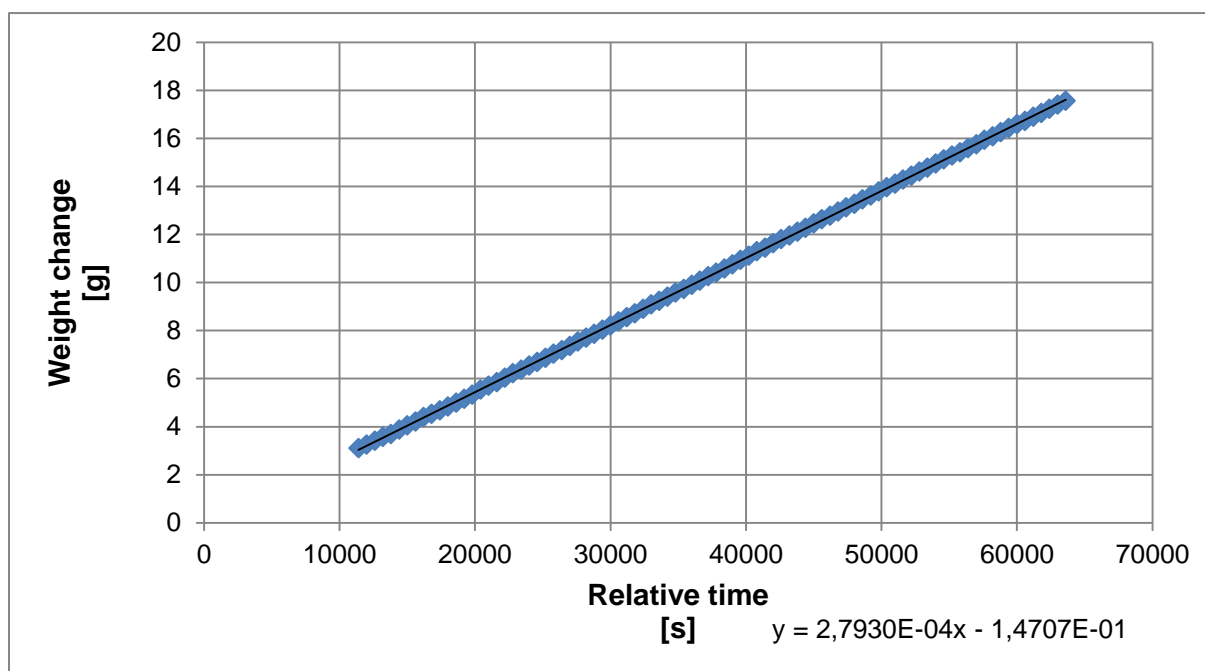**Figure 8-21: Plot of the amount of salt that has permeated to the feed, versus time for the Membrane D reference test.**

C.d   Membrane D 20 % HC test

The measured values of weight plotted versus time, is shown in Figure 8-22. The plot is consists of 97 points of data.
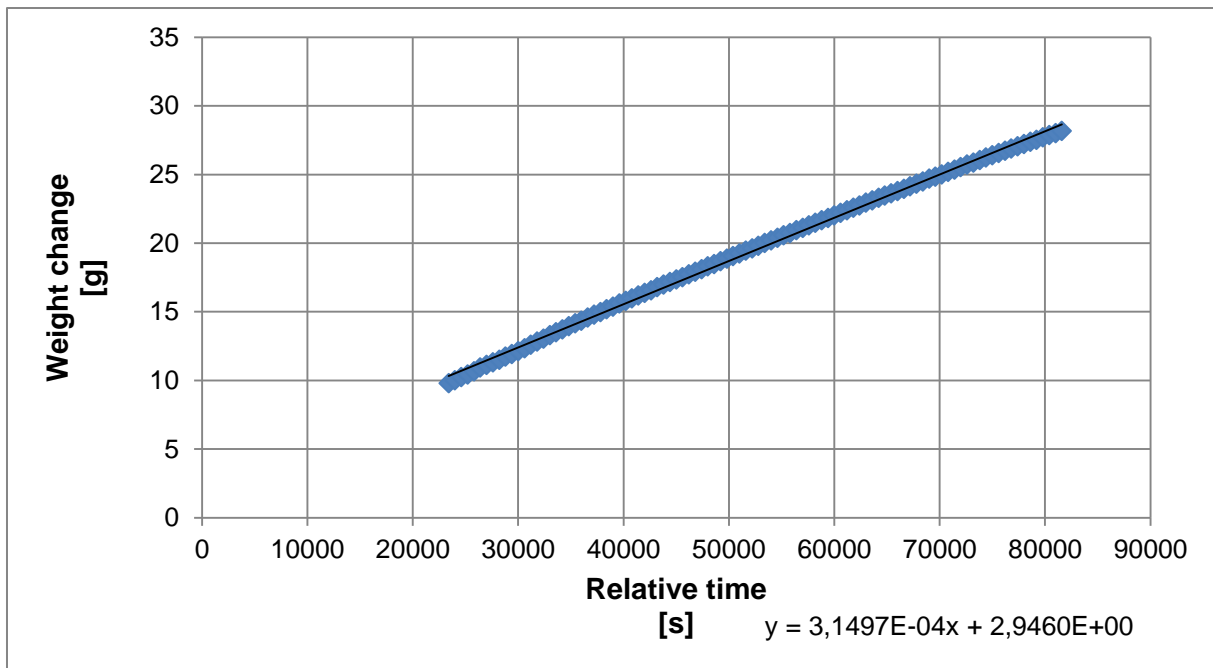
Figure 8-22: Plot of weight versus time for the Membrane D, 20 % HC test.

C.e   Membrane D 50 % HC test

Figure 8-23 shows the measured values of weight plotted versus time. The plot is based on 125 data points.
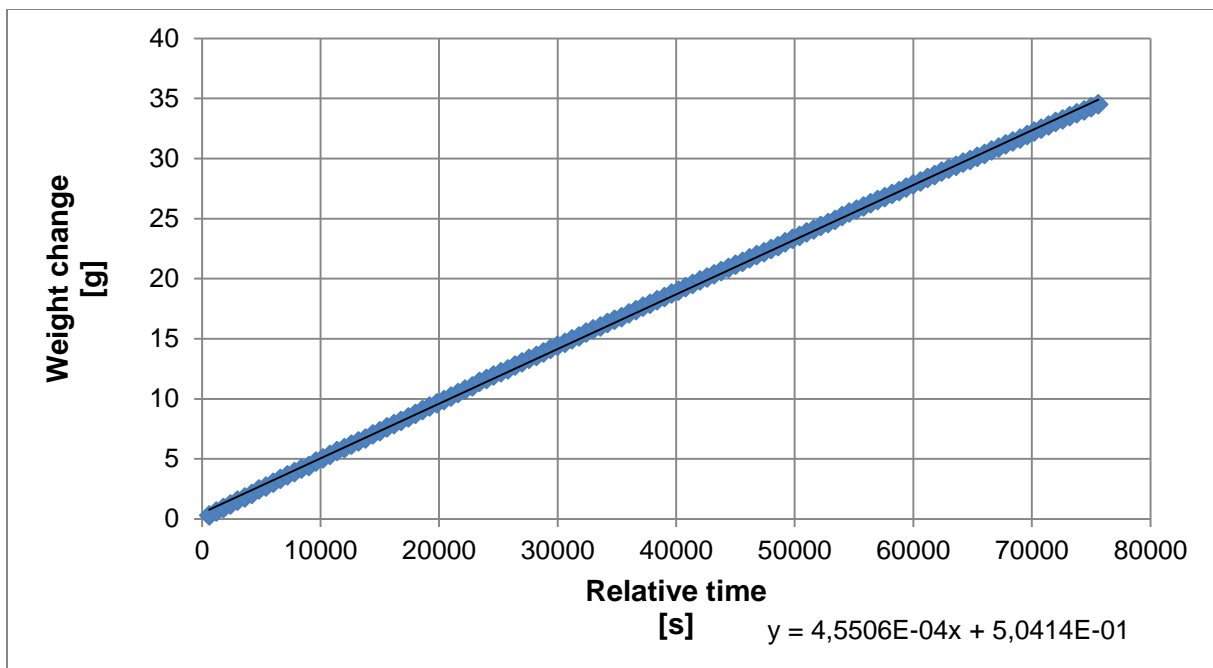
Figure 8-23: Plot of weight versus time for the Membrane D, 50 % HC test.

C.f   Membrane D 80 % HC test

The measured values of weight plotted versus time, is shown in Figure 8-24. The plot consists of 96 points of data.
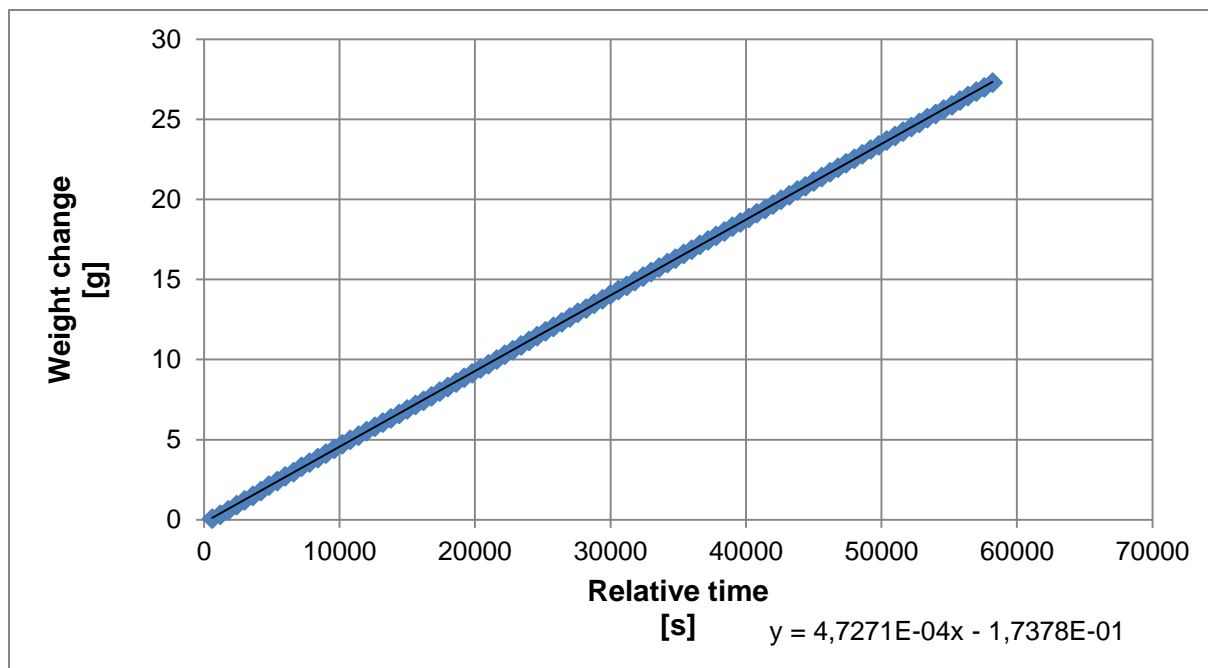
Figure 8-24: Plot of weight versus time for the Membrane D, 80 % HC test.

C.g   Membrane F reference test

Figure 8-25 shows the measured values of weight plotted versus time. The plot is created using 102 data points.
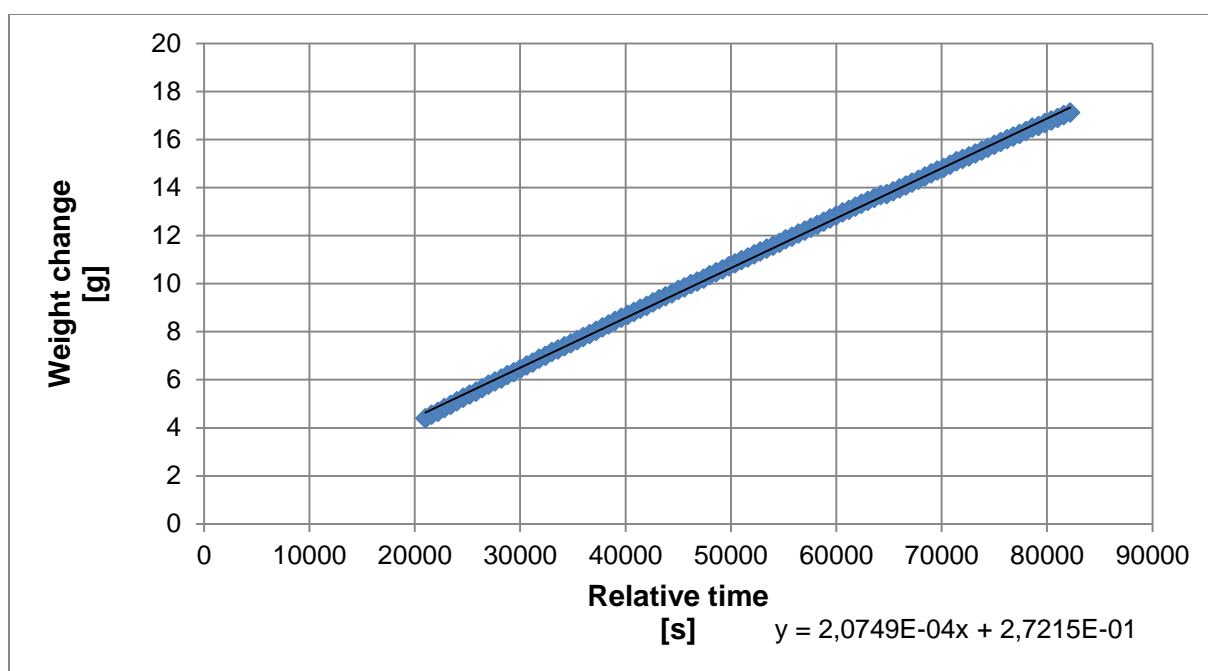
Figure 8-25: Plot of weight versus time for the Membrane F reference test.

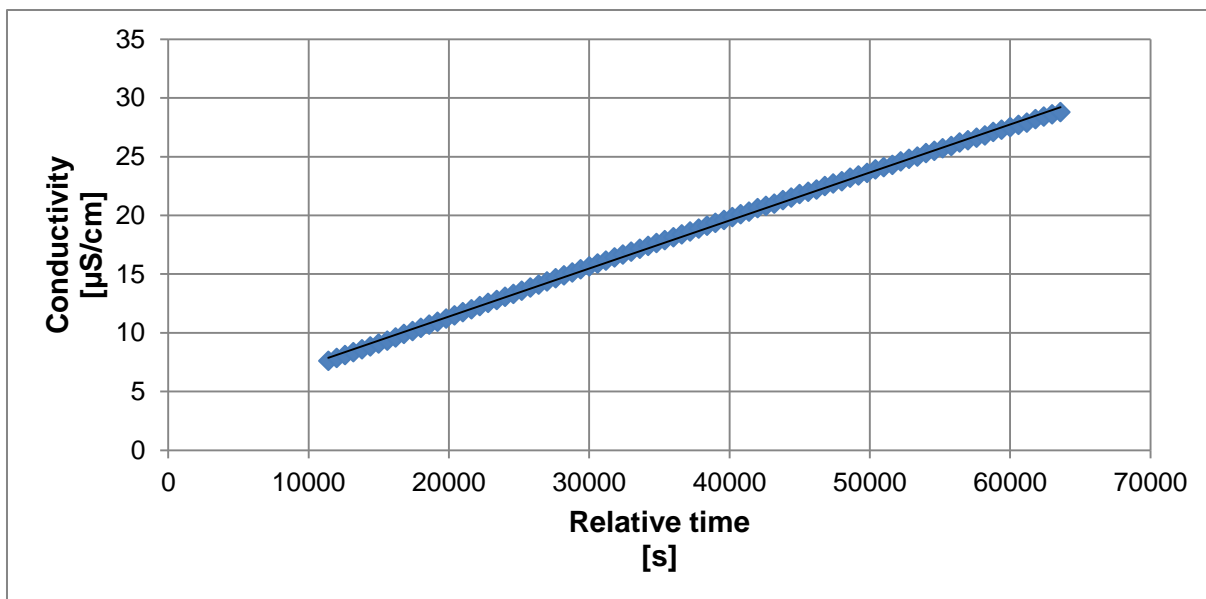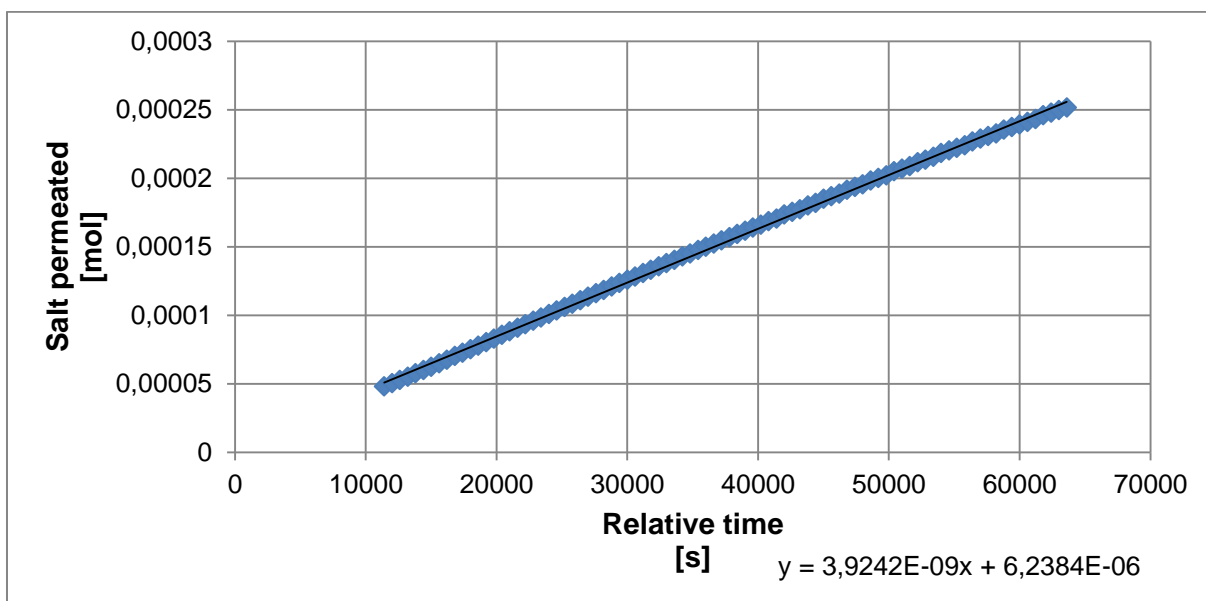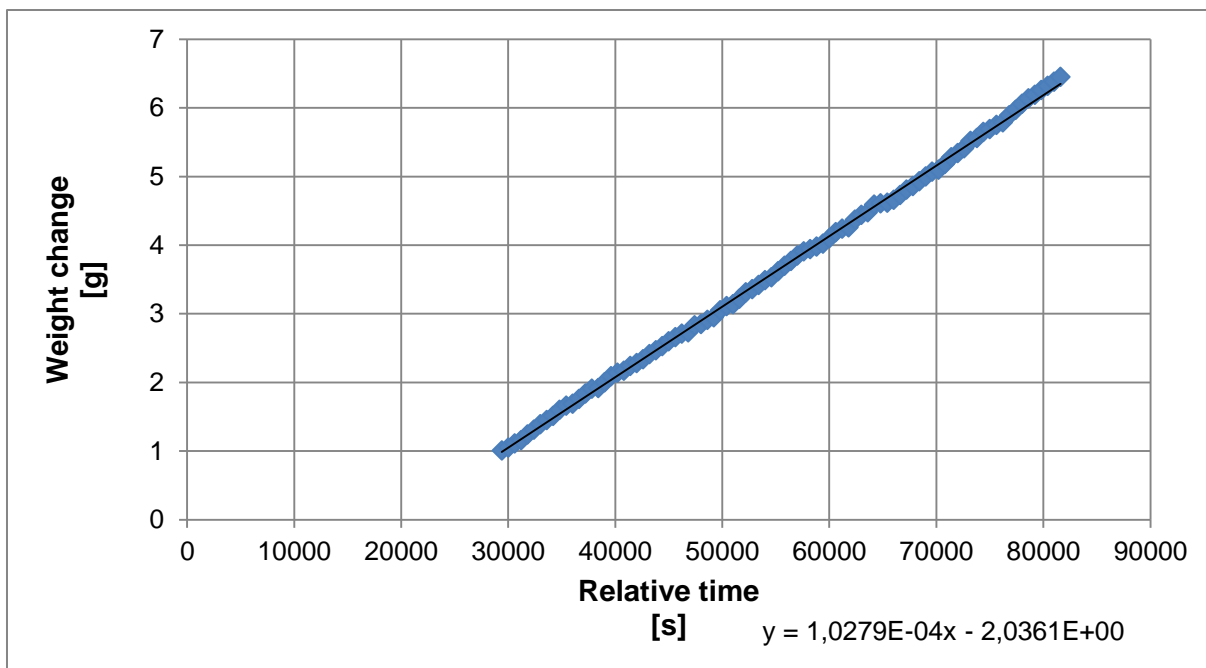In Figure 8-26 the measured conductivity is plotted versus time. The plot consists of 102 data points.
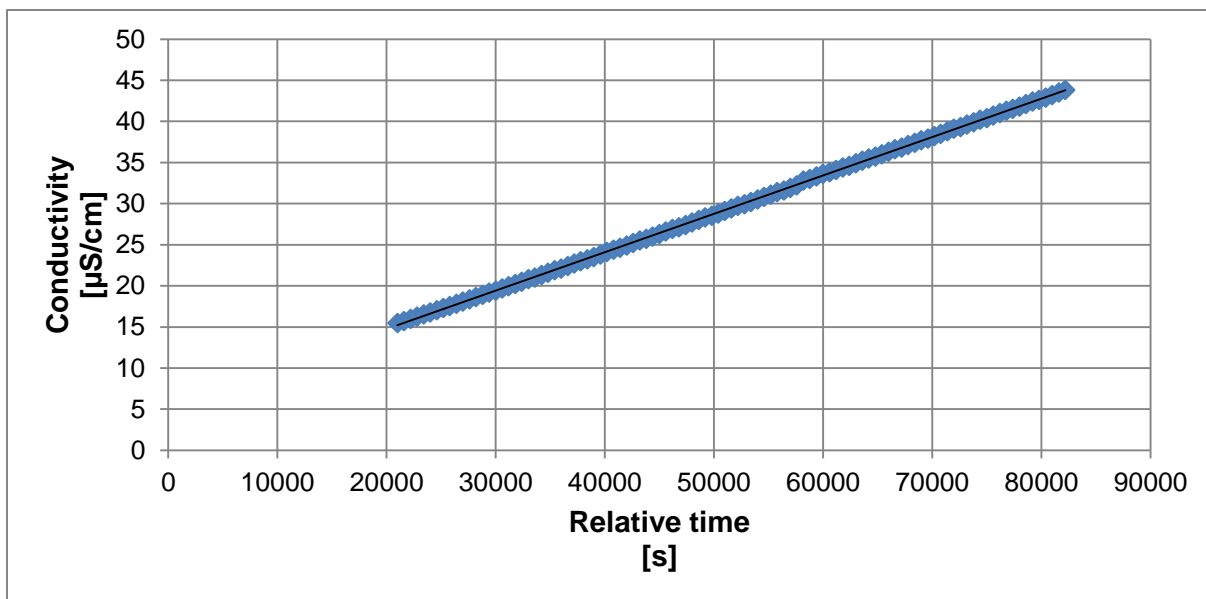
Figure 8-26: Plot of conductivity versus time for the Membrane F reference test.

In Figure 8-27 the calculated amount of salt permeated is plotted versus time.

$$y = 4,4773E\text{-}09x + 2,8293E\text{-}05$$

Figure 8-27: Plot of the amount of salt that has permeated to the feed, versus time for the Membrane F reference test.

C.h   Membrane F 20 % HC test

The measured values of weight plotted versus time, is shown in Figure 8-28. The plot is consists of 111 points of data.
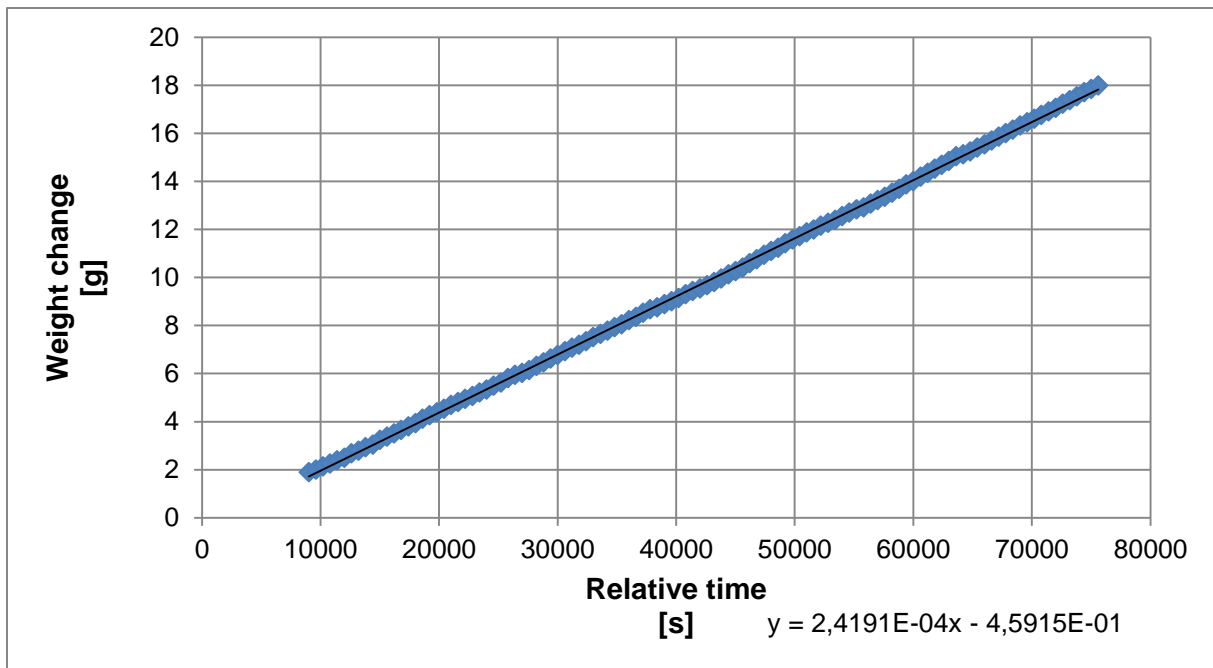
Figure 8-28: Plot of weight versus time for the Membrane F, 20 % HC test.

C.i Membrane F 50 % HC test

Figure 8-29 shows the measured values of weight plotted versus time. The plot is created using 250 data points.
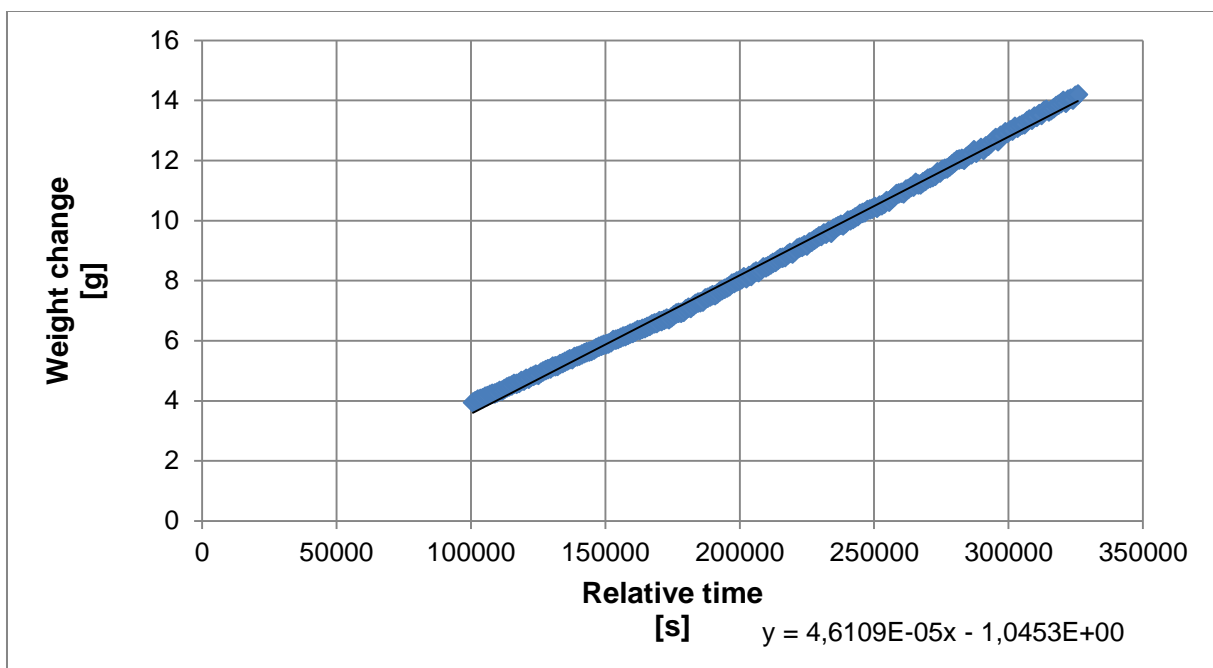
Figure 8-29: Plot of weight versus time for the Membrane F, 50 % HC test.

C.j Membrane G reference test 1

The measured values of weight plotted versus time, is shown in Figure 8-30. The plot consists of 112 points of data.
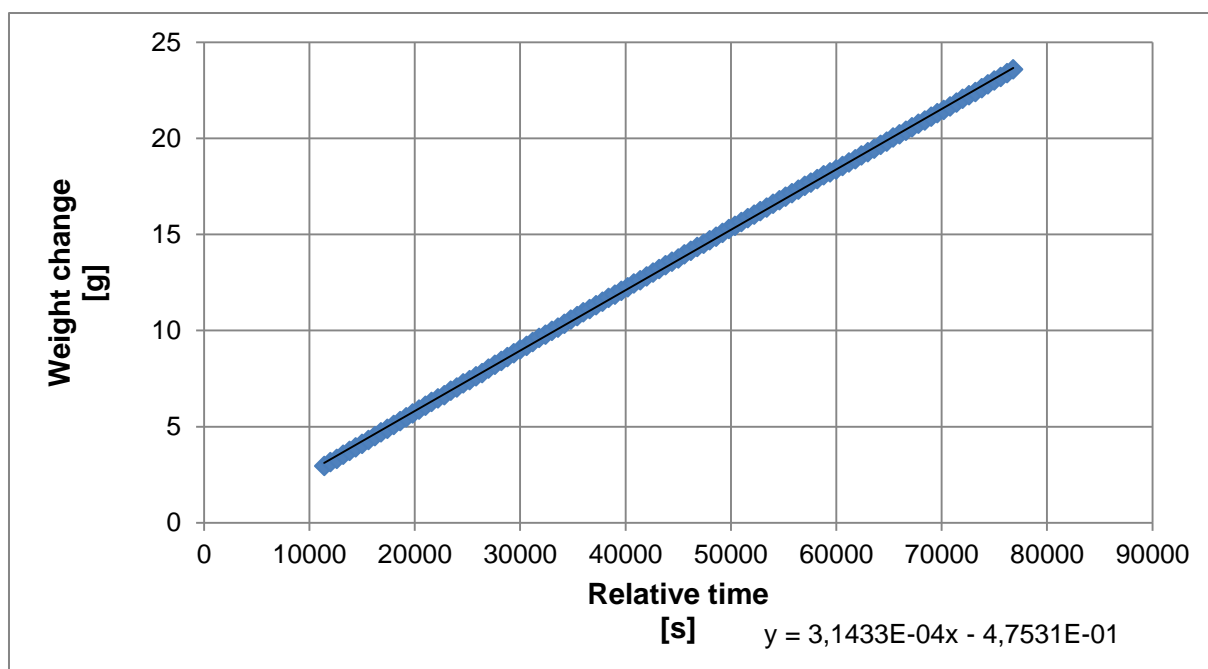
Figure 8-30: Plot of weight versus time for Membrane G reference test 1.

In Figure 8-31 the measured conductivity is plotted versus time. The plot consists of 112 data points.
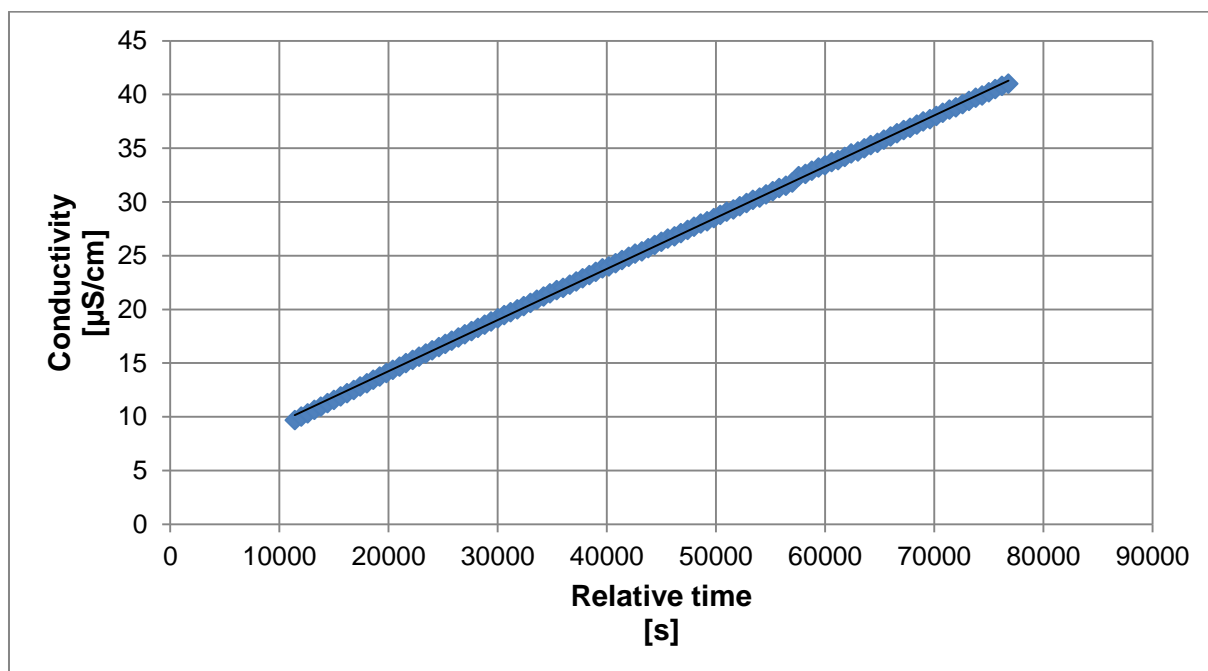

Figure 8-31: Plot of conductivity versus time for Membrane G reference test 1.

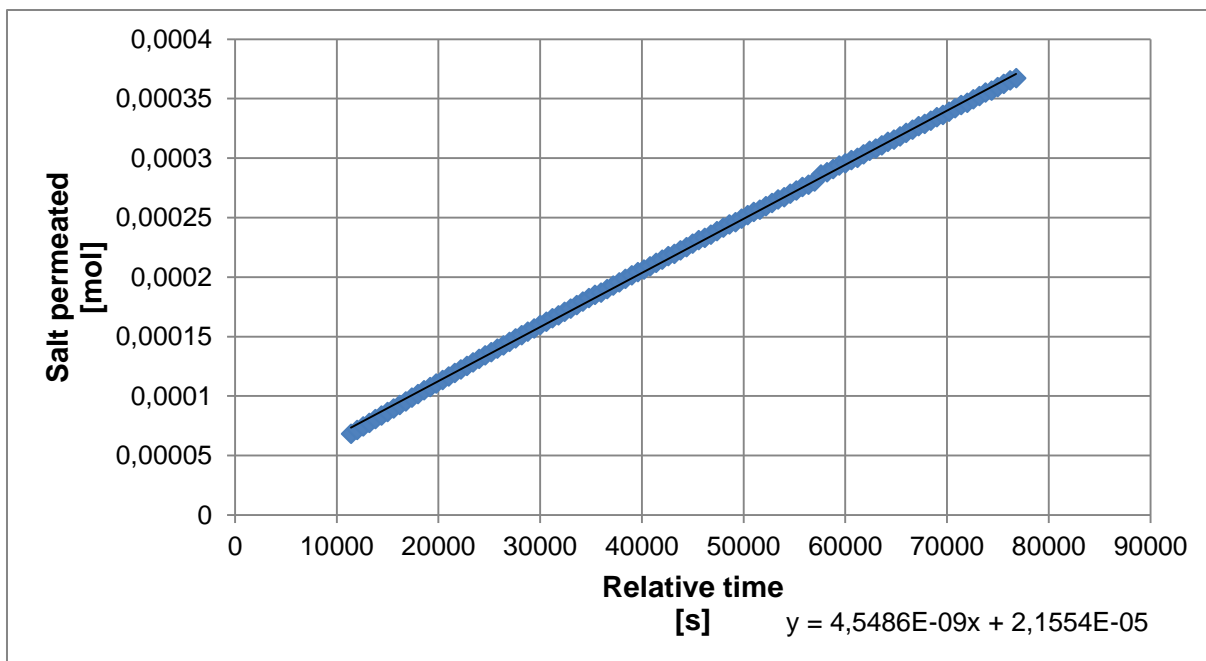Figure 8-32 shows the calculated amount of salt plotted versus time.

Figure 8-32: Plot of the amount of salt that has permeated to the feed, versus time for Membrane G reference test 1.

C.k Membrane G 20 % HC test 1

Figure 8-33 shows the measured values of weight plotted versus time. The plot is created using 112 data points.

Figure 8-33: Plot of weight versus time for Membrane G 20 % HC test 1.

Figure 8-34 shows the measured conductivity is plotted versus time. These points are used in the calculation of permeated salt which is plotted in Figure 8-35. The plots consist of 2 measurements.
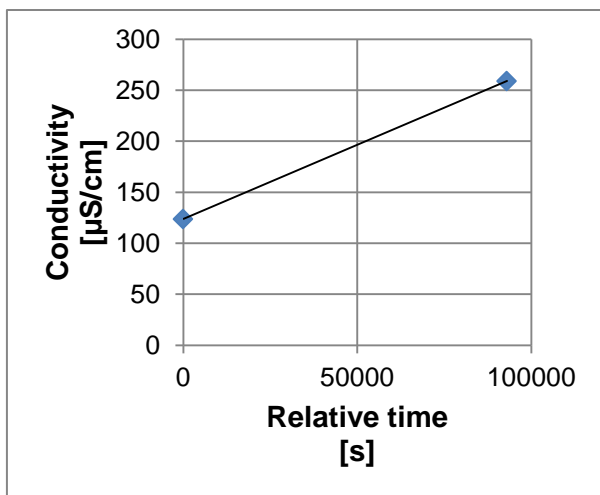
Figure 8-34: Plot of conductivity versus time for Membrane G 20 % HC test 1.

$$y = 3,7803E-09x + 3,3204E-04$$
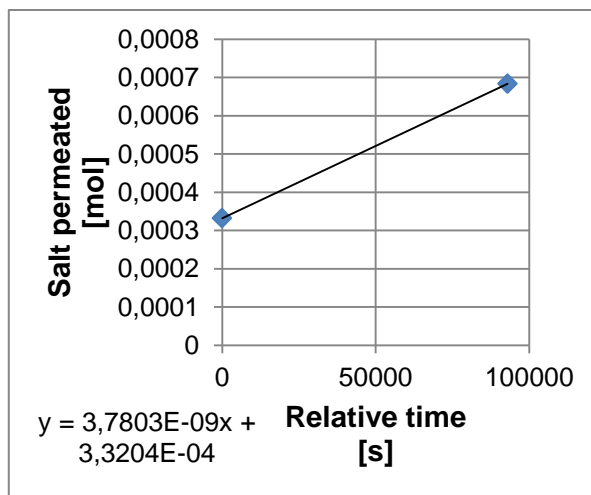
Figure 8-35: Plot of the amount of salt that has permeated to the feed, versus time for Membrane G 20 % HC test 1.

C.I   Membrane G reference test 2

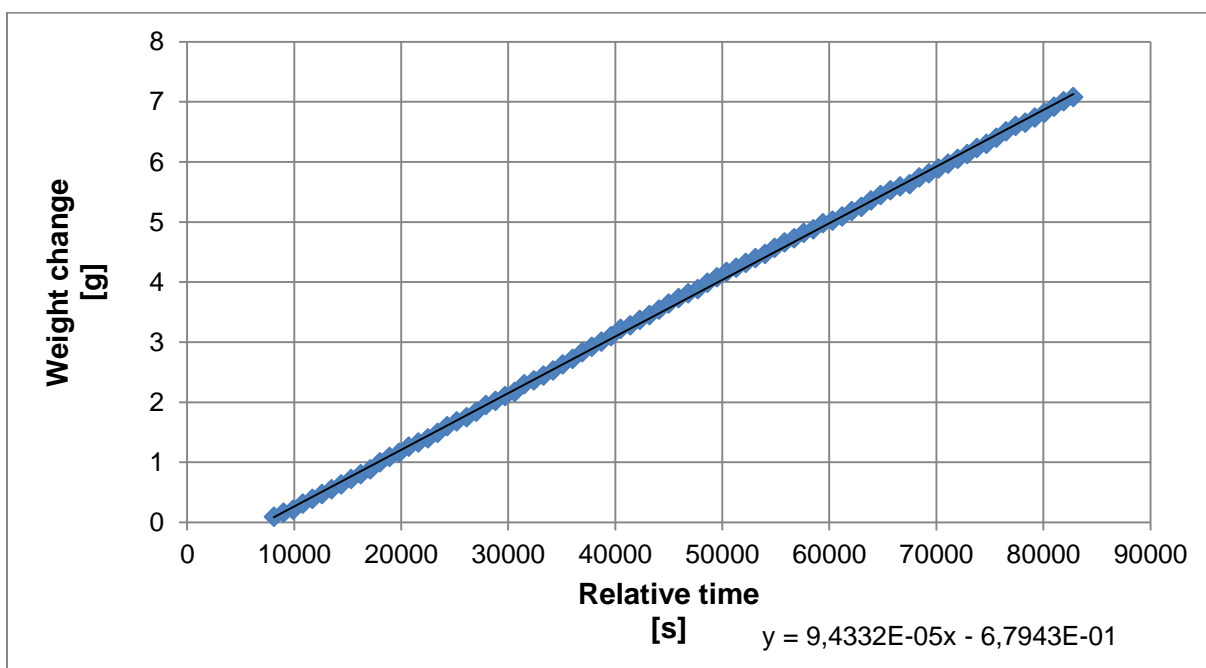Figure 8-36 shows the measured values of weight plotted versus time. The plot is created using 87 data points.
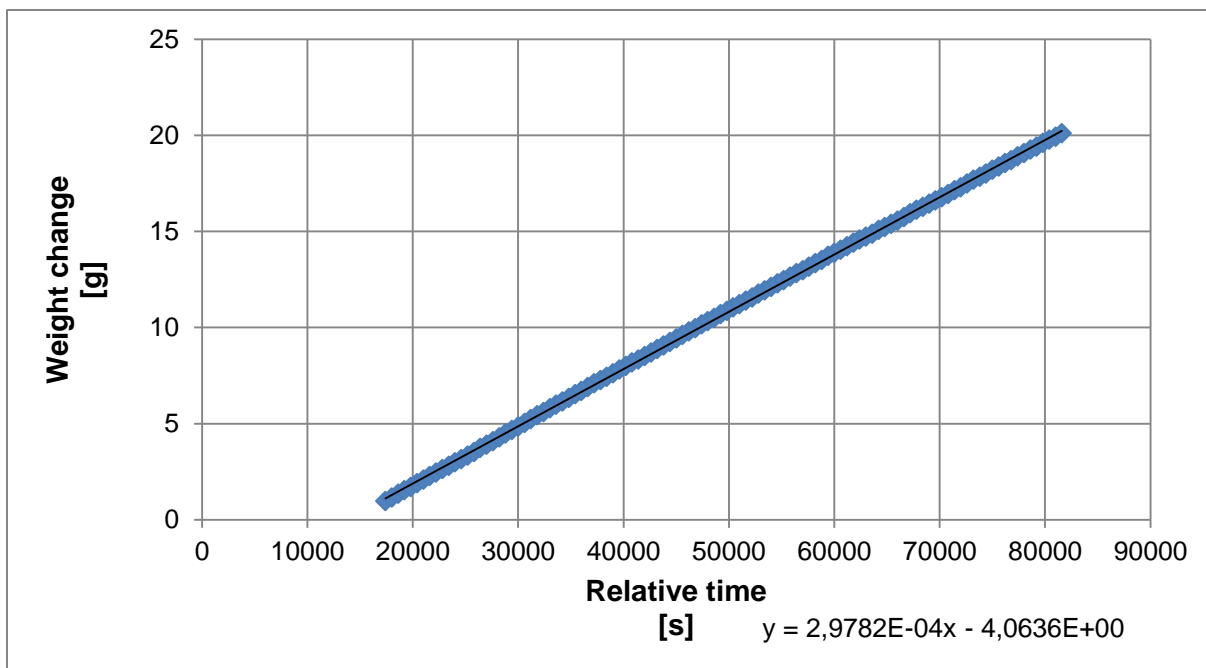

$$y = 2,7930E-04x - 1,4707E-01$$

Figure 8-36: Plot of weight versus time for Membrane G reference test 2.

Figure 8-37 the measured conductivity is plotted versus time. The plot consists of 87 data points.
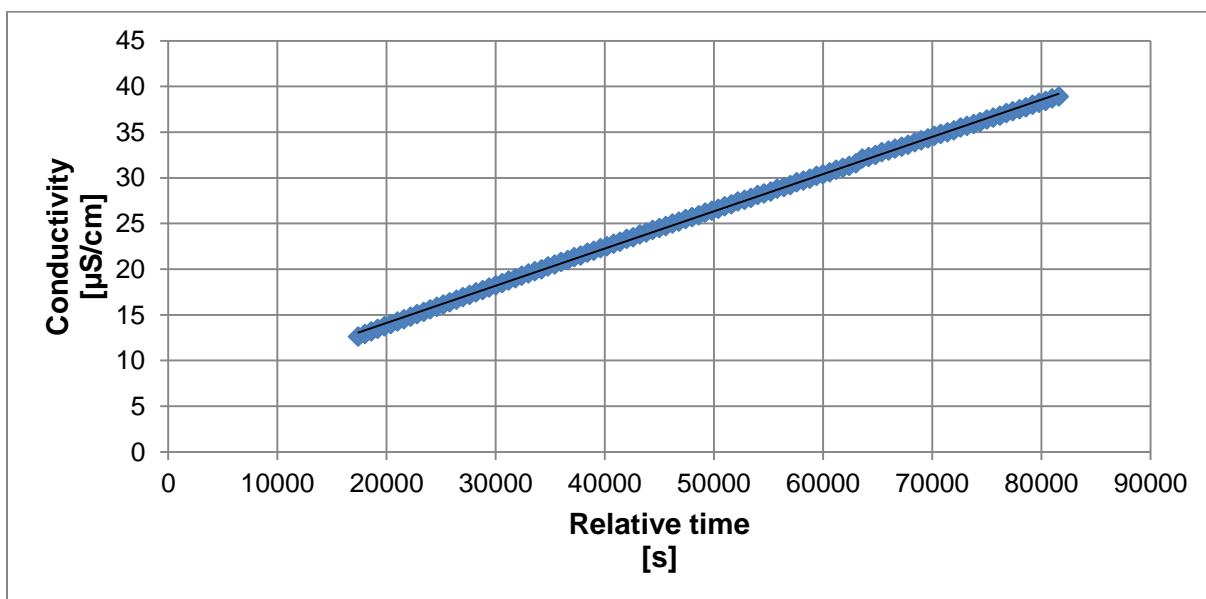
Figure 8-37: Plot of conductivity versus time for Membrane G reference test 2.

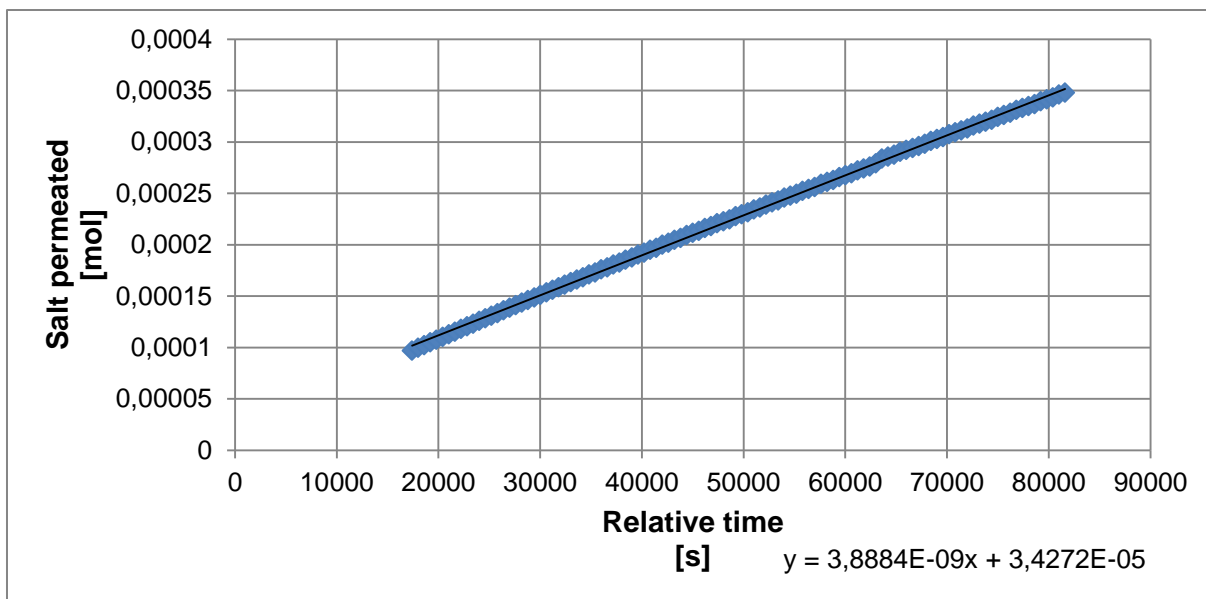Figure 8-38 shows the calculated amount of salt plotted versus time.

$$y = 3{,}9242E\text{-}09x + 6{,}2384E\text{-}06$$

Figure 8-38: Plot of the amount of salt that has permeated to the feed, versus time for Membrane G reference test 2.

C.m   Membrane G 50 % HC test 1

Figure 8-39 shows the measured values of weight plotted versus time. The plot is created using 87 data points.
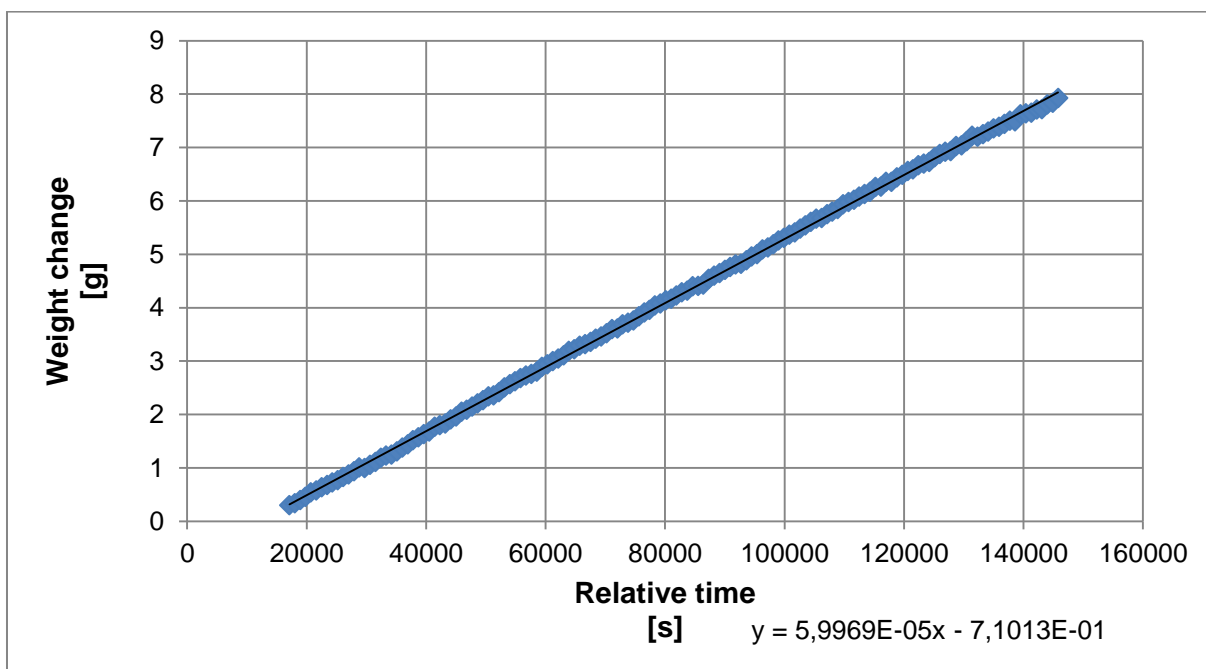
Figure 8-39: Plot of weight versus time for Membrane G 50 % HC test 1.

Figure 8-40 shows the measured conductivity is plotted versus time. These points are used in the calculation of permeated salt which is plotted in Figure 8-41. The plots consist of 2 measurements.
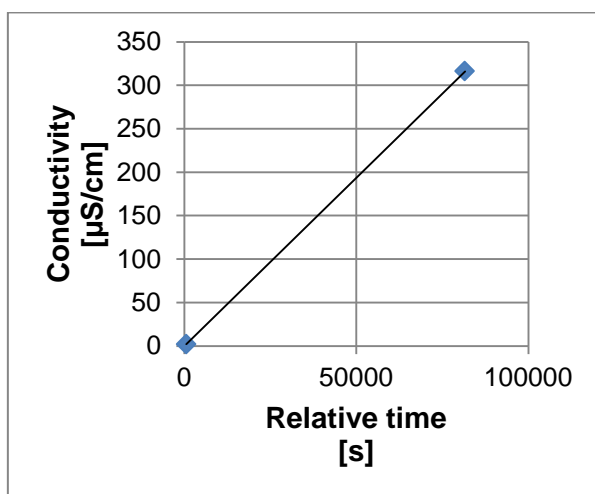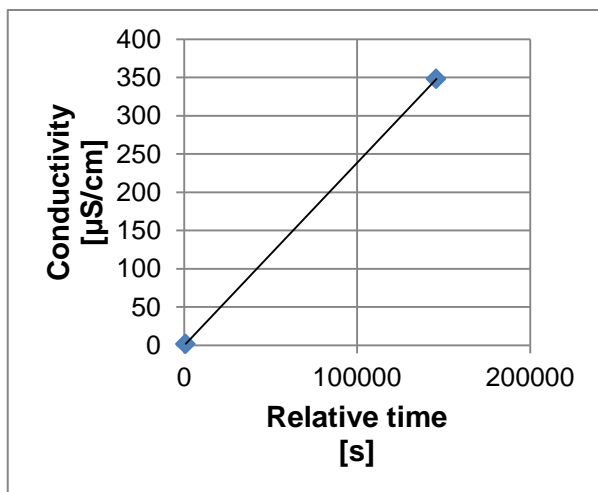

Figure 8-40: Plot of conductivity versus time for Membrane G 50 % HC test 1.
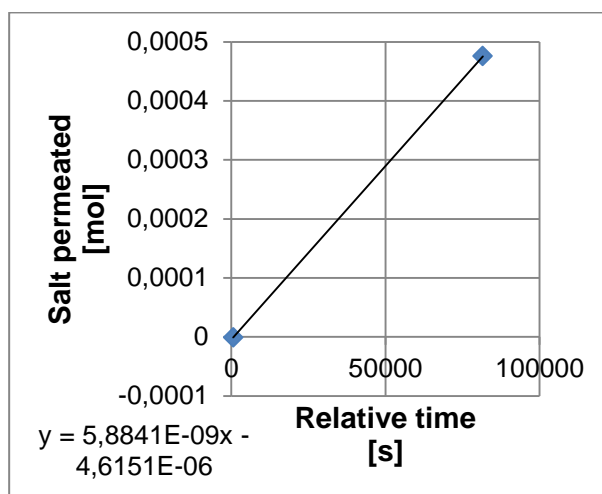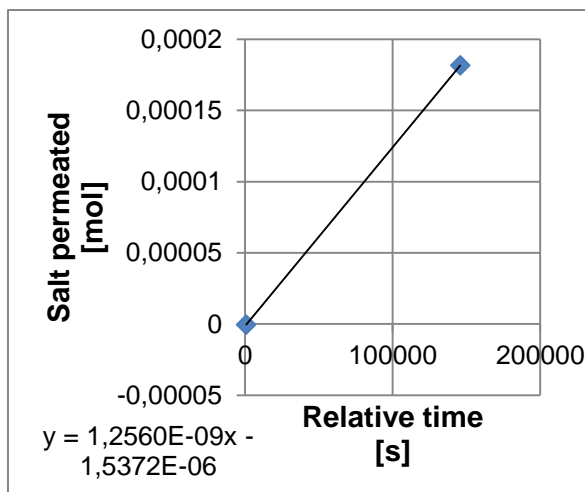

Figure 8-41: Plot of the amount of salt that has permeated to the feed, versus time for Membrane G 50 % HC test 1.

C.n   Membrane G reference test 3

In Figure 8-42 the measured values of weight is plotted versus time. The plot consists of 119 points of data.
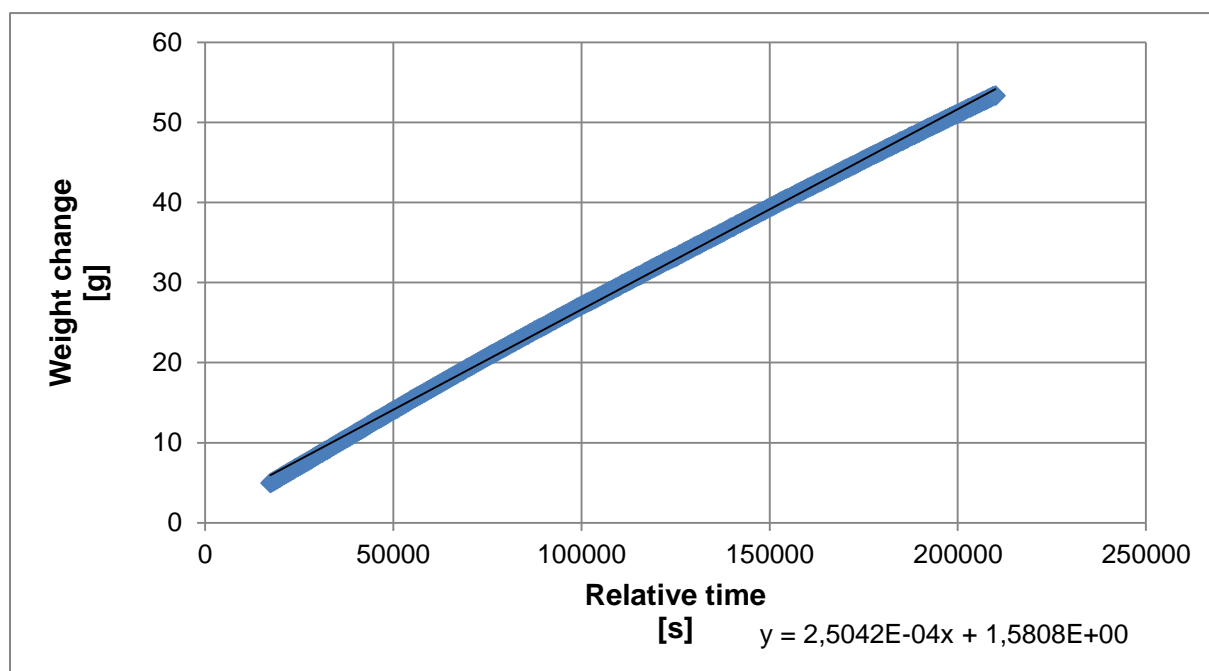
Figure 8-42: Plot of weight versus time for Membrane G reference test 3.

Figure 8-43 the measured conductivity is plotted versus time. The plot is based on 119 data points. These points are used to calculate the amount of salt permeated.
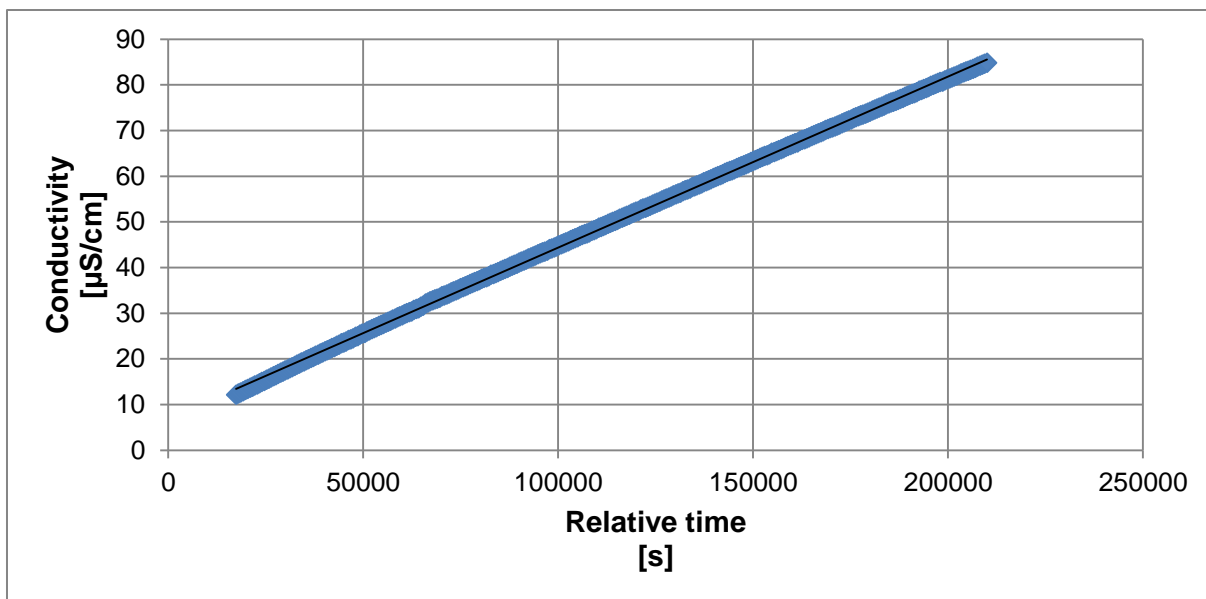

Figure 8-43: Plot of conductivity versus time for Membrane G reference test 3.

Figure 8-44 shows the calculated amount of salt plotted versus time.

Figure 8-44: Plot of the amount of salt that has permeated to the feed, versus time for Membrane G reference test 3.

C.o Membrane G 80 % HC test 1

Figure 8-45 shows the measured values of weight plotted versus time. The plot is created using 83 data points.

Figure 8-45: Plot of weight versus time for Membrane G 80 % HC test 1.

C.p Membrane G reference test 4

Figure 8-46 shows the measured values of weight plotted versus time. The plot is created using 107 data points.

Figure 8-46: Plot of weight versus time for Membrane G reference test 4.

Figure 8-47 the measured conductivity is plotted versus time. The plot is based on 107 data points.

Figure 8-47: Plot of conductivity versus time for Membrane G reference test 4.

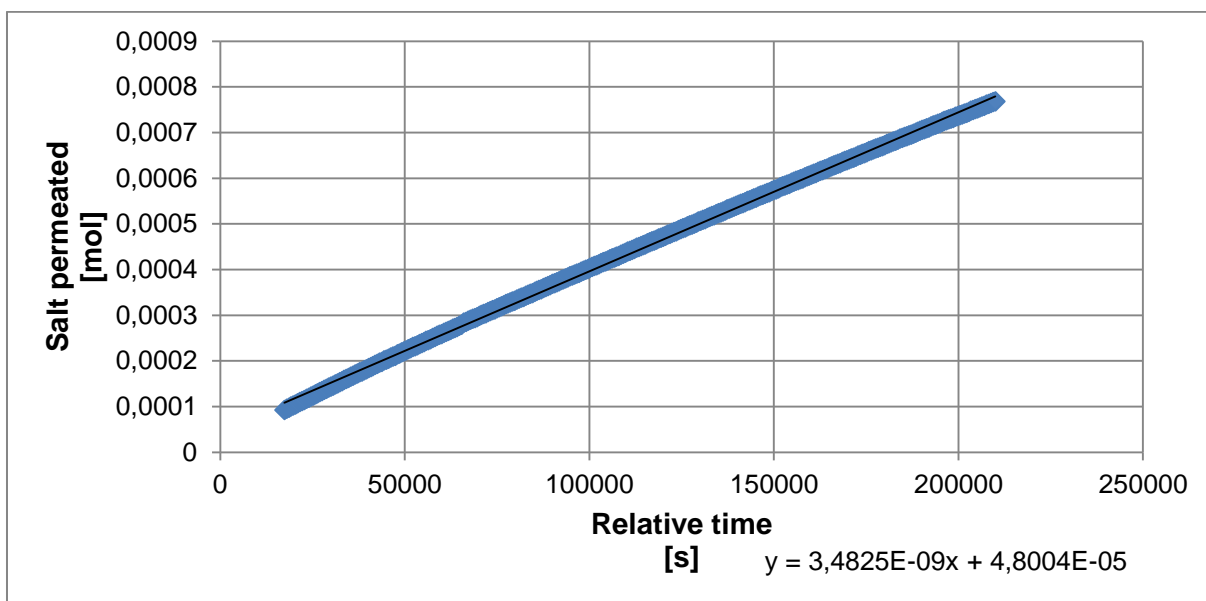Figure 8-48 shows the calculated amount of salt plotted versus time.

Figure 8-48: Plot of the amount of salt that has permeated to the feed, versus time for Membrane G reference test 4.

C.q   Membrane G 80 % HC test 2

Figure 8-49 shows the measured values of weight plotted versus time. The plot consists of 143 data points.
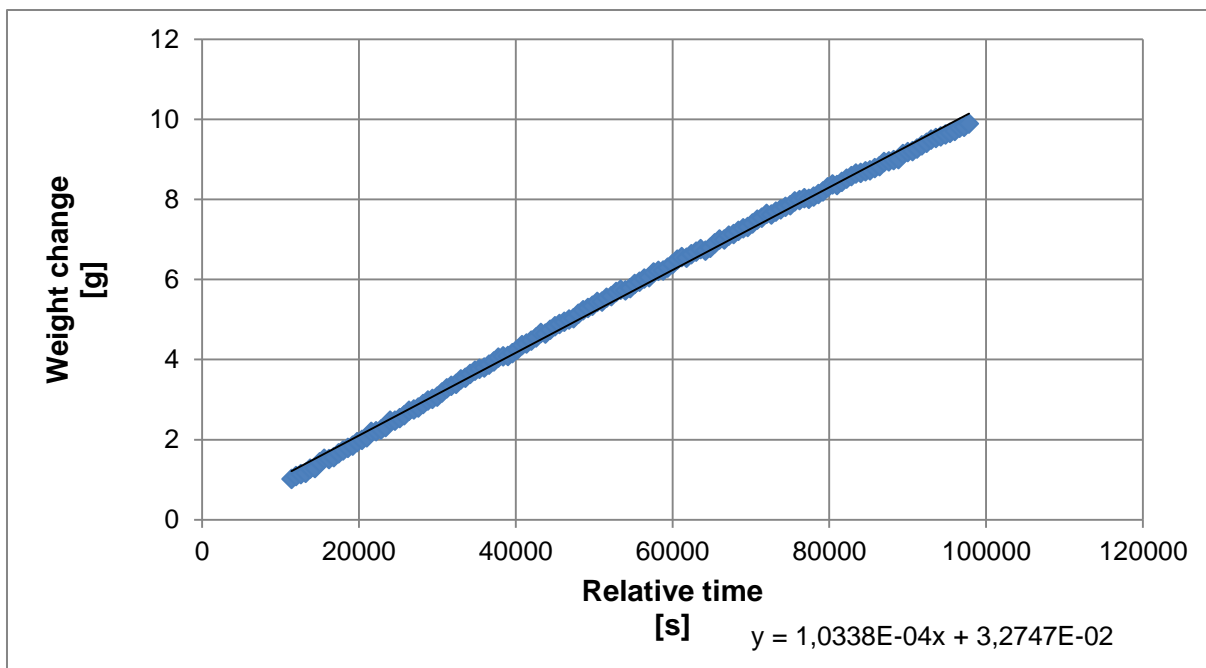

Figure 8-49: Plot of weight versus time for Membrane G 80 % HC test 2.

Figure 8-50 shows the measured conductivity is plotted versus time. These points are used in the calculation of permeated salt which is plotted in Figure 8-51. The plots consist of 2 measurements.
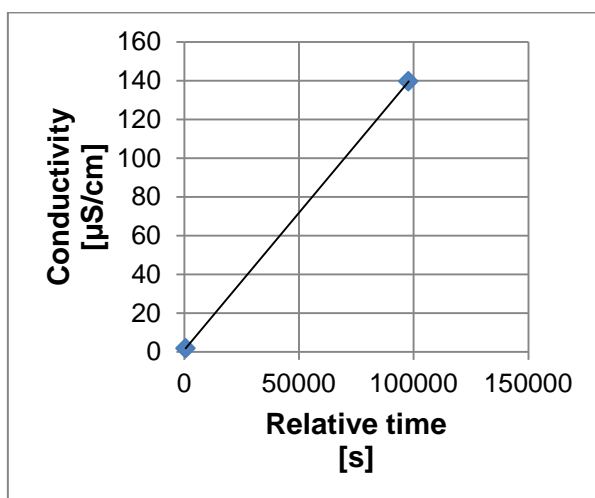
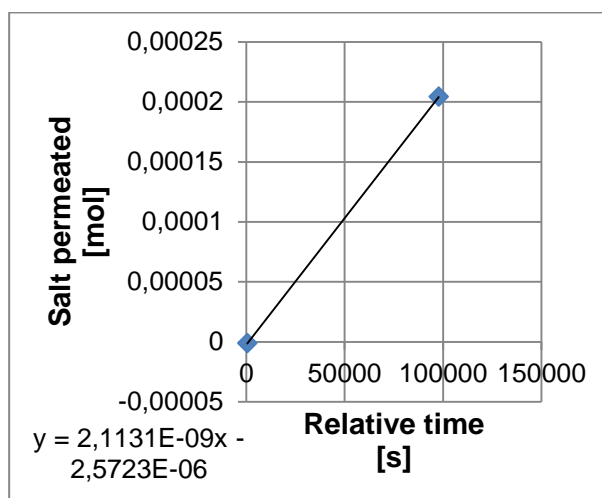**Figure 8-50: Plot of conductivity versus time for Membrane G 80 % HC test 2.**

Figure 8-51: Plot of the amount of salt that has permeated to the feed, versus time for Membrane G 80 % HC test 2.

C.r   Membrane G reference test 5

Figure 8-52 shows the measured values of weight plotted versus time. The plot is created using 321 data points.
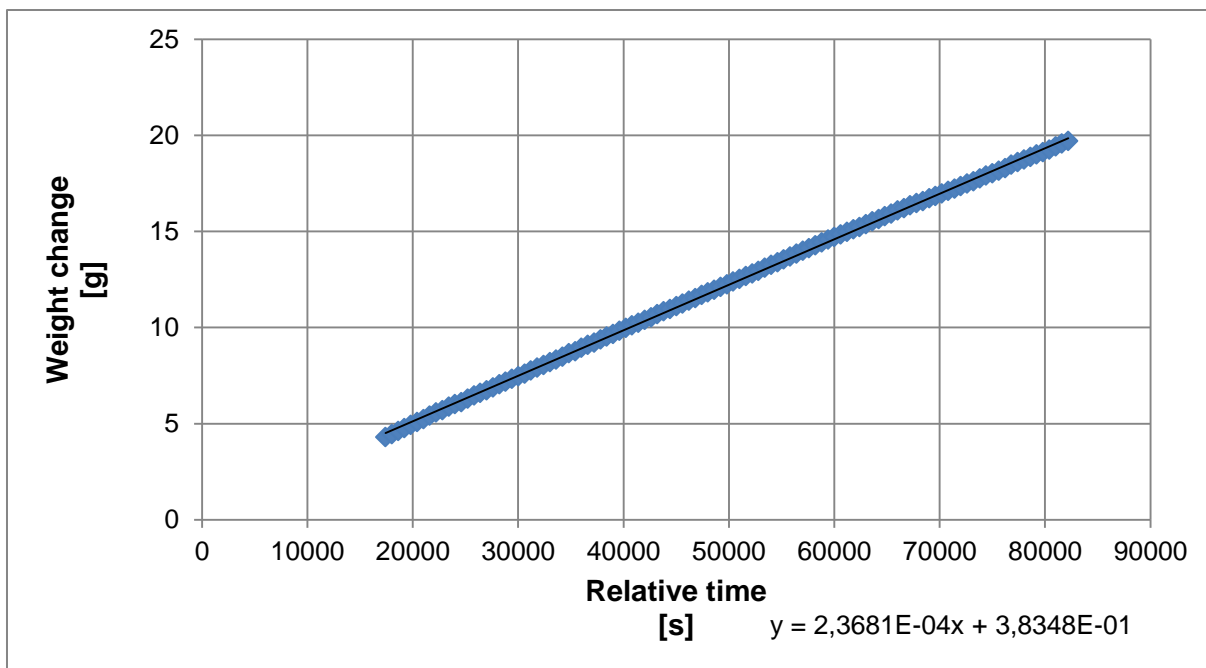

Figure 8-52: Plot of weight versus time for Membrane G reference test 5.

Figure 8-53 the measured conductivity is plotted versus time. The plot is based on 321 data points.

Figure 8-53: Plot of conductivity versus time for Membrane G reference test 5.

Figure 8-54 shows the calculated amount of salt plotted versus time.

y = 3,4825E-09x + 4,8004E-05

Figure 8-54: Plot of the amount of salt that has permeated to the feed, versus time for Membrane G reference test 5.

C.s   Membrane G 50 % HC test 2

Figure 8-55 shows the measured values of weight plotted versus time. The plot is created using 144 data points.

Figure 8-55: Plot of weight versus time for Membrane G 50 % HC test 2.

Figure 8-56 shows the measured conductivity is plotted versus time. These points are used in the calculation of permeated salt which is plotted in Figure 8-57. The plots consist of 2 measurements.
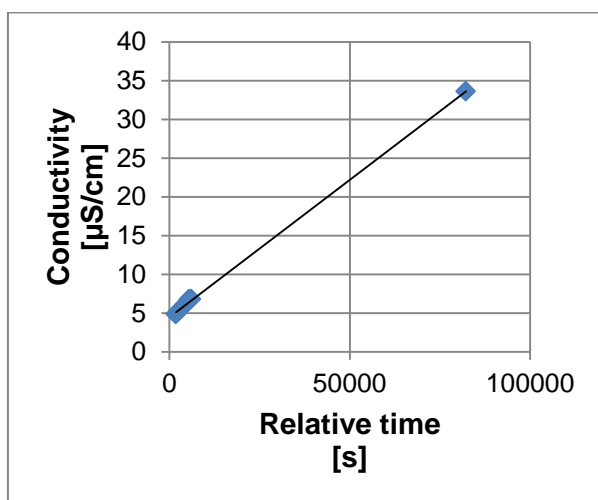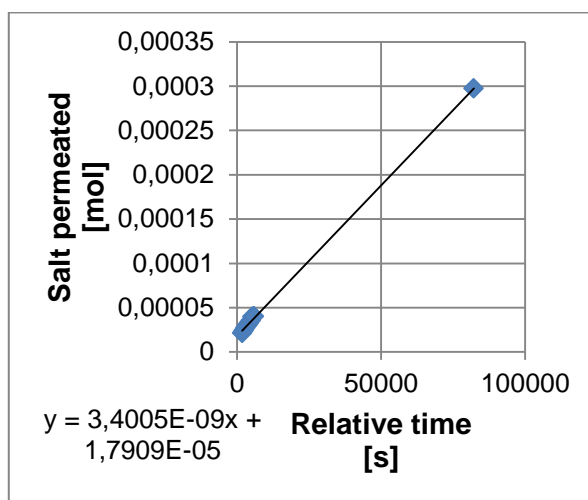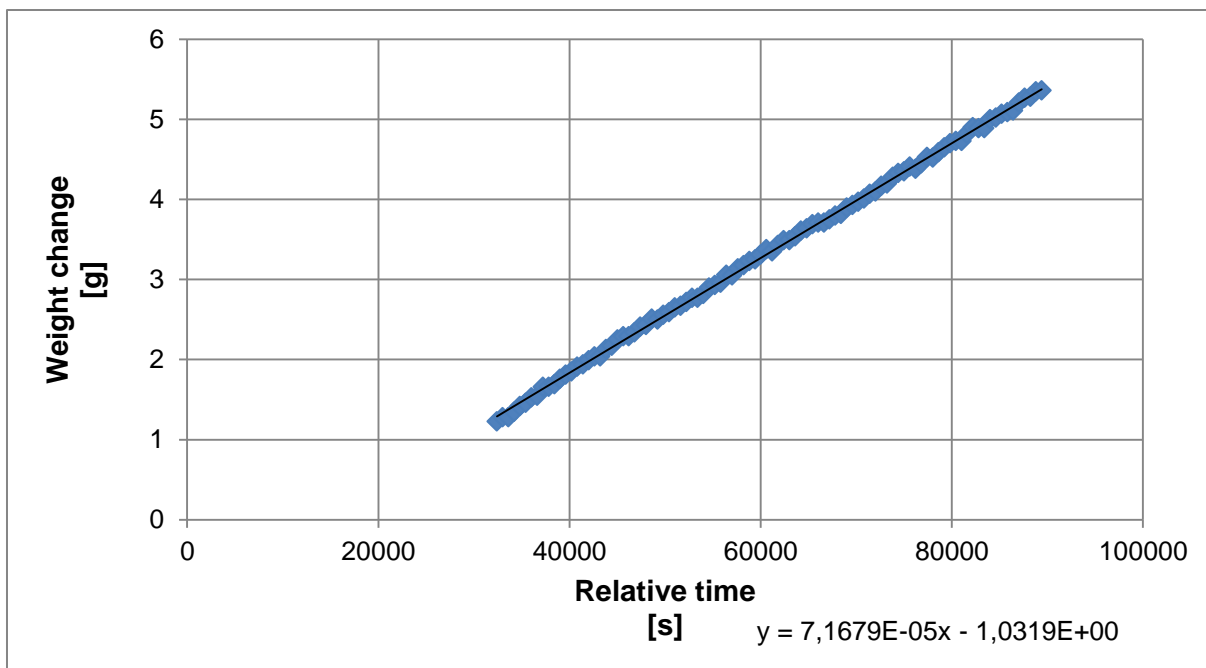

Figure 8-56: Plot of conductivity versus time for Membrane G 50 % HC test 2.

Figure 8-57: Plot of the amount of salt that has permeated to the feed, versus time for Membrane G 50 % HC test 2.

C.t   Membrane G reference test 6

Figure 8-58 shows the measured values of weight plotted versus time. The plot is created using 108 data points.

74

Figure 8-58: Plot of weight versus time for Membrane G reference test 6.

Figure 8-59 shows the measured conductivity is plotted versus time. These points are used in the calculation of permeated salt which is plotted in Figure 8-60. The plots consist of 11 measurements due to an error in the conductivity data logging.
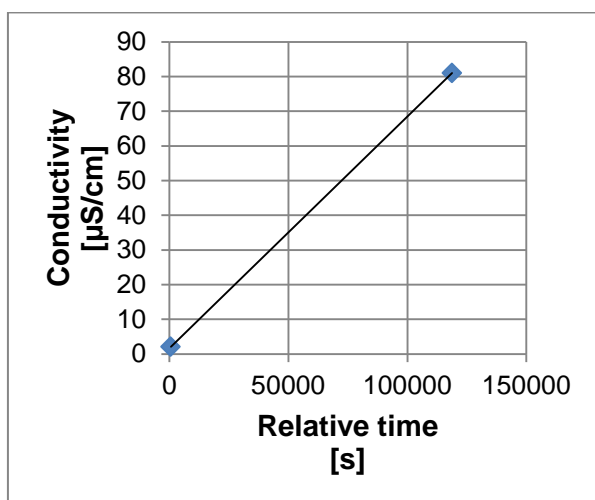

Figure 8-59: Plot of conductivity versus time for Membrane G reference test 6.

Figure 8-60: Plot of the amount of salt that has permeated to the feed, versus time for Membrane G reference test 6.

C.u   Membrane G 20 % HC test 2

Figure 8-61 shows the measured values of weight plotted versus time. The plot is created using 95 data points.

Figure 8-61: Plot of weight versus time for Membrane G 20 % HC test 2.

$y = 7,1679E\text{-}05x - 1,0319E\text{+}00$

Figure 8-62 shows the measured conductivity is plotted versus time. These points are used in the calculation of permeated salt which is plotted in Figure 8-63. The plots consist of 2 measurements.

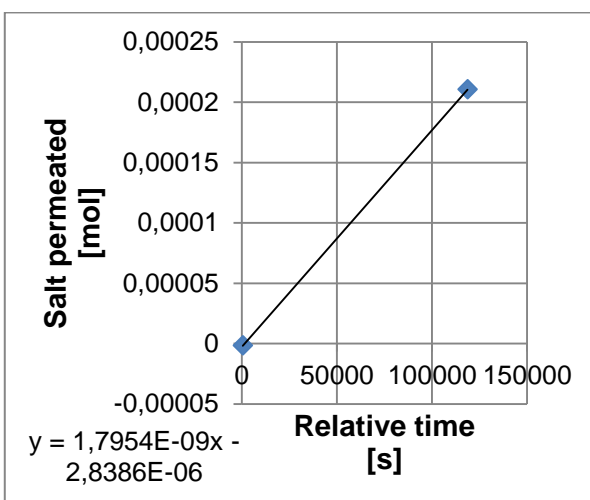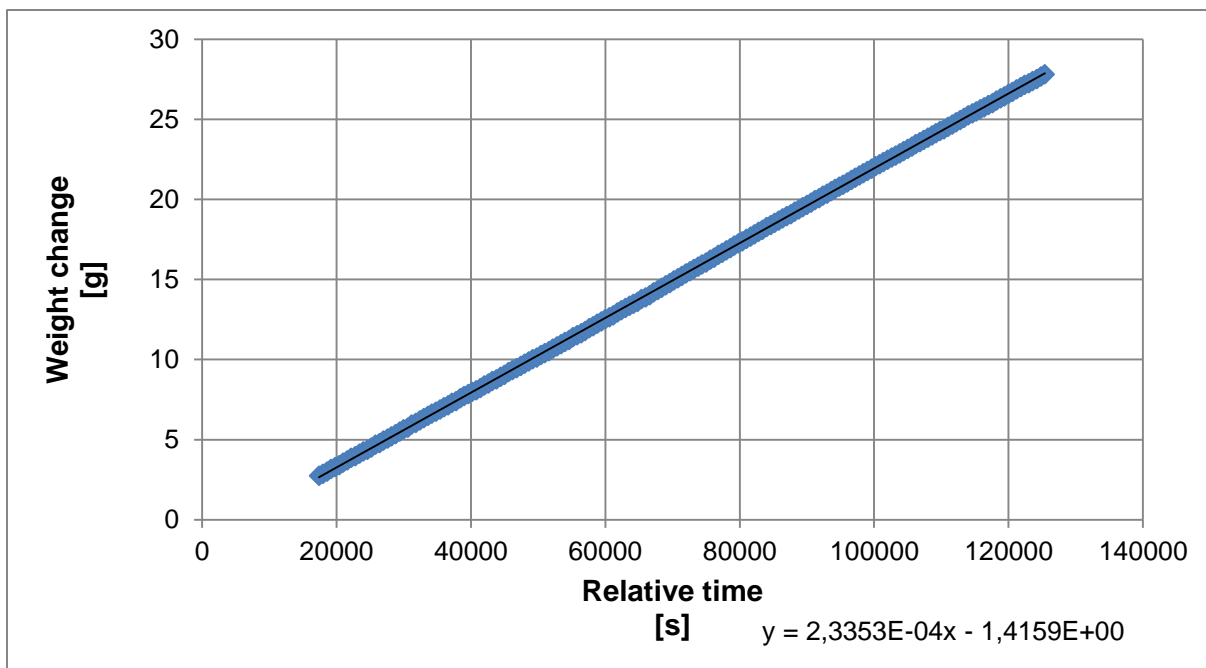**Figure 8-62: Plot of conductivity versus time for Membrane G 20 % HC test 2.**

$y = 1,7954E\text{-}09x - 2,8386E\text{-}06$

Figure 8-63: Plot of the amount of salt that has permeated to the feed, versus time for Membrane G 20 % HC test 2.

C.v   Membrane G reference test 7

Figure 8-64 the measured values of weight is plotted versus time. The plot consists of 180 points of data.

Figure 8-64: Plot of weight versus time for Membrane G reference test 7.

In Figure 8-65 the measured conductivity is plotted versus time. The plot is based on 180 data points.
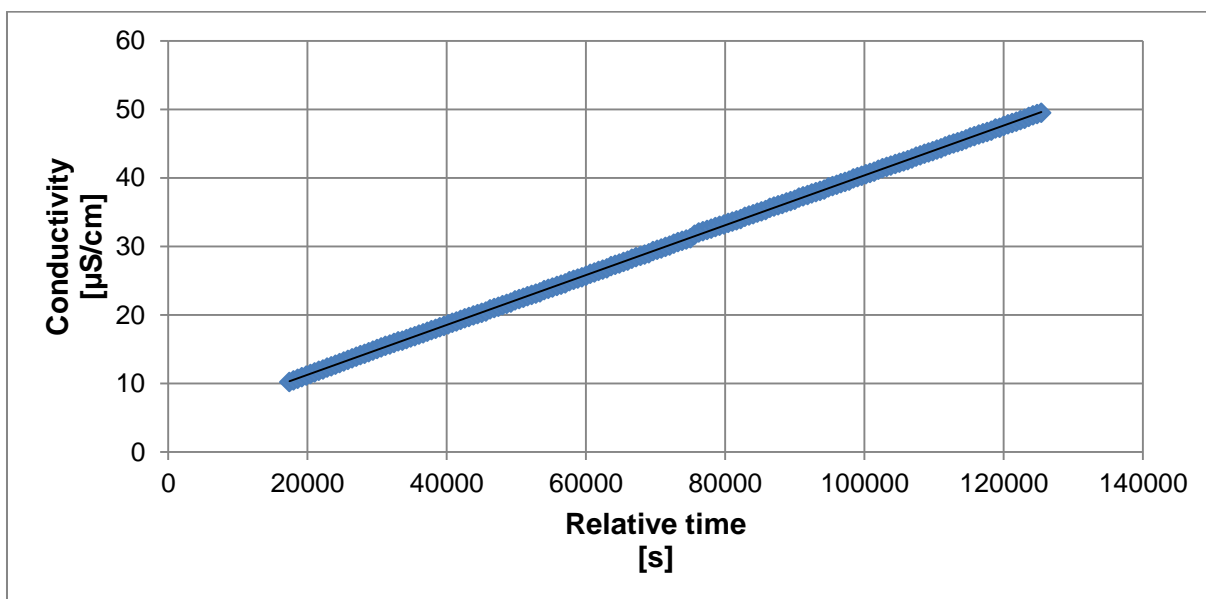

Figure 8-65: Plot of conductivity versus time for Membrane G reference test 7.

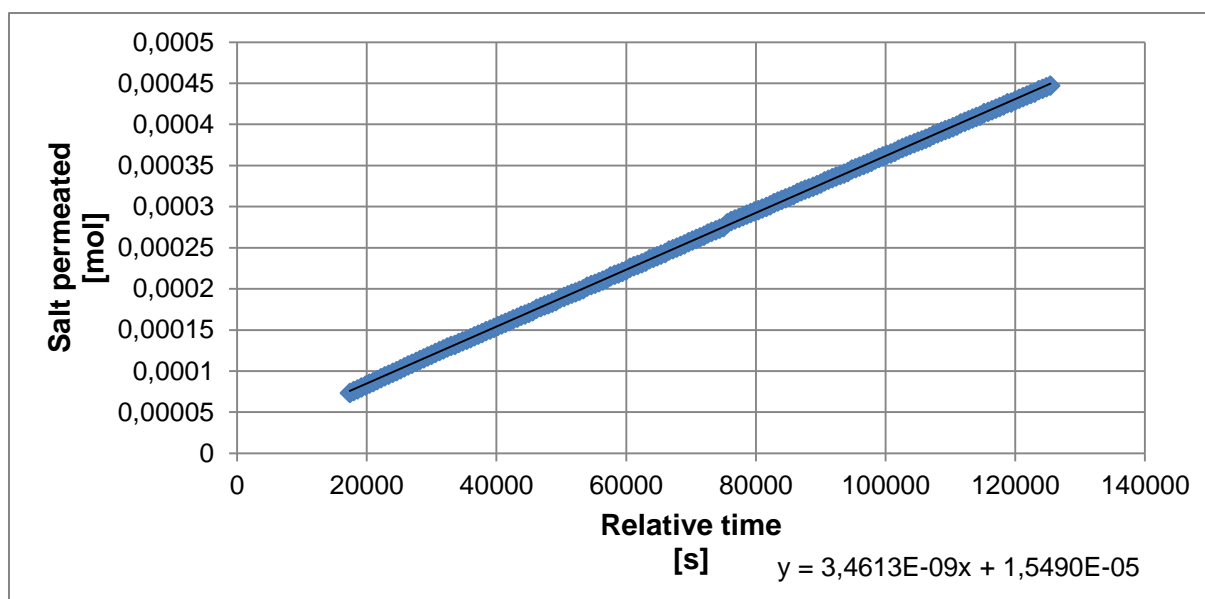Figure 8-66 shows the calculated amount of salt plotted versus time.

Figure 8-66: Plot of the amount of salt that has permeated to the feed, versus time for Membrane G reference test 7.

D   Data for the PRO experiments

In this chapter, the measured data of the PRO experiments is presented. Calculations of the water flux were performed in the same manner shown in Appendix B.

D.a   Investigation of membrane performance in PRO

Figure 8-67, Figure 8-68 and Figure 8-69 show the measured values of the weight of the feed bottle plotted versus time for ΔP = 8,0 bar, 1,4 bar and 12,8 bar respectively.
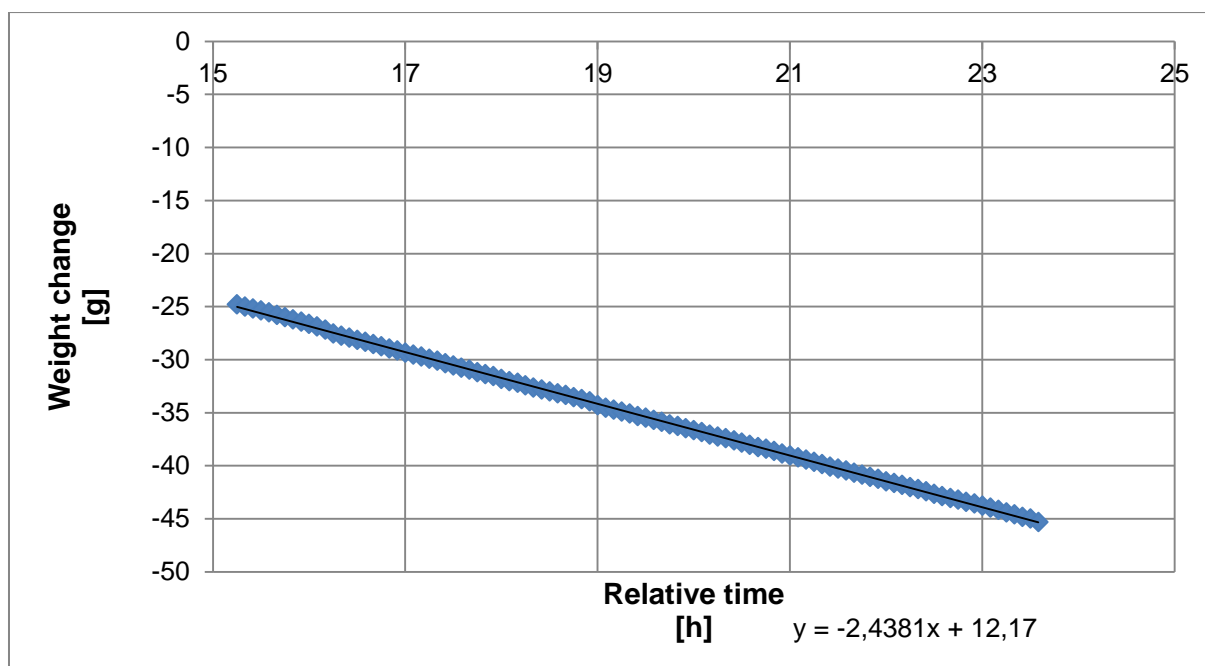

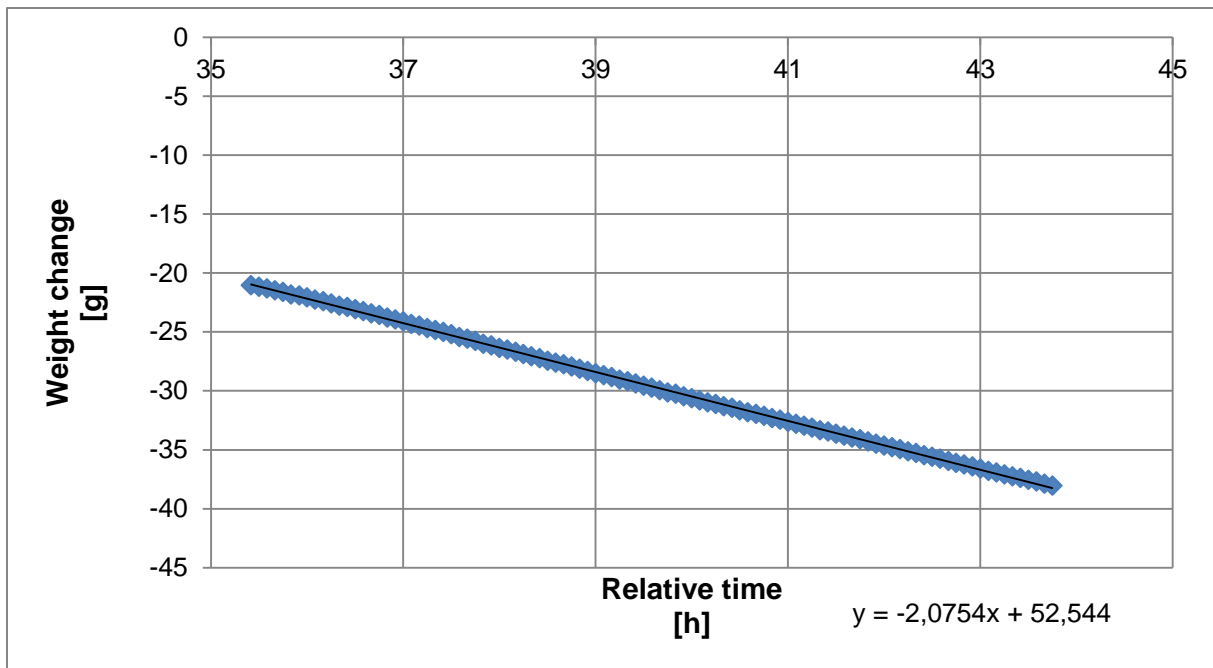**Figure 8-67: Plot of the weight change of the feed versus time for ΔP = 8,0 bar.**

Figure 8-68: Plot of the weight change of the feed versus time for ΔP = 1,4 bar.
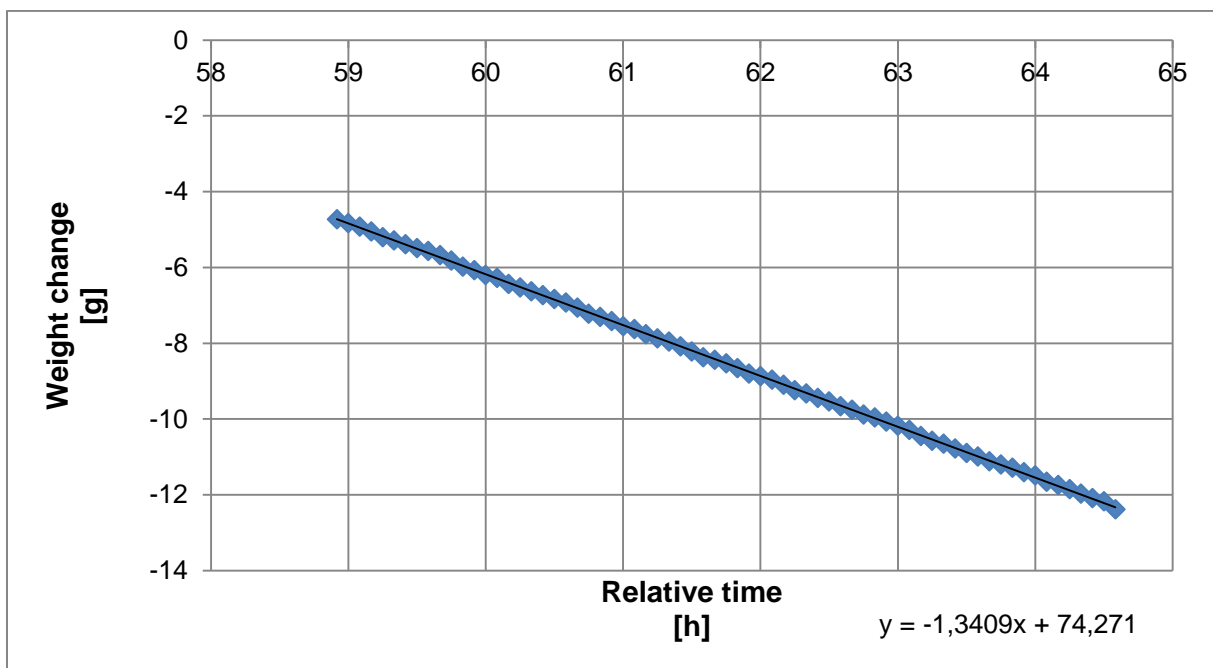

Figure 8-69: Plot of the weight change of the feed versus time for ΔP = 12,8 bar.

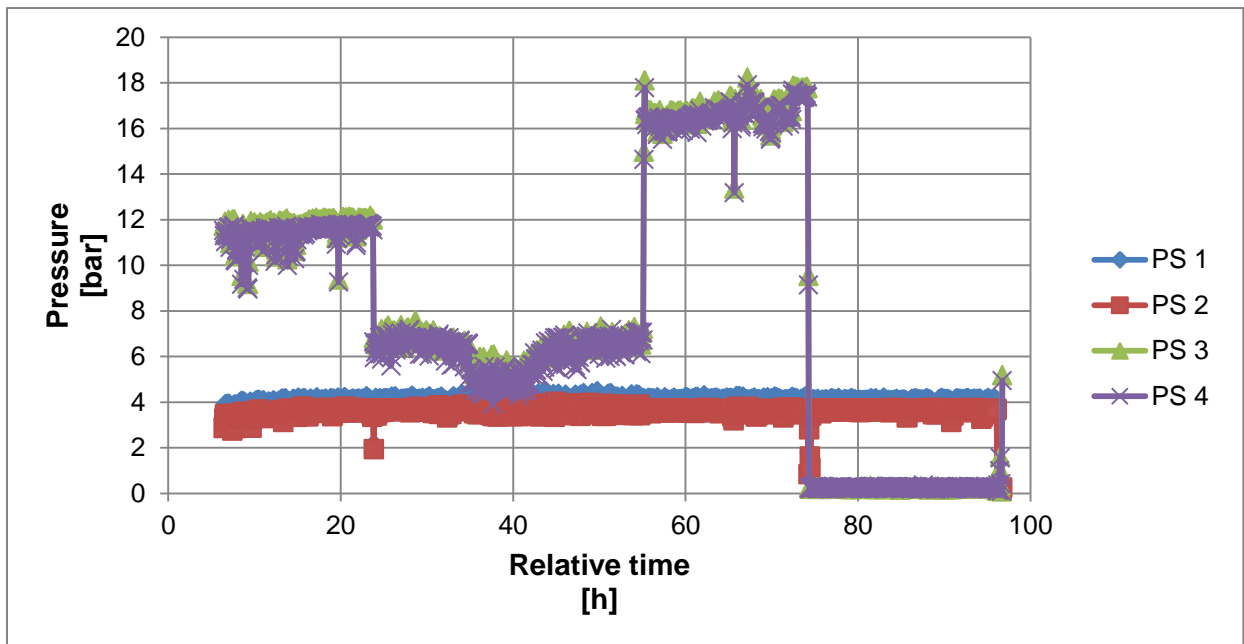Figure 8-70 shows the measured pressure during the experiment plotted versus time.

Figure 8-70: Plot of the pressure versus time for the different pressure indicators.

Figure 8-71 shows the measured temperature during the experiment plotted versus time. Temperature sensor 3 vas not connected.
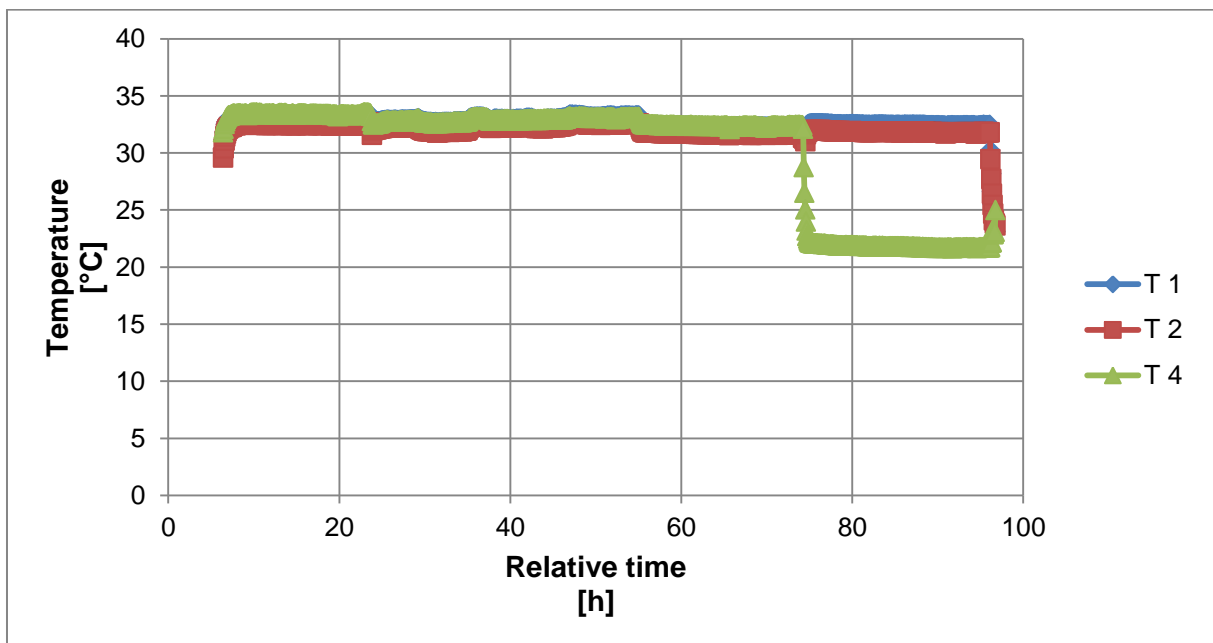

Figure 8-71: Plot of the temperature versus time for the different temperature indicators.

Figure 8-72 shows the measured flow rate during the experiment plotted versus time.
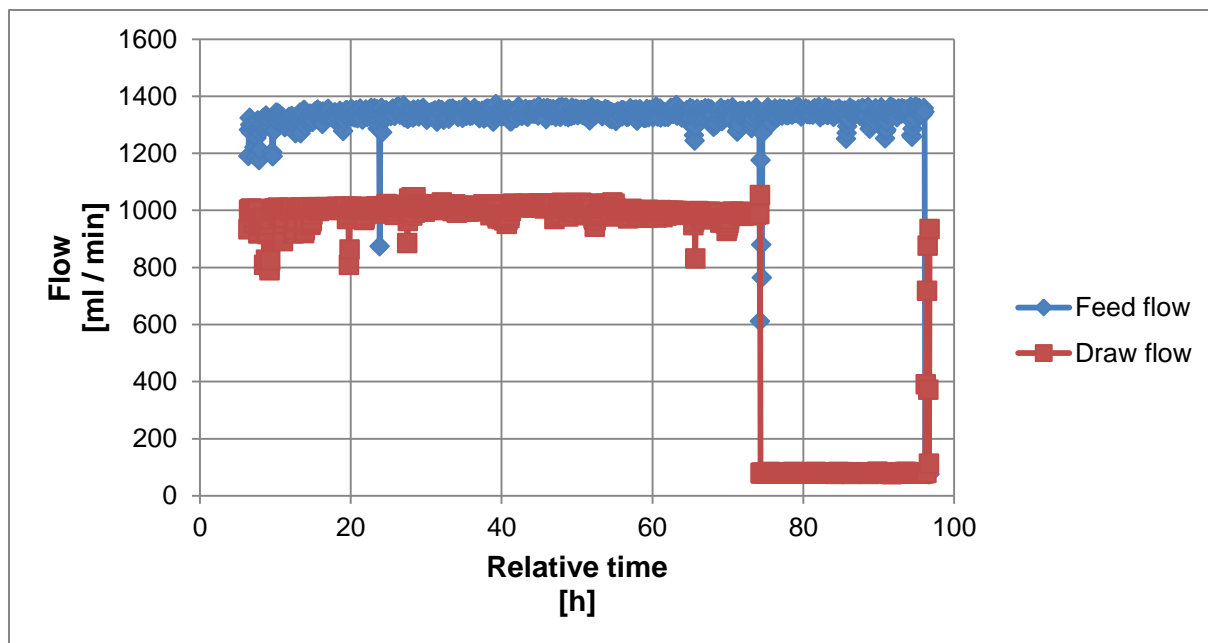
Figure 8-72: Plot of the feed and draw flow rate versus time.

D.b   The effect of hydrocarbons on the generated pressure in PRO

The measured pressures, temperatures and flow rates are plotted versus time in Figure 8-73, Figure 8-74 and Figure 8-75 respectively, for the reference test.
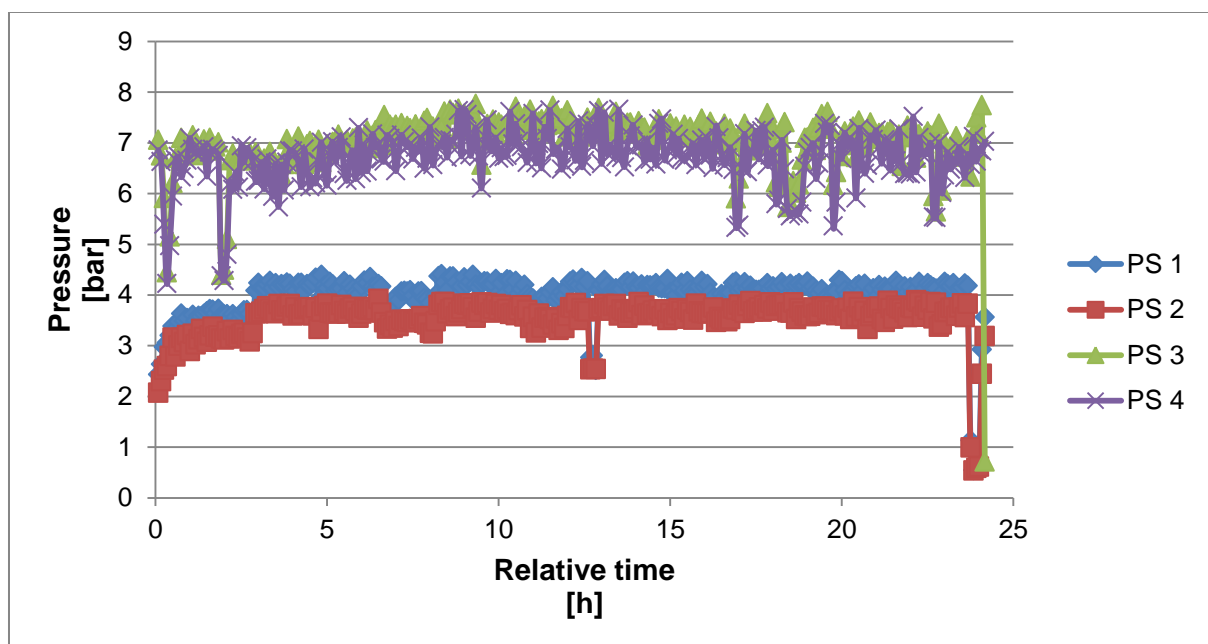

Figure 8-73: Plot of the pressure versus time for the different pressure indicators for the reference test.
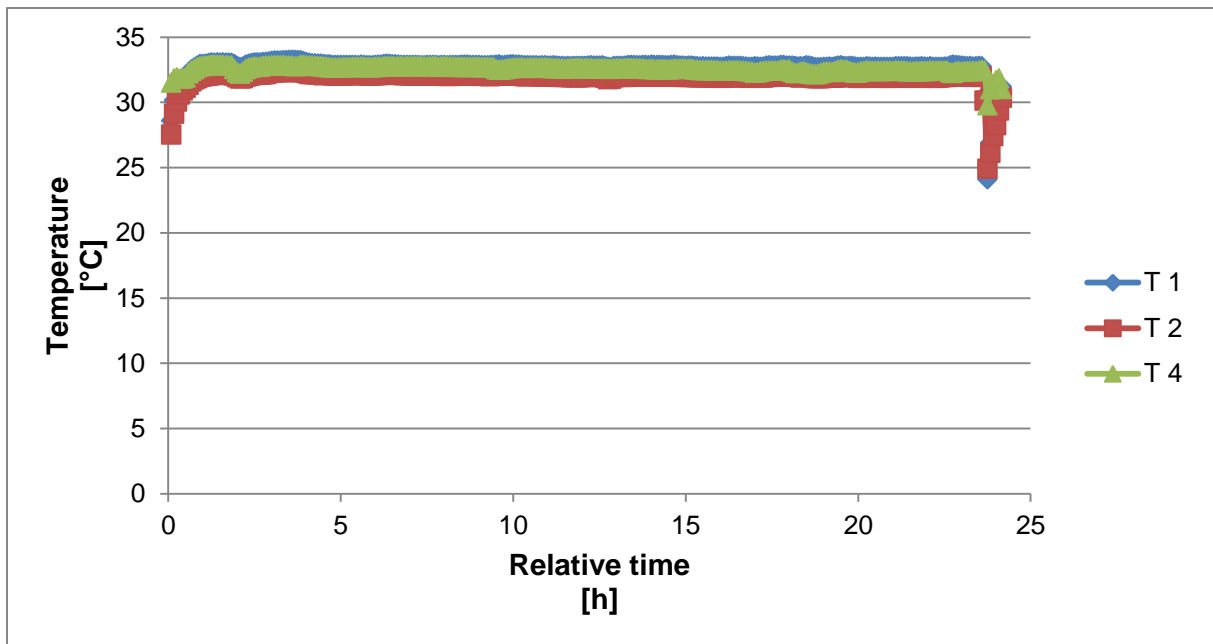
Figure 8-74: Plot of the temperature versus time for the different temperature indicators for the reference test.
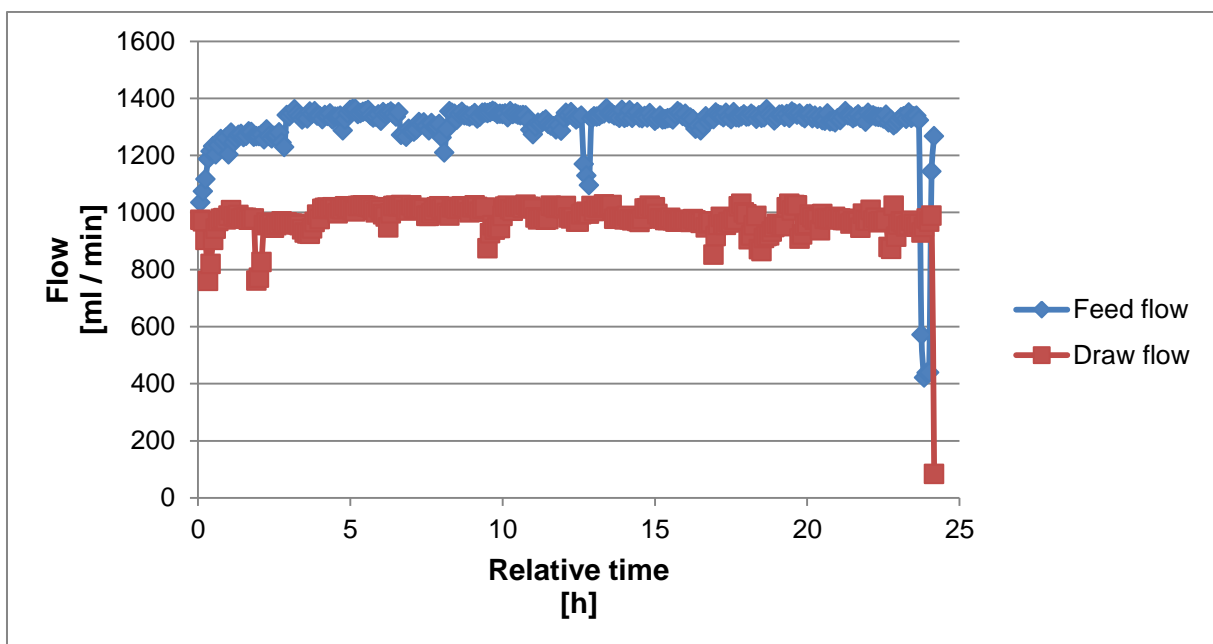

Figure 8-75: Plot of the feed and draw flow rate versus time for the reference test.

The measured pressures, temperatures and flow rates are plotted versus time in Figure 8-76, Figure 8-77, and Figure 8-78 respectively, for the 0 % HC test.

82

Figure 8-76: Plot of the pressure versus time for the different pressure indicators for the 0 % HC test.

Figure 8-77: Plot of the temperature versus time for the different temperature indicators for the 0 % HC test.

Figure 8-78: Plot of the feed and draw flow rate versus time for the 0 % HC test.

The measured pressures, temperatures and flow rates are plotted versus time in Figure 8-79, Figure 8-80 and Figure 8-81 respectively, for the 20 % HC test.
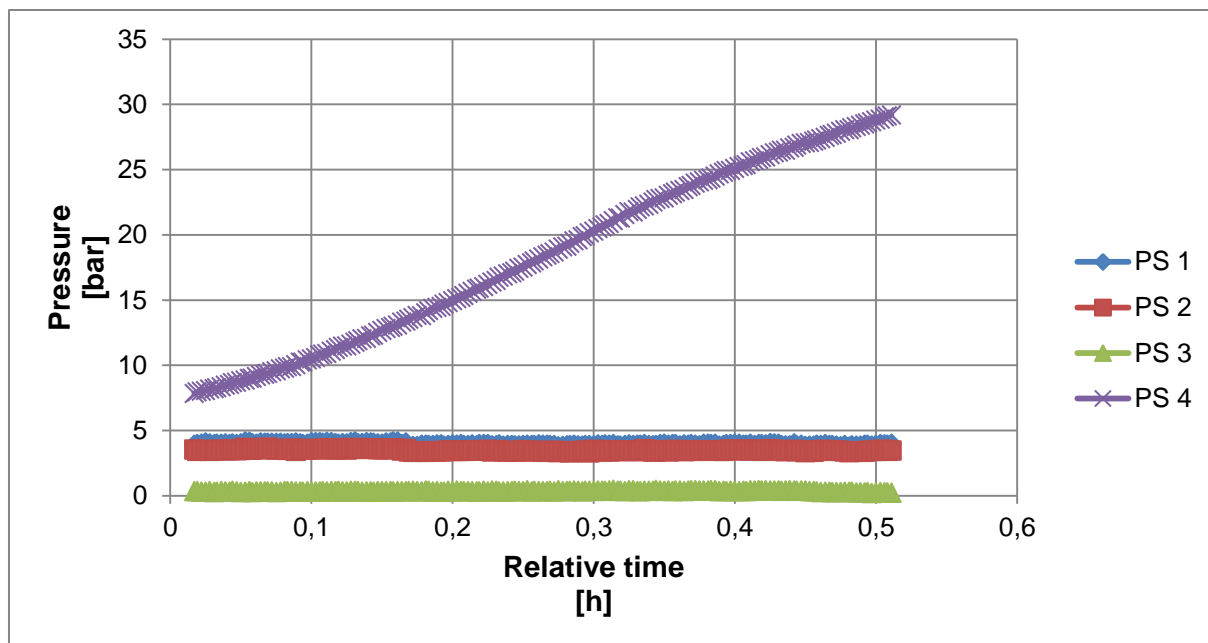

Figure 8-79: Plot of the pressure versus time for the different pressure indicators for the 20 % HC test.
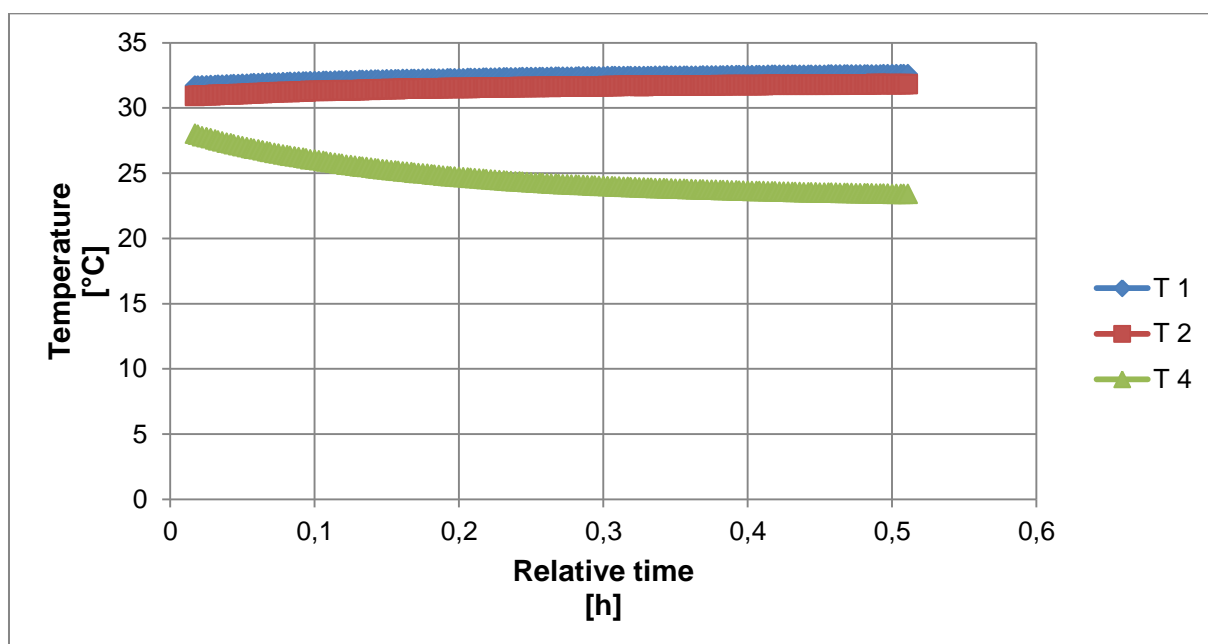
Figure 8-80: Plot of the temperature versus time for the different temperature indicators for the 20 % HC test.
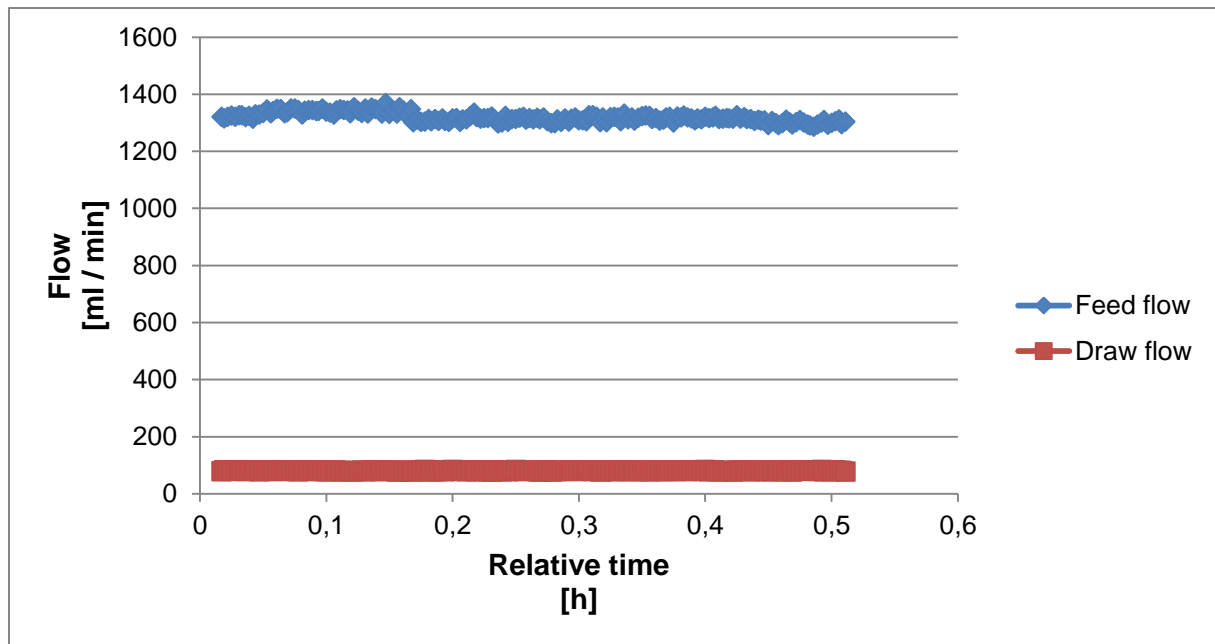

Figure 8-81: Plot of the feed and draw flow rate versus time for the 20 % HC test.

The measured pressures, temperatures and flow rates are plotted versus time in Figure 8-82, Figure 8-83 and Figure 8-84 respectively, for 50 % HC test 1.

Figure 8-82: Plot of the pressure versus time for the different pressure indicators for 50 % HC test 1.

Figure 8-83: Plot of the temperature versus time for the different temperature indicators for 50 % HC test 1.

Figure 8-84: Plot of the feed and draw flow rate versus time for 50 % HC test 1.

The measured pressures, temperatures and flow rates are plotted versus time in Figure 8-85, Figure 8-86 and Figure 8-87 respectively, for 50 % HC test 2.
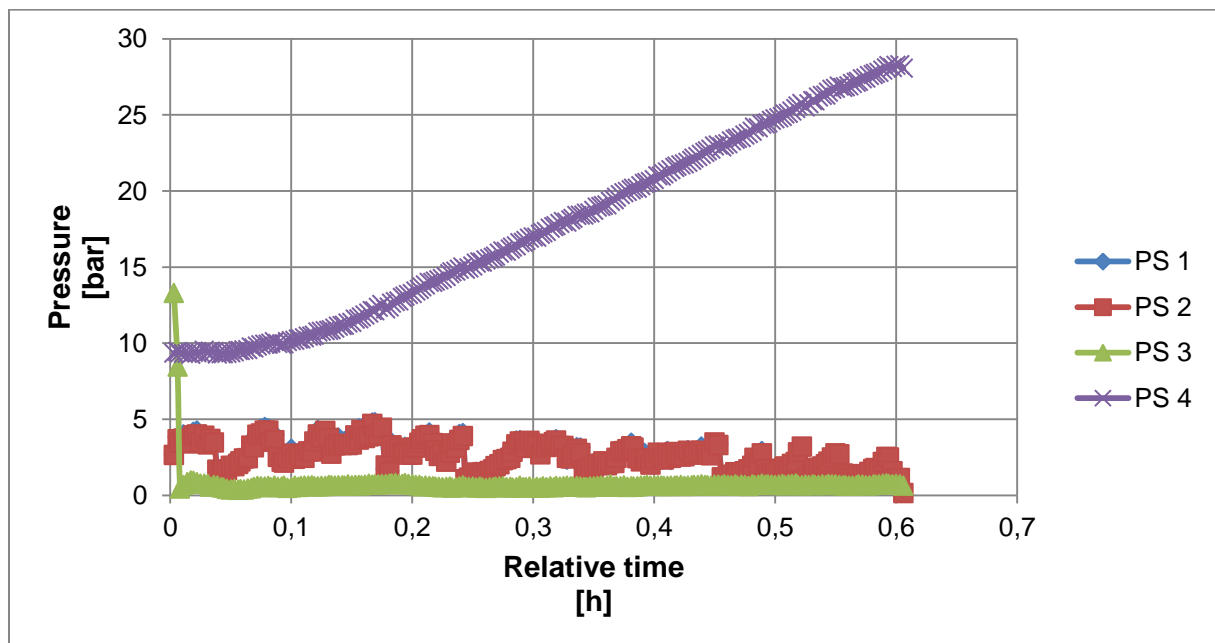

Figure 8-85: Plot of the pressure versus time for the different pressure indicators for 50 % HC test 2.
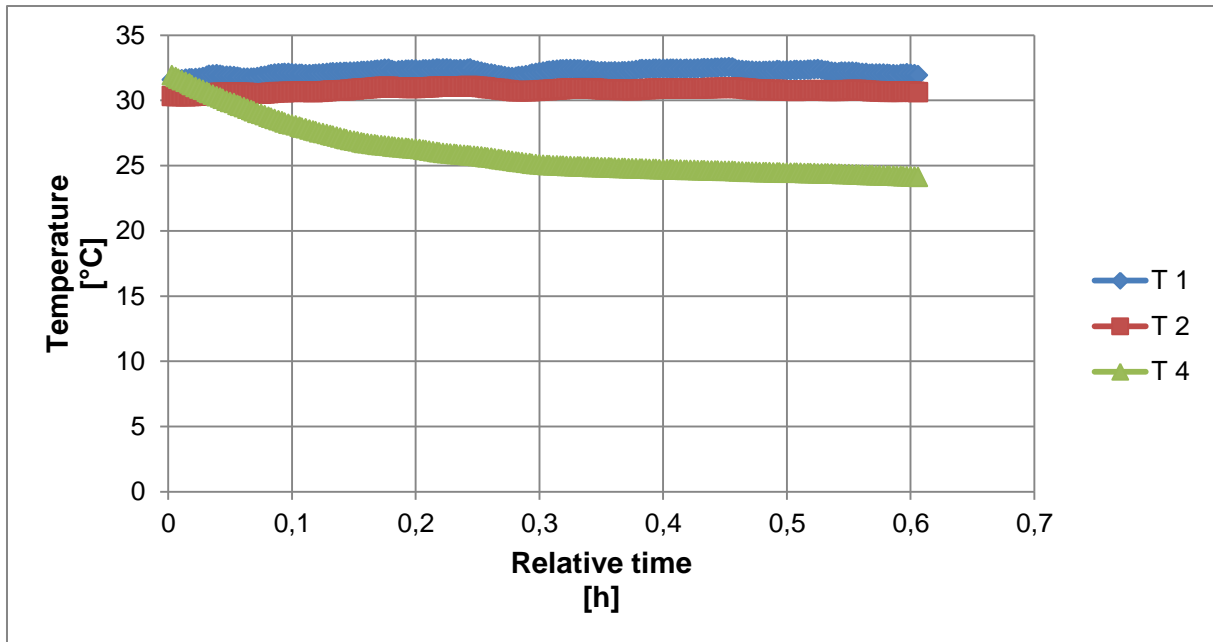
Figure 8-86: Plot of the temperature versus time for the different temperature indicators for 50 % HC test 2.
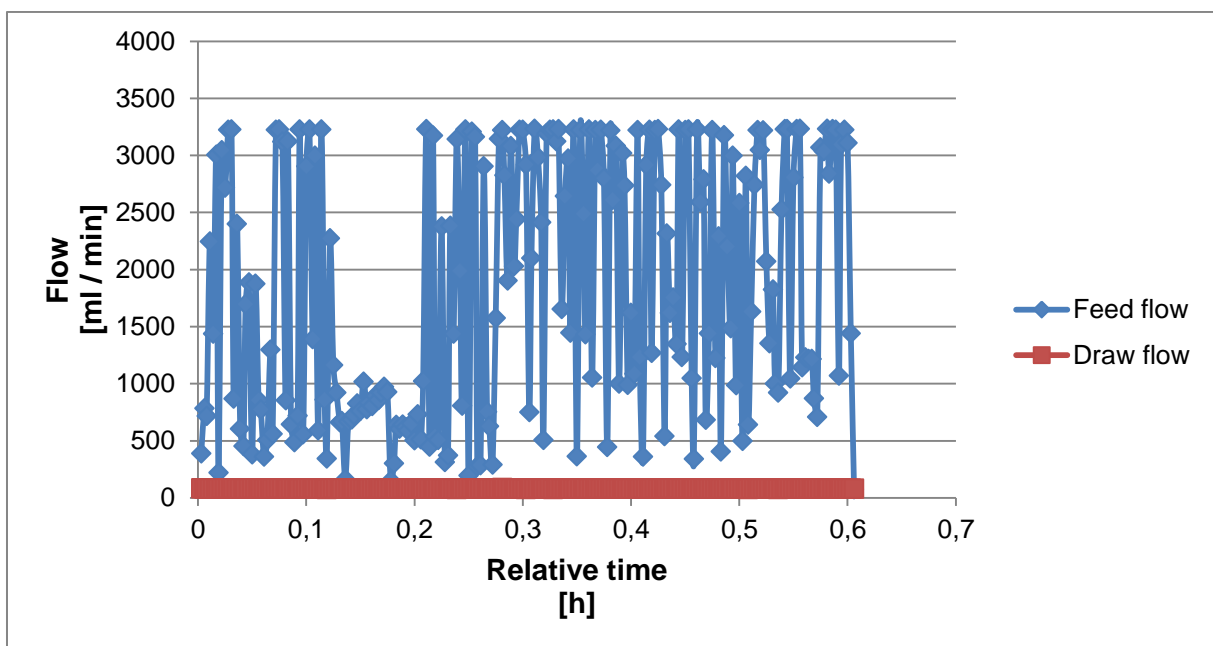

Figure 8-87: Plot of the feed and draw flow rate versus time for 50 % HC test 2.

The measured pressures, temperatures and flow rates are plotted versus time in Figure 8-88, Figure 8-89 and Figure 8-90 respectively, for 80 % HC test 1.
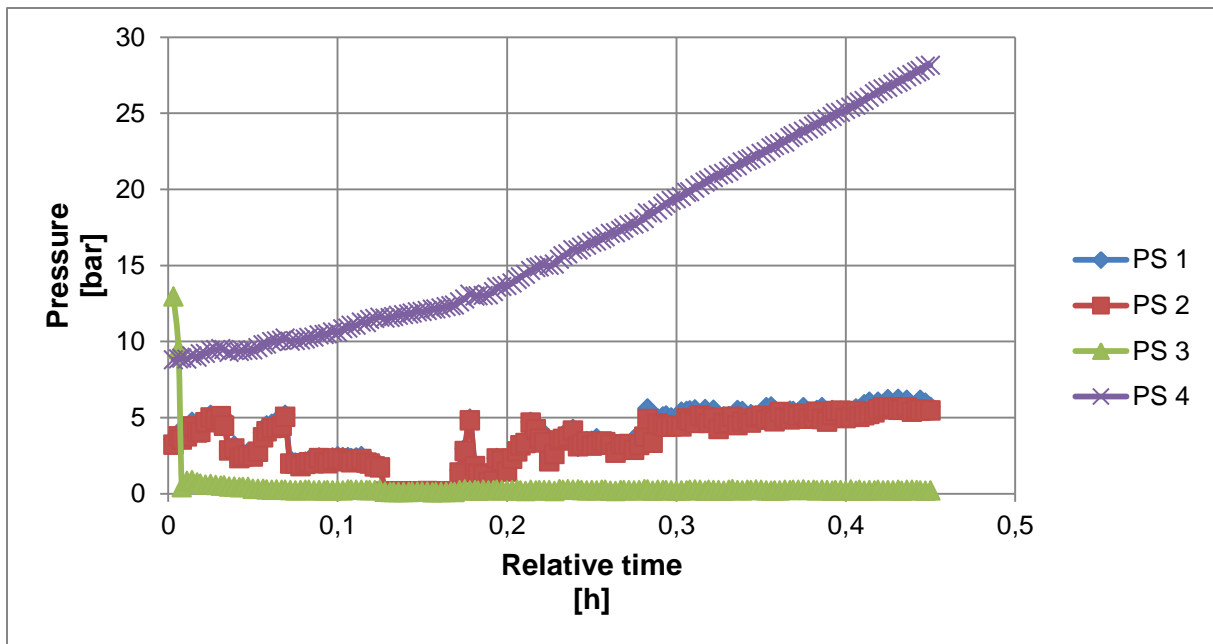
Figure 8-88: Plot of the pressure versus time for the different pressure indicators for 80 % HC test 1.

Figure 8-89: Plot of the temperature versus time for the different temperature indicators for 80 % HC test 1.

Figure 8-90: Plot of the feed and draw flow rate versus time for 80 % HC test 1.

The measured pressures, temperatures and flow rates are plotted versus time in Figure 8-91, Figure 8-92 and Figure 8-93 respectively, for 80 % HC test 2.

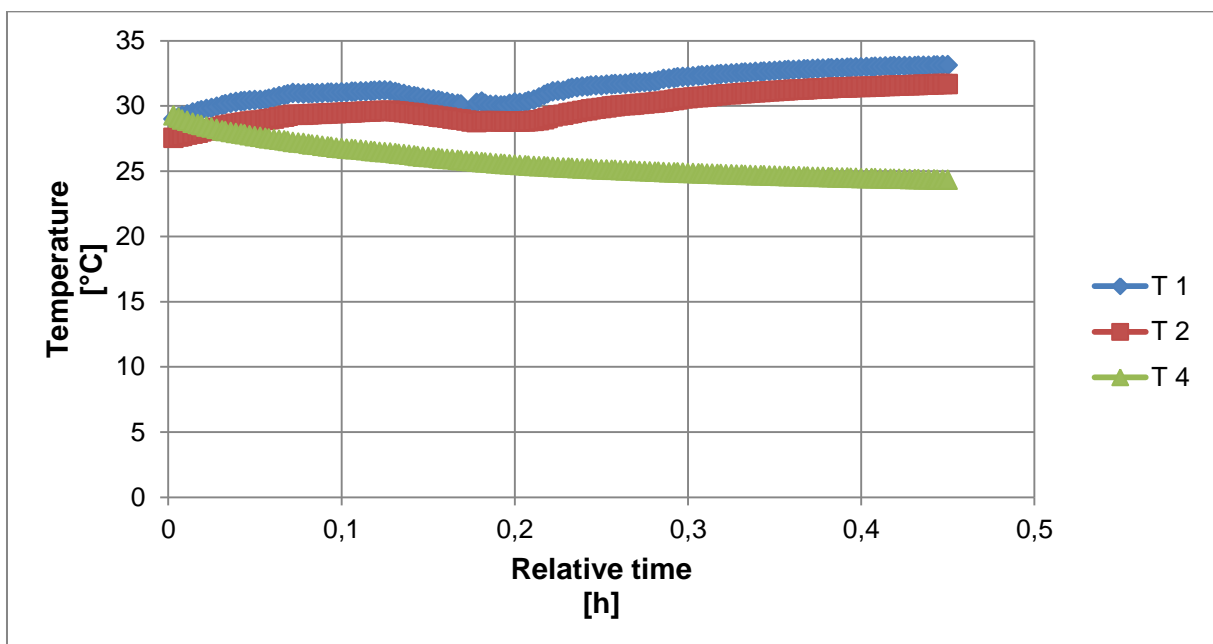**Figure 8-91: Plot of the pressure versus time for the different pressure indicators for 80 % HC test 2.**
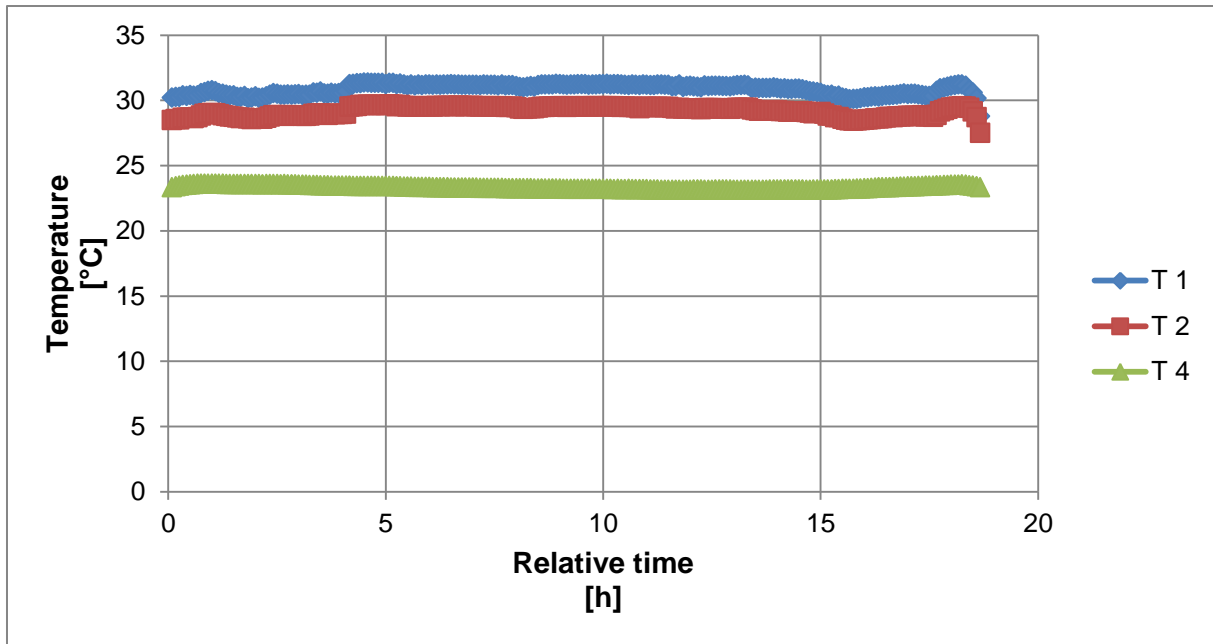
Figure 8-92: Plot of the temperature versus time for the different temperature indicators for 80 % HC test 2.
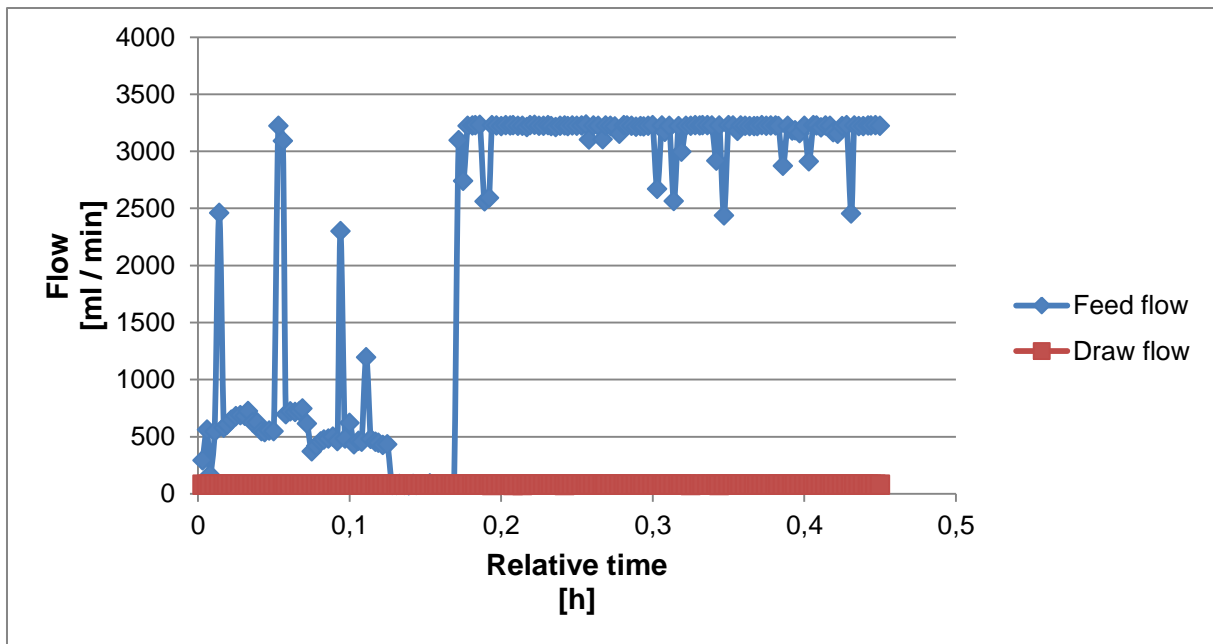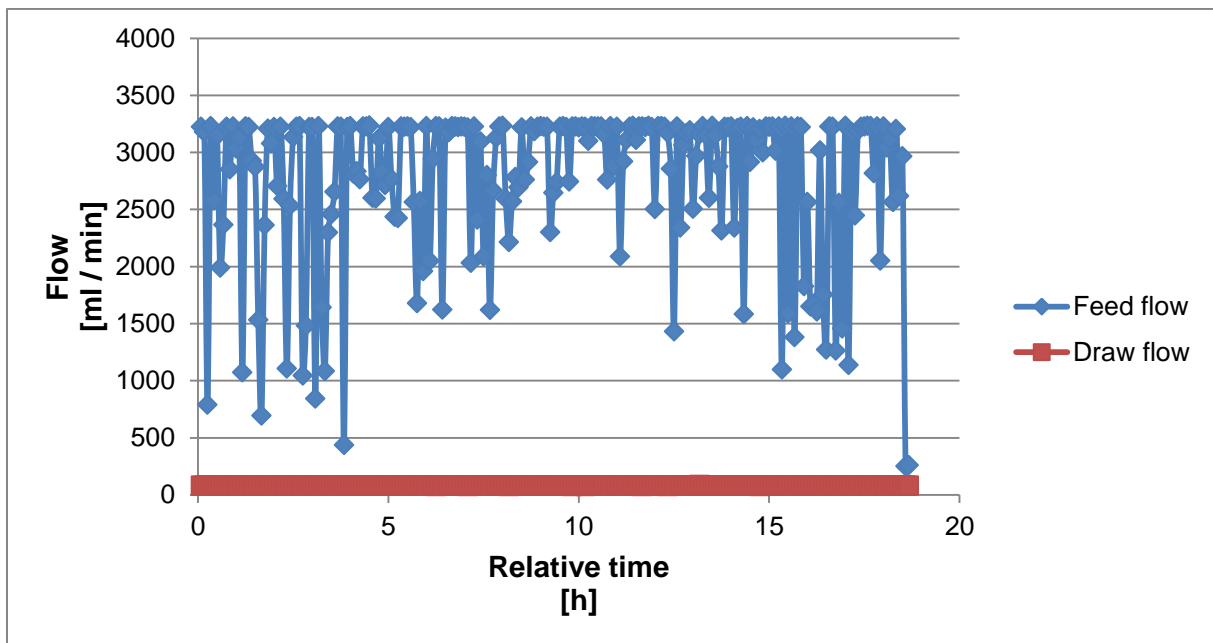

Figure 8-93: Plot of the feed and draw flow rate versus time for 80 % HC test 2.

The measured pressures, temperatures and flow rates are plotted versus time in Figure 8-94, Figure 8-95 and Figure 8-96 respectively, for the 100 % HC test.
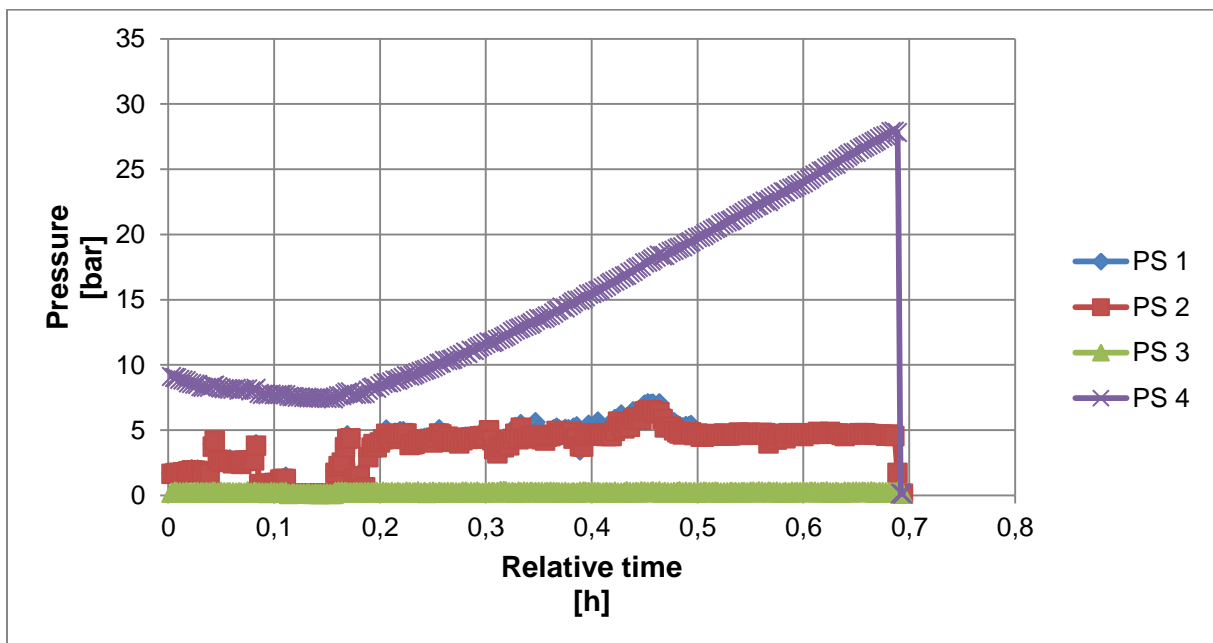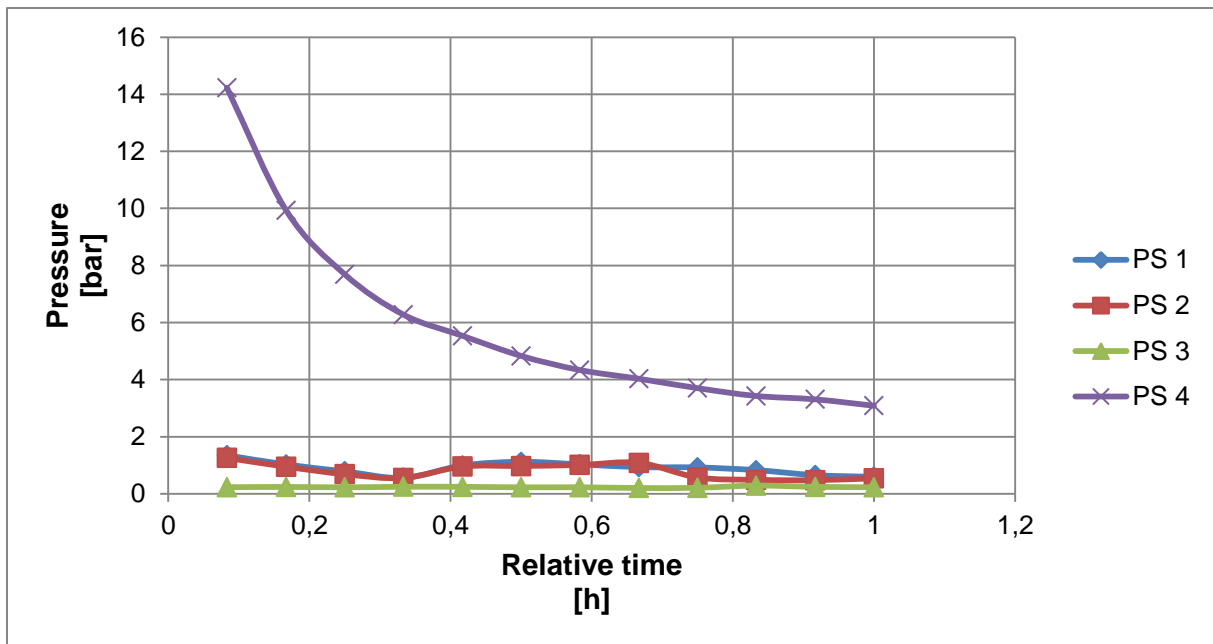
Figure 8-94: Plot of the pressure versus time for the different pressure indicators for the 100 % HC test.
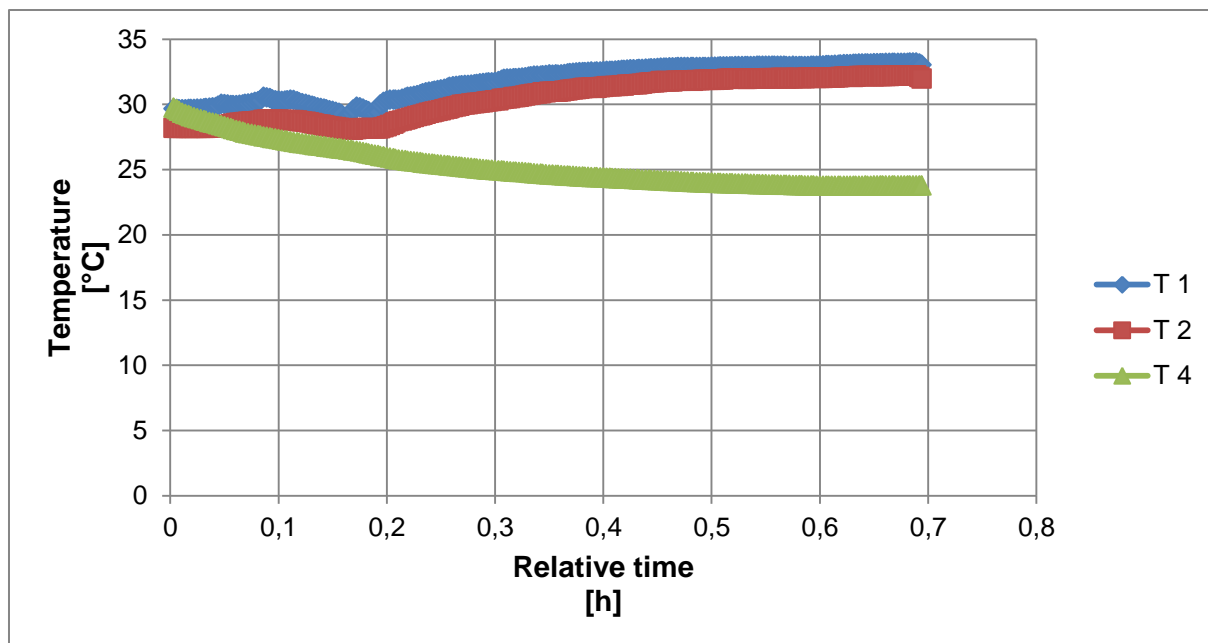

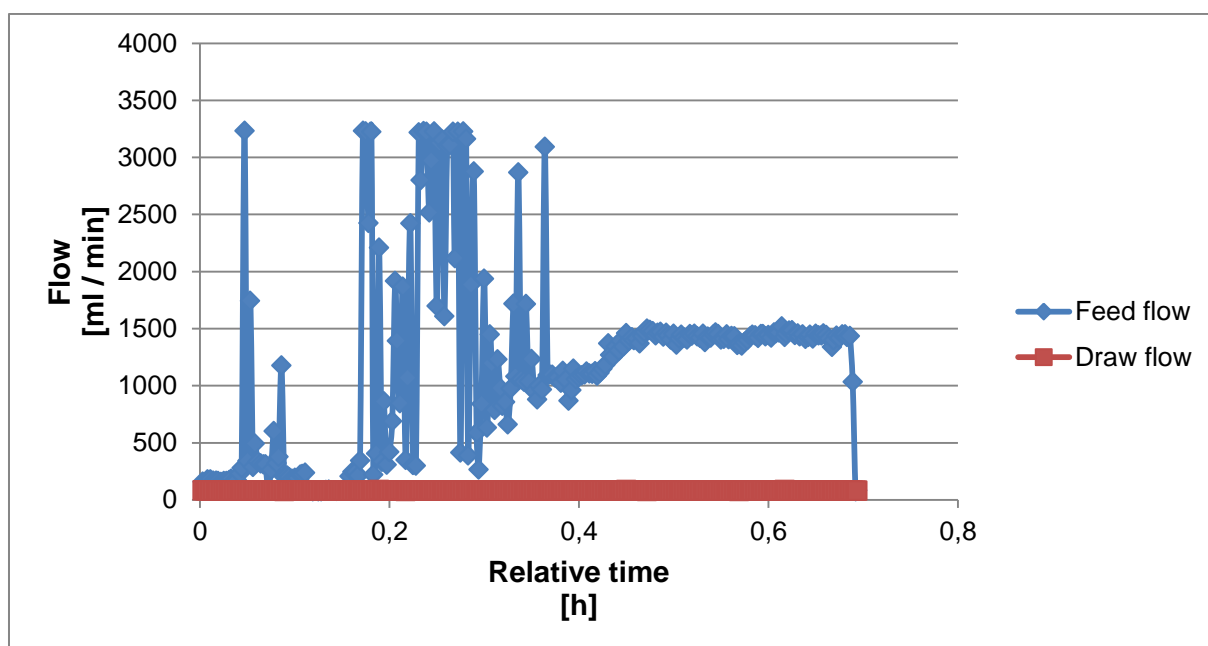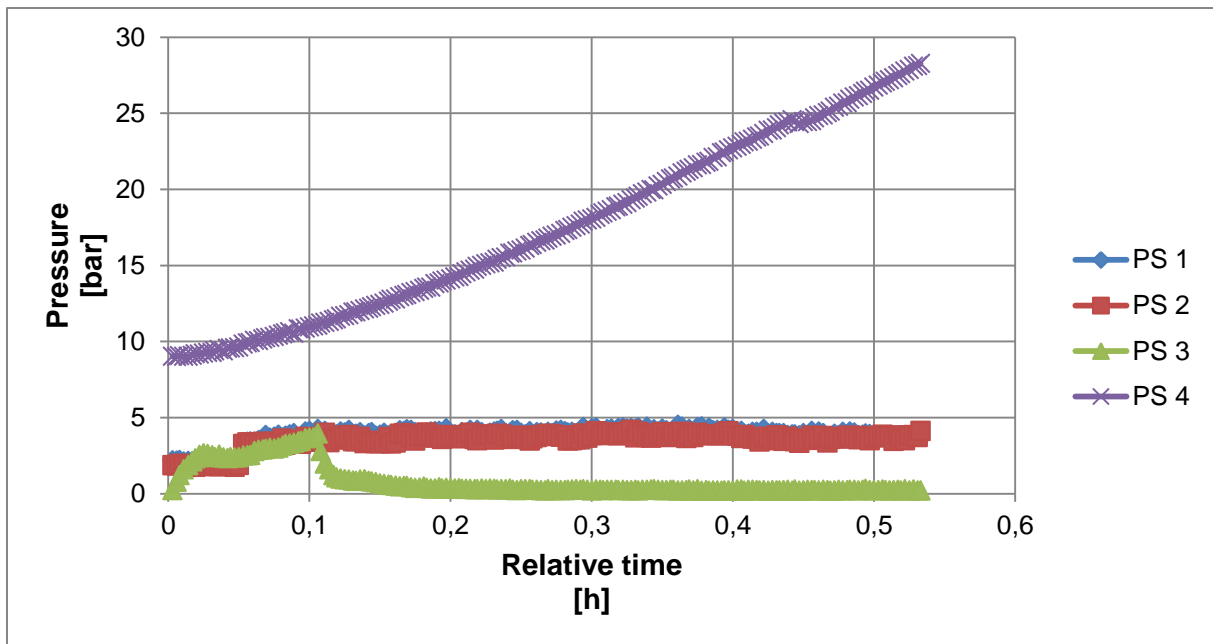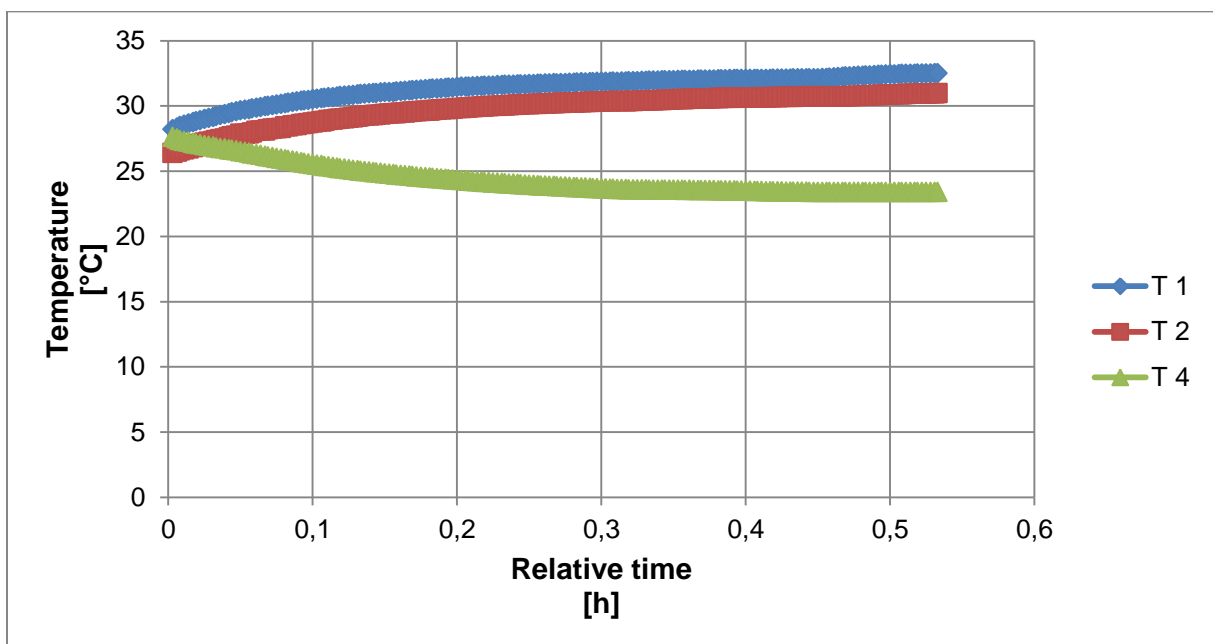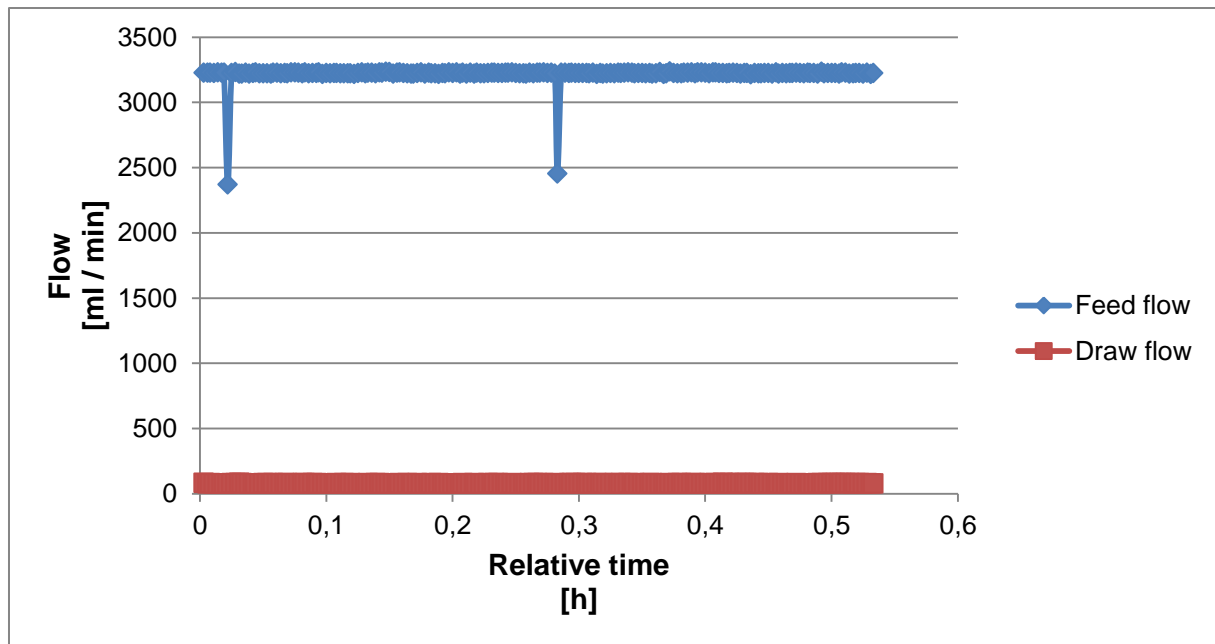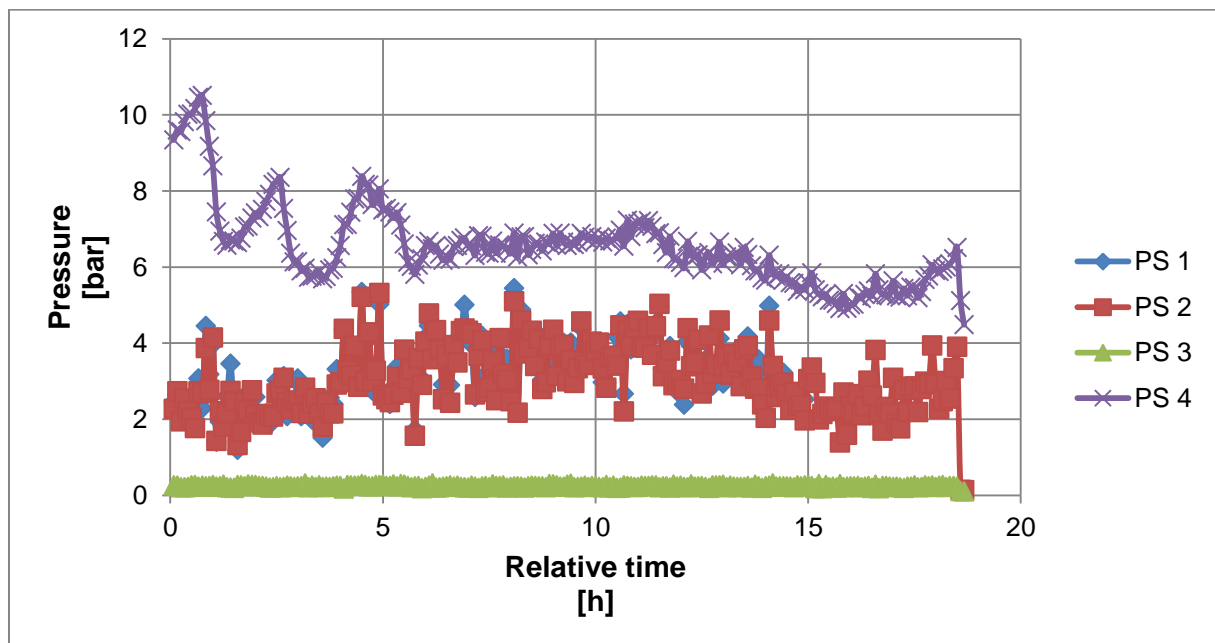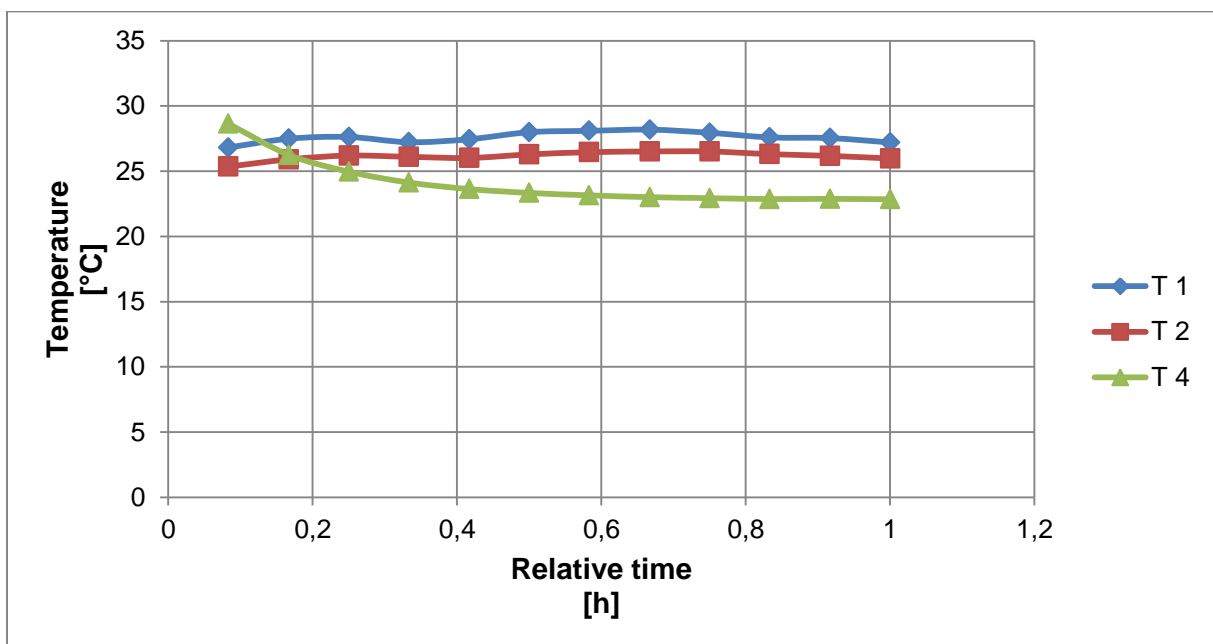**Figure 8-95: Plot of the temperature versus time for the different temperature indicators for the 100 % HC test.**

92
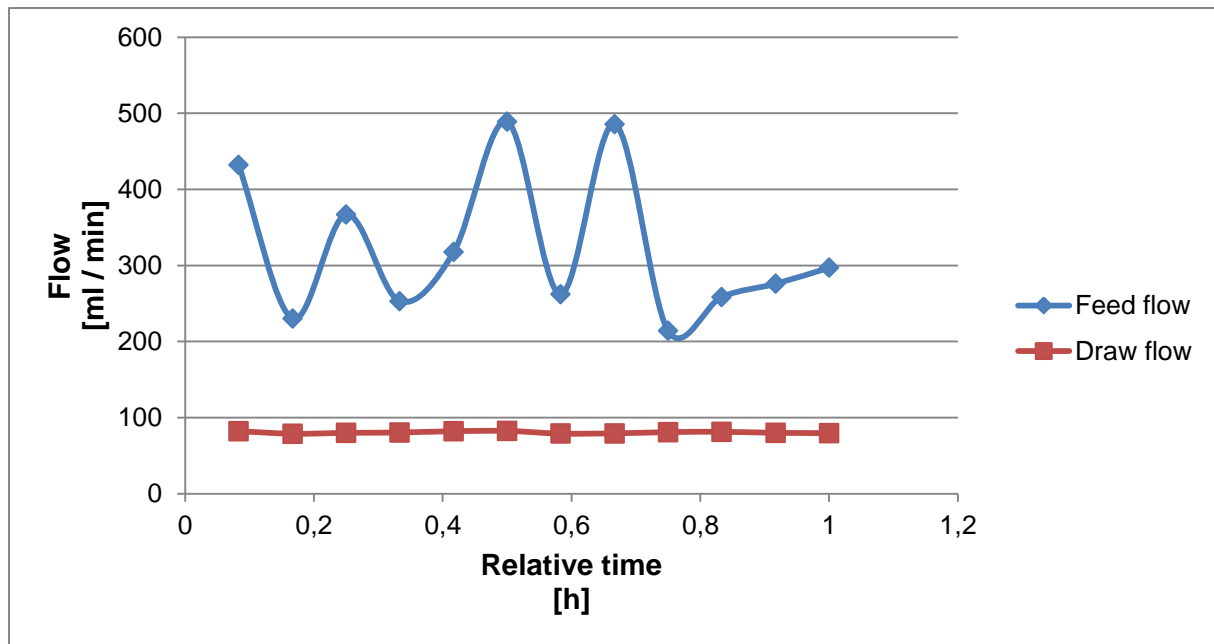
Figure 8-96: Plot of the feed and draw flow rate versus time for the 100 % HC test.

E   Membrane thickness measurements

Table 8-6 shows the measured thickness on different points of the wet Membrane B.

Table 8-6: Measured thickness on different points of the new Membrane B.

									Average
Measured thickness [μm]	45	45	45	53	44	41	43	45	**45**

Table 8-7 shows the measured thickness on different points of the wet Membrane C.

Table 8-7: Measured thickness on different points of the new Membrane C.

									Average
Measured thickness [μm]	44	40	45	38	43	48	44	48	**44**

Table 8-8 shows the measured thickness on different points of the wet Membrane D.

Table 8-8: Measured thickness on different points of the new Membrane D.

									Average
Measured thickness [μm]	47	42	42	32	46	41	47	41	**44**

Table 8-9 shows the measured thickness on different points of the wet Membrane D.

Table 8-9: Measured thickness on different points of the new Membrane E.

									Average
Measured thickness [μm]	61	66	70	72	63	74	68	80	**69**

Table 8-10 shows the measured thickness on different points of the wet Membrane F before it was used in any experiments.

Table 8-10: Measured thickness on different points of the new Membrane F.

										Average
Measured thickness [µm]	46	46	50	42	43	46	44	48	48	**46**

Table 8-11 shows the measured thickness on different points of the wet Membrane F after it was used in experiments and had been immersed in water for one week.

Table 8-11: Measured thickness on different points of Membrane F after breaking.

										Average
Measured thickness [µm]	51	53	54	52	50	51	55	50	57	**53**

Table 8-12 shows the measured thickness on different points of the wet Membrane F after it had been immersed in HC for one week.

Table 8-12: Measured thickness on different points of Membrane F after immersion in HC.

											Average
Measured thickness [µm]	51	58	55	53	50	58	55	63	56	51	**55**

Table 8-13 shows the measured thickness on different points of the wet Membrane F after it had been immersed in water and HC for one week.

Table 8-13: Measured thickness on different points of Membrane F after immersion in water and HC.

														Average
Measured thickness [µm]	57	56	67	60	60	57	64	57	64	62	60	60	58	58	**59**

Table 8-14 shows the measured thickness on different points of the wet Membrane D.

Table 8-14: Measured thickness on different points of the new Membrane G.

											Average
Measured thickness [µm]	49	53	48	50	53	53	49	51	44	48	49	**50**

F   Volume of the FO feed loop

In Table 8-15 the measured volume of the feed side is shown. Due to a leak in the cap the feed bottle could only be filled up to the bottom of the cap. The cap volume had to be subtracted from the total volume for calculations.

Table 8-15: The measured volume of the feed loop.

	Full bottle and tubes	Cap	Volume for calculations
Volume [mL]	1263	17,02	1245,98

In some experiments a magnet was put inside the feed flask. The volume of the magnet would then also have to be subtracted from the volume for calculations. This is presented in Table 8-16.

Table 8-16: The measured volume of the feed loop.

	Bottle and tubes - cap	Magnet	Volume for calculations
Volume [mL]	1245,98	12,85	1233,13

G   Risk assessment

NTNU		Hazardous activity identification process	Prepared by	Number	Date	
			HSE section	HMSRV-26/01	01.12.2006	
			Approved by	Page	Replaces	
HSE			The Rector	1 out of 1	15.12.2003	

Unit: Department of Chemical Engineering   **Date:** 07.03.14
Line manager: Edd Blekkan
Participants in the risk assessment (including their function): Student: Gaute Trondsen. Co-supervisor: Qiang Yu

Activity/process	Responsible person	Laws, regulations etc.	Existing documentation	Existing safety measures	Comment
Characterization of membranes: Microscopy, calorimetry etc.	Qiang Yu				
Forward Osmosis testing: Salt solutions and alkanes are used.	Qiang Yu			Fume hood	
Pressure Retarded Osmosis testing: Salt solutions and alkanes are used.	Qiang Yu			Fume hood	

Unit: Department of Chemical Engineering   **Date:** 07.03.14
Line manager: Edd Blekkan
Participants in the risk assessment (including their function): Student: Gaute Trondsen. Co-supervisor: Qiang Yu

Activity from the identification process form	Potential undesirable incident/strain	Likelihood: Likelihood (1-4)	Consequence: Human (1-4)	Environment (1-4)	Economy/ materiel (1-4)	Risk value	Comments/status Suggested measures
Characterization of membranes	None	2	A	A	A	A2	
Forward Osmosis testing	Leakage of water, salt, alkanes.	3	A	A	A	A3	When alkanes are used the test rig is kept in a fume hood.
Pressure Retarded Osmosis testing	Leakage of water, salt, alkanes.	3	A	A	A	A3	Test rig is placed inside a fume hood.
	Release of pressure	3	A	A	A	A3	

Likelihood, e.g.:
1. *Minimal*
2. *Low*
3. *Medium*
4. *High*
5. *Very high*

Consequence, e.g.:
1. *Safe*
2. *Relatively safe*
3. *Dangerous*
4. *Critical*
5. *Very critical*

Risk value (each one to be estimated separately):
Human = Likelihood x Human Consequence
Environmental = Likelihood x Environmental consequence
Financial/material = Likelihood x Consequence for Economy/materiel

Potential undesirable incident/strain
Identify possible incidents and conditions that may lead to situations that pose a hazard to people, the environment and any materiel/equipment involved.

Criteria for the assessment of likelihood and consequence in relation to fieldwork
Each activity is assessed according to a worst-case scenario. Likelihood and consequence are to be assessed separately for each potential undesirable incident. Before starting on the quantification, the participants should agree what they understand by the assessment criteria:

The likelihood of something going wrong is to be assessed according to the following criteria:
1 Minimal Once every 10 years or less
2 Low Once a year
3 High Once a month
4 Very high Once a week or more often

Human consequence is to be assessed according to the following criteria:
1 Relatively safe Injury that does not involve absence from work; insignificant health risk
2 Dangerous Injury that involves absence from work; may produce acute sickness
3 Critical Permanent injury; may produce serious health damage/sickness
4 Very critical Injury that may produce fatality/ies

Environmental consequences are assessed according to the following criteria:
1 Relatively safe Insignificant impact on the environment
2 Dangerous Possibility of undesirable long term effects; some cleanup is to be expected
3 Critical Undesirable long term effects; cleanup to be expected
4 Very critical Damaging to living organisms; irreversible impact on the environment; cleanup must be undertaken

The unit makes its own decision as to whether opting to fill in or not consequences for economy/materiel, for example if the unit is going to use particularly valuable equipment. It is up to the individual unit to choose the assessment criteria for this column.

Risk = Likelihood x Consequence
Please calculate the risk value for "Human", "Environment" and, if chosen, "Economy/materiel", separately. For activities with a risk value of 16 or 12, or a single value of 4, safety measures (designed to both reduce the likelihood and to limit the consequences) must be documented with descriptions of measures and allocation of responsibility.

About the column "Comments/status, suggested preventative and corrective measures":
Measures can impact on both likelihood and consequences. Prioritise measures that can prevent the incident from occurring; in other words, likelihood-reducing measures are to be prioritised above greater emergency preparedness, i.e. consequence-reducing measures.

H   Finished in the lab form

Finished in the lab?

NAME: Gaute Tolås Trondsen   Supervisor: May-Britt Hägg

		What has been done	Accepted by Gøril	Accepted by the apparatus responsible
1. Solutions	- waste or - give to someone who needs it	Removed solutions removed labels	*Gøril*	
	Clean flasks (remove labels from them)	Flasks have been cleaned and labels removed		
2. Remove samples	Remove samples from shelves, drawers, freezers and fridges. IF they can't be removed, talk to Gøril or your supervisor about it.	Removed samples from the lab	*Gøril*	
	Clean sample bottles, remove labels	No bottles were used		
3. Lab-jacket	Return lab-coat to Arne.	No lab coat was borrowed	Hadde ikke	
4. Check chemicals.	If someone is going to use these chemicals, re-register to the other user.	Chemicals have been re-registered	Hadde ikke	
	If nobody needs them, deliver them to Arne.			
5. Apparatus	Clean the apparatus and surroundings, remove all solutions, +tell the apparatus responsible if something is not working!	Apparatus cleaned		*Martin Fossen*
6. All other equipment / glassware	If you have been using equipment/glass ware which you picked up from Arne/Frode, please return them.	Glassware returned	Hadde ikke	

Instructions:

- Please fill the form. THEN talk to Gøril and explain what has been done.
- All points except point number 5 will be signed by Gøril.
- Point 5: The tidiness of the apparatus will be accepted by the apparatus responsible (see apparatus card).

If you are unsure what to do, talk to your supervisor/ Gøril/Lily/May-Britt. We will help!